A reappraisal of tyrannosauroid fossils from the Iren Dabasu Formation (Coniacian–Campanian), Inner Mongolia, People's Republic of China

Thomas D. Carr

View supplementary material

Published online: 31 May 2023.

Submit your article to this journal

Article views: 4226

View related articles

View Crossmark data

ARTICLE

A REAPPRAISAL OF TYRANNOSAUROID FOSSILS FROM THE IREN DABASU FORMATION (CONIACIAN–CAMPANIAN), INNER MONGOLIA, PEOPLE'S REPUBLIC OF CHINA

THOMAS D. CARR*

Department of Biology, Carthage College, 2001 Alford Park Drive, Kenosha WI, 53140, U.S.A.; tcarr@carthage.edu

ABSTRACT—The hind limb of the lectotype of *Alectrosaurus olseni* is described in comparison with other tyrannosauroids. In addition to the autapomorphies described for *Alectrosaurus* by previous workers, the taxon possesses a specialized pes, where the distal condyles of the metatarsals and most phalanges are strongly elevated beyond the dorsal and ventral surfaces of the shaft of each bone, described here as the 'pediculate' condition. In comparison with the lectotype, previously reported *Alectrosaurus* and *Tyrannosaurus bataar* material from the Turonian of Uzbekistan, and fossils from the Kyzylkum Desert, are not referable to *Alectrosaurus*. A partial skull from the Iren Dabasu Formation is not referable to *A. olseni* because of the lack of shared diagnostic bones between it and the lectotype. Several features are shared between the skull, the holotype of *Raptorex*, and an isolated juvenile *T. rex* lacrimal, to the exclusion of other derived tyrannosauroids.

INTRODUCTION

By the Late Cretaceous, tyrannosauroids were well-established top predators in the terrestrial ecosystems of Laurasia and their biogeographic history included dispersal events between Asia and Laramidia that were controlled by eustatic variation in sea level (Loewen et al., 2013; Brusatte & Carr, 2016). Owing to a relatively complete fossil record, the diversity and relationships of Laramidian tyrannosaurs of the Campanian and Maastrichtian is well understood. In contrast, a comparable high quality fossil record in Asia is limited to the Nemegt Formation of Mongolia. The depauperate fossil record of the early Late Cretaceous on both land masses limits our understanding of the faunal exchanges between them and how those dispersals affected their phylogenetic relationships (Loewen et al., 2013).

Specifically, the diversity and relationships of tyrannosauroids from the Coniacian-Campanian Iren Dabasu Formation is poorly understood, owing to a poor fossil record. Likewise, the fossil record of early tyrannosaurs in Laramidia are limited to the Cenomanian-Turonian (Nesbitt et al., 2019; Zanno et al., 2019). The most complete tyrannosauroid fossils from the Iren Dabasu Formation includes the lectotype of *Alectrosaurus olseni* (AMNH FARB 6554) and a partial skull (AMNH FARB 6266). The hind-limb of *Alectrosaurus* has been described, whereas the skull material, including teeth, has not been documented in the literature. This raises the question of whether or not the Iren Dabasu fauna included a single tyrannosauroid taxon or a pair of sympatric taxa. A related issue is the referral of fossils to *Alectrosaurus* from other units and localities, which, if not securely made, results in inaccurate hypotheses of diversity and relationships.

Alectrosaurus is currently understood as a medium-sized and possibly early branching tyrannosaurid from central Asia (Gilmore, 1933; Mader and Bradley, 1989; Molnar et al., 1990; Currie and Eberth, 1993; Currie, 2000a; Holtz, 2001; Loewen et al., 2013). Gilmore named and first described the holotype (AMNH FARB 6554) of *Alectrosaurus olseni*, which was collected in China from the Iren Dabasu Formation, thought to be Coniacian–Campanian, or 89.8–83.6 million years in age (Gilmore, 1933; Currie and Eberth, 1993). Mader and Bradley (1989) later redescribed the specimen and corrected problems with bones originally thought to be part of the holotype. Specifically, Mader and Bradley (1989) verified the tyrannosaurid identity of the specimen and identified several autapomorphies (see below).

At the time of its first description, *Alectrosaurus* was the most complete tyrannosaurid known from central Asia (Gilmore, 1933). Gilmore distinguished *Alectrosaurus* from *Albertosaurus libratus* on the basis of its smaller size and slenderness, shorter and narrower astragalus, and "less robust" fourth trochanter (1933:37). Gilmore also mentioned that the "pes has the peculiar and specialized character of the ornithomimids very exactly reproduced," but without explanation of what he meant (1933).

In their description of the lectotype of *Alectrosaurus*, Mader and Bradley (1989) identified three diagnostic characters – a short pedal digit III, the distal joint surface of metatarsal III is offset from the plantar surface of the shaft by a lip, and large flexor tubercles on the pedal unguals. The authors noted that Gilmore's contention that the ascending process of the astragalus was narrower than in other tyrannosaurids could not be substantiated because most of the medial margin of the process is missing (1989). Also, the authors regarded the reduced fourth trochanter to be the result of poor preservation (1989). They also observed that metatarsals II and IV are longer and narrower in *Alectrosaurus* (1989) than in *Albertosaurus libratus* and *Daspletosaurus torosus*, but they cited published evidence that the long hind limb proportions may represent typical growth trends of subadult tyrannosaurids.

Mader and Bradley noted that the manual unguals are "small, strongly recurved, and laterally compressed … unlike the manual unguals of any tyrannosaur with which we are familiar" (1989:46). They considered the unguals to be more similar to dromaeosaurids, therizinosauroids, and oviraptorids (1989). However, they did not consider this morphology diagnostic and raised doubts regarding the referral of the unguals to the partial pelvis and hind limb even though the specimens were found associated in the field (1989). If the unguals are absolutely larger than in similar-sized tyrannosaurids, then this size may be plesiomorphic and is comparable to the condition seen in *Dryptosaurus*. Finally, in contrast to Mader and Bradley (1989:47), the fibula is visible in the field photograph of the specimen, which is exposed distal to the fibular process of the tibia.

Fossils Referred to *A. olseni*

Additional material collected from Mongolia was referred to *Alectrosaurus* based on hind limb proportions (Perle, 1977). However, the basis for this referral has been questioned (Mader and Bradley, 1989) and hind limb proportions are conservative among tyrannosaurids (Currie, 2000b). Nondenticulate premaxillary tyrannosaurid teeth from Inner Mongolia have been referred to *Alectrosaurus* owing to the presence of such teeth in the skull material described by Perle (1977; Currie and Eberth, 1993; Currie et al., 1990; Currie, 2000a). Isolated postcranial bones and teeth from Uzbekistan were also referred to *Alectrosaurus* (Nessov, 1995). These referrals are unjustified given that the lectotype only consists of an isolated hind limb (Fig. 1) and that the more complete fossils are questionably assigned to that taxon (Perle, 1977; Mader and Bradley, 1989). Thus, *Alectrosaurus* is still an enigmatic form that has not received detailed comparative treatment with other tyrannosauroids.

Several authors (e.g., Molnar et al., 1990; Currie and Eberth, 1993) have suggested *Alectrosaurus* is a basally branching species, but this hypothesis was not accompanied by comparative data. Currie (2000a) enumerated several characters that typified *Alectrosaurus*, including a high maxillary and dentary tooth count, long and low skull, smooth nasals, and large front limb. Holtz (2001) concluded that *Alectrosaurus* is a member of the tyrannosaurid subclade "Aublysodontinae" based on his cladistic analysis, and he characterized the taxon as primitive. However, "*Alectrosaurus*" in both works is a composite taxon that combines data from the lectotype and the referred fossils. Loewen et al. (2013) recovered *Alectrosaurus* as a basally branching taxon outside of Tyrannosauridae based exclusively on data from the lectotype.

Craniodental Fossils from the Iren Dabasu Formation—The cranial material is important since it is the only tyrannosauroid skull material that was unambiguously collected from the Iren Dabasu Formation. The skull of tyrannosaurs from this unit is currently unknown and this specimen is the best evidence there is of its morphology and how it compares with other taxa. The only other skull material of early Tyrannosauridae-line tyrannosaurs from Asia includes the Perle (1977) material, the maxilla

and dentary of *Jinbeisaurus* (Wu et al., 2020), the complete skull of the Aptian-Albian *Xiongguanlong* (Li et al., 2009), and the partial skull of the Turonian *Timurlengia* (Brusatte et al., 2016). The Iren Dabasu specimen will help to fill in our picture of cranial evolution among Asian tyrannosaurs.

Justification and Objectives—In terms of the larger framework of tyrannosauroid evolution, comparative descriptions of the Iren Dabasu fossils will help to clarify the morphological differences between presumably basally branching tyrannosauroids and the later branching tyrannosaurids. A comparative description is also justified by the recent spate of discoveries of basally branching tyrannosauroid taxa from Asia (Wu et al., 2020) and North America (Brownstein, 2021; Nesbitt et al., 2019; Zanno et al., 2019) that are based on incomplete fossils. Although the Iren Dabasu fossils are fragmentary, their high quality of preservation permits detailed osteological descriptions to be done. A new look at the fossils will help to maximize the number of phylogenetically informative characters among the successive sister taxa of Tyrannosauridae that are based on partial specimens. Therefore, the objectives of this paper are to (1) redescribe the hind limb of the lectotype of *A. olseni* in comparison with other tyrannosauroids, (2) identify autapomorphies of *A. olseni*, and (3) describe a partial tyrannosauroid skull (AMNH FARB 6266) from the Iren Dabasu Formation to help clarify tyrannosauroid diversity in that unit. A cladistic analysis of the hindlimb and partial skull is deferred until a complete hindlimb data set for tyrannosauroids is compiled.

Materials

Most of the specimens mentioned in the text were studied first-hand (Table S1); those not studied first-hand, for which the published illustrations were consulted, were the holotypes of *Shanshanosaurus* (Currie and Dong, 2001), and one specimen of *Albertosaurus libratus* (USNM 12814; Lambe, 1917; Matthew and Brown, 1923); photographs were used to document the characters in the MgD specimens. The pedal bones of the holotype of *Alioramus altai* were excluded from this work; owing to their small size relative to the rest of the skeleton, it is not clear if the bones are from the same individual or from the same taxon.

Terminology

The anatomical and orientation terminology used in this article follows that of Baumel and Witmer (1993), where "plantar" is used in place of "ventral" for the metatarsals and phalanges. As a result, constructions such as "plantolateral" and "plantomedial" are used here. For clarity, three novel terms used in this article are defined here:

Pedicle—A pedicle is an elevation of bone that extends abruptly (like a stalk) from the dorsal or plantar surface of a diaphysis that supports a joint surface. The joint surface may extend beyond the pedicle as a ridge or crest.

Elevation—An elevation differs from a pedicle in that it extends at a low angle from the surface of a diaphysis to support a joint surface. The joint surface does not extend beyond an elevation.

Cranial Process of the Lateral Cnemial Process—This term refers to the "cranial process" of the proximal end of the tibia of Molnar et al. (1990). In the Nomina Anatomica Avium, the lateral ramus of bone that supports the joint surface for the femur is termed the "lateral cnemial process" (Baumel and Witmer, 1993); thus it is appropriate to coin a term for the subordinate projection, which is not present in all theropods.

Taxonomy

The taxonomy used here follows that of Carr and Williamson (2010), where *Albertosaurus libratus* and *A. sarcophagus* are equivalent to *Gorgosaurus* and *Albertosaurus*, respectively, of

other workers; and *Tyrannosaurus bataar* and *T. rex* are equivalent to *Tarbosaurus* and *Tyrannosaurus*, respectively, of other workers. The purpose of this approach is to maximize the information content of the taxonomy by aligning it with sister group relationships as recovered by phylogenetic analyses (Brusatte & Carr, 2016; Carr et al., 2017; Brownstein, 2021).

I consider *Shanshanosaurus* (IVPP V4878) to represent a juvenile *T. bataar*, and, following Carr et al. (2017), I consider *Alioramus altai* as a subjective junior synonym—a subadult—of *A. remotus* (Carr et al., 2017). However, the name "*A. altai*" is used wherever the holotype specimen (IGM 100/1844) is specifically discussed. When used on their own, the names *Albertosaurus*, *Daspletosaurus*, and *Tyrannosaurus* include both species of those clades.

The phylogenetic scheme and terminology of Brusatte et al. (2010) is followed here, with the following terminological conventions. As used here "derived tyrannnosauroids" refers to *Appalachiosaurus*, *Bistahieversor*, and Tyrannosauridae; "tyrannosaurines" refers to *Alioramus* and successive sister groups of *Tyrannosaurus rex*; and "derived tyrannosaurines" refers to *Teratophoneus* and successive sister groups of *T. rex*.

Raptorex—The taxon *Raptorex kriegsteini* was based on the skeleton of a small subadult tyrannosauroid that was purportedly collected from Lower Cretaceous in China (Sereno et al., 2009). Later, the validity of the taxon and its relative maturity were challenged and its geological age and provenance were revised (Fowler et al., 2011, Newbrey et al., 2013). Although the revisions to geological age and provenance are based on overwhelming evidence, the assessment of the taxonomic identity and relative maturity are not. The skull and teeth of the holotype specimen (LH PV18) were restudied by this author to assess these issues.

Fowler et al. (2011) made seven primary claims about LV PV18: (1) Closure of the internasal suture, variable neurocentral suture closure, and tooth width do not indicate a subadult level of maturity; (2) the plexiform bone histology and distance between LAGs indicate a skeletally immature animal in an exponential growth phase; (3) the chronological age of the animal at death was between 3–6 years or, assuming rapid early growth, it was between 2–3 years; (4) the skull differences between *R. kriegsteini* and juvenile *Tyrannosaurus bataar* are "minor" (2011:5); (5) the identity of the specimen is equivocal: "LH PV18 is a juvenile of a much larger tyrannosaurid species, and may indicate affinity with *Tarbosaurus*, although not necessarily being assignable to *T. bataar*" (2011:5); (6) the uncertain stratigraphy and provenance, and its juvenile growth stage make LH PV18 a problematic holotype; and (7) "*Raptorex* should be considered a *nomen dubium*" (2011:5).

In agreement with Fowler et al. (2011), this restudy of LH PV18 done for this article found that the specimen is a juvenile, but it is a valid taxon. In addition to its small size and the histological data (Fowler et al., 2011), LH PV18 possesses numerous juvenile skeletodental features that are seen across Tyrannosauridae (Carr, 1999, 2020). Although this is not an exhaustive list, the most salient juvenile features seen in LH PV18 include noninflated pneumatic facial bones, absence of enhanced facial ornaments, shallow jaws, narrow teeth, shallow skull frame, smooth joint surfaces, long contribution of the frontal to the orbital fenestra, and a long tibia relative to the femur.

Also, this restudy found several features that indicate LH PV18 does pertain to a new taxon. This observation is not unusual, as species-level diagnostic features are seen in juveniles of other tyrannosaurids, including *T. rex* (Carr, 1999, 2020; Carr and Williamson, 2004). LH PV18 differs from other tyrannosaurids (juveniles and adults) in several ways, the most obvious of these include: (1) The ventral ramus of the lacrimal is thin and subtly curved (vs. stout and distinctly curved), (2) the suborbital ligament scar is a distinct flange (vs. a subtle convexity), (3) the rostroventral ala of the lacrimal extends halfway up the ventral ramus (vs. extends up the ventral quarter of the ramus); (4) the

rostrolateral extent of the dorsotemporal fossa on the frontal is deeply concave (vs. convex in juveniles or shallowly concave in adults). Finally, the subcutaneous flange of the maxilla (Carr & Napoli et al., 2022), which is a diagnostic character of *T. bataar* that is seen in small juveniles (Currie and Dong, 2001; Tsuihiji et al., 2011), is absent from PH LV18. These discrete differences from other tyrannosaurids are clear evidence that *R. kriegsteini* is a reliably diagnosable and valid taxon. Based on this evidence, adult *R. kriegsteini* will be found to have unusually straight preorbital bars and dorsotemporal fossae with pocket-like corners, resembling the condition seen in some dromaeosaurids (Turner, Makovicky, & Norell, 2012).

Institutional Abbreviations

AMNH FARB, American Museum of Natural History Fossil Fishes, Amphibians, Reptiles, and Birds, New York, New York, U.S.A.; **ANSP**, Academy of Natural Sciences, Philadelphia, PA, U.S.A.; **BMRP**, Burpee Museum of Natural History, Rockford, IL, U.S.A.; **BYU**, Brigham Young University, Salt Lake City, UT, U.S.A.; **CM**, Carnegie Museum, Pittsburgh, PA, U.S.A.; **CMN**, Canadian Museum of Nature, Aylmer, Canada; **DDM**, Dinosaur Discovery Museum, Kenosha, WI, U.S.A.; **DMNH**, Denver Museum of Natural History, Denver, CO, U.S.A.; **FMNH PR**, Field Museum, Chicago, IL, U.S.A.; **IGM**, Institute of Geology, Mongolian Academy of Sciences, Ulan Bataar, Mongolia; **IVPP**, Institute of Paleontology and Paleoanthropology, Beijing, China; **MgD**, Institute of Paleobiology, Polish Academy of Sciences, Warsaw, Poland; **MOR**, Museum of the Rockies, Bozeman, MT, U.S.A.; **LACM**, Los Angeles County Museum, Los Angeles, CA, U.S.A.; **OMNH**, Oklahoma Museum of Natural History, Norman, OK, U.S.A.; **NMMNH**, New Mexico Museum of Natural History and Science, Albuquerque, NM, U.S.A.; **PIN**, Palaeontological Institute, Moscow, Russia; **ROM**, Royal Ontario Museum, Toronto, Canada; **RMM**, Red Mountain Museum, Birmingham, AL, U.S.A.; **TMP**, Royal Tyrrell Museum of Palaeontology, Drumheller, Canada; **USNM**, United States National Museum, Washington, DC, U.S.A.

SYSTEMATIC PALEONTOLOGY

SAURISCHIA Seeley, 1888

THEROPODA Marsh, 1881
TYRANNOSAUROIDEA Osborn, 1905
ALECTROSAURUS Gilmore, 1933

Type Species—*Alectrosaurus olseni* Gilmore, 1933.
Diagnosis—As for the type and only species.

ALECTROSAURUS OLSENI Gilmore, 1933
(Figs. 1–25)

Alectrosaurus olseni Gilmore, 1933:35:figs. 8–10 (original description).
Lectotype—AMNH FARB 6554, manual unguals, partial pelvis, and hindlimbs (Fig. 1).
Remarks—The fossils referred to this taxon from Baishin Tsav and Uzbekistan by Perle (1977), and by Nessov (1995), respectively, to *Alectrosaurus* sp. are not referable to *A. olseni*; the reasons for revising these referrals are given in the Discussion. Nessov's referral of tyrannosaurid material from Dhzarakuduk was based on its relatively small size and geological age, not shared derived characters. Perle's referral of the fossils from Baishin Tsav were based, problematically, on similarity of undisclosed hindlimb proportions (Mader and Bradley, 1989). For the present time these fossils are best regarded as Tyrannosauroidea indeterminate.

FIGURE 1. The stylopodium and zeugopodium of the right hind limb of the lectotype (AMNH FARB 6554) of *Alectrosaurus olseni*, including **A**, femur; **B**, tibia; and **C**, fibula in lateral view. Illustrations © Dino Pulerà. All rights reserved, used with permission.

0   5 cm

FIGURE 1 continued. The proximal acropodium of the right hind limb of the lectotype (AMNH FARB 6554) of *Alectrosaurus olseni*, including meta-tarsals **D**, V; **E**, VI; **F**, III; **G** II; and **H**, I in lateral view. Illustrations © Dino Pulerà. All rights reserved, used with permission.
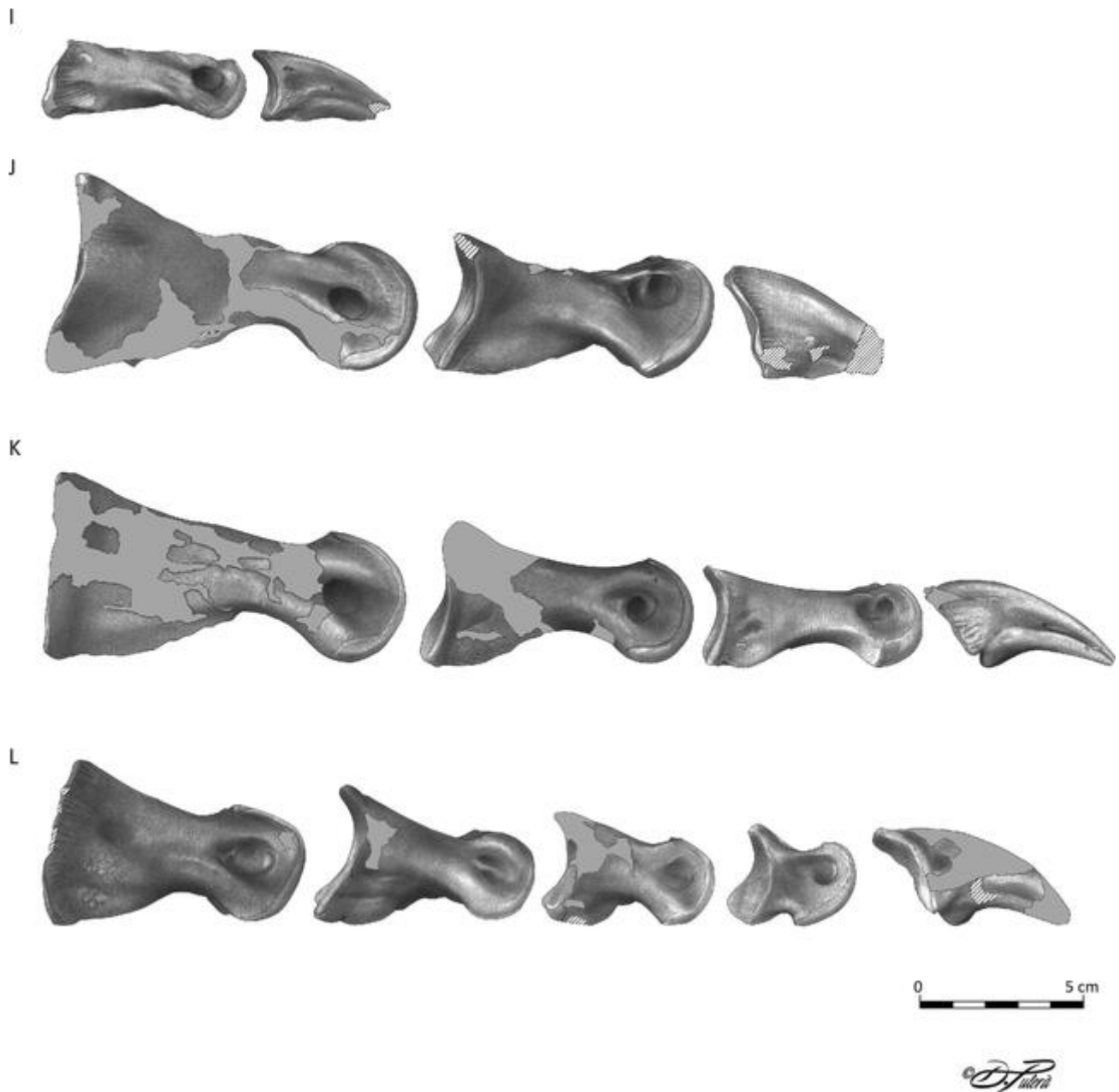
FIGURE 1 continued. The distal acropodium of the right hind limb of the lectotype (AMNH FARB 6554) of *Alectrosaurus olseni*, including digits **I**, I; **J**, II; **K**, III; and **L**, IV in lateral view. Unguals of digits III and IV are switched; i.e., the ungual with D III should be with D IV and vice versaI. Illustrations © Dino Pulerà. All rights reserved, used with permission.

Locality and Horizon—Third Asiatic Expedition field site 136, Republic of China (what is now the People's Republic of China); a field photograph (Neg. no. 108720) shows the articulated right hind limb (femur, tibia, fibula, pes) and a partial and slightly dissociated left metatarsus *in situ*; Iren Dabasu Formation.

Revised Diagnosis—In addition to the diagnostic characters identified by Mader and Bradley (1989) added here include: spike-like process extends from the caudodorsal surface of the medial condyle of the femur; oval scar on the caudal surface of the femur is lateral to the midline; abrupt expansion in length of the cranial margin of the fibula at the distal joint surface for the tibia; tendon pit adjacent to the ventrolateral buttress of the astragalus undercuts the medial surface of the buttress; expanded and, in several cases, pediculate distal joint surfaces on the metatarsals and phalanges; lateral flange of MTT I is triangular; center of the flexor groove of II-2 is convex; lateral ridge that bounds the flexor groove of III-2 is a prominent keel; rugosities absent above the collateral ligament pits of III-3; in dorsal view, wide caudal region of the shaft of III-3 is limited to the caudal third of the shaft; scar caudodorsal to the medial collateral ligament pit is low in III-3; dorsal ridge of III-4 extends medial the midline of the bone; longitudinal groove excavates the distal third of the ventral surface of IV-5.

Remarks—The most notable feature of the hind limb of *Alectrosaurus* is the dilated (expanded) distal ends of the pedal bones. In most bones (MTT II, II-2, MTT III, III-1, III-2, III-3, MTT IV, IV-1, IV-2, IV-4), the joint surfaces are pediculate. *Alectrosaurus* is the only tyrannosauroid in which pedicles are present in MTTs II and IV.

DESCRIPTION

Femur

In contrast to other tyrannosauroids, the femur of *Alectrosaurus* is autapomorphic. In medial view, a spike-like process extends from the dorsal surface of the medial condyle (Figs. 1A, 2B, C). This process is absent from *Appalachiosaurus* (RMM 6670), *Albertosaurus* (CMN 2120, CMN 11315, ROM 1247, TMP 1984.064.0001, USNM 12814; Fig. 2F; Lambe, 1917; Matthew and Brown, 1923), *Tyrannosaurus* (CM 9380, FMNH PR2081, PIN 551-2, PIN 552-2), and juvenile *T. bataar* (IVPP V4878). Both condyles are damaged in the holotype of *Alioramus altai* (IGM 100/1844). The lateral condyle of *Alectrosaurus* is damaged, so the presence of a spike there is indeterminate. Measurements of the femur are given in Table 1; polymorphic and ontogenetic characters are listed in Table S2 and Table S3, respectively.

The caudal surface of the femur in all tyrannosauroids bears an oval scar approximately at the midheight of the diaphysis. In *Alectrosaurus* the scar is lateral to the caudal midline (Fig. 2D), whereas the scar is medial to the midline in *Appalachiosaurus* (RMM 6670), *Bistahieversor* (NMMNH P-25049), *Albertosaurus* (AMNH FARB 5458, CMN 2120, CMN 11315, CMN 11593, ROM 1247, TMP 1986.144.0001; Fig. 2G), *Teratophoneus* (BYU 13719), and in *Daspletosaurus* (FMNH PR308, MOR 590). In *Tyrannosaurus* (CM 9380, FMNH PR2081, IVPP V4878, MOR 555, PIN 551-2, PIN 552-2), the scar is on the caudomedial edge of the bone, which is almost certainly a synapomorphy for this clade. Individual variation is evident in one specimen of *A. sarcophagus* (ROM 807), where the scar is on the caudomedial edge of the bone. This indicates that the position of the scar is either taxonomically uninformative or that ROM 807 (a headless skeleton) is misidentified. In the holotype of *Alioramus altai* (IGM 100/1844), the caudal surface of the shaft is damaged, preventing assessment of the condition. The work of Carrano and Hutchinson (2002) on *T. rex* shows that the medial scar marks the insertion of the M. adductor femoris 1 and the lateral scar marks the insertion of M. adductor femoris 2. If the "oval scar" is not homologous between *Alectrosaurus* and other taxa, then it is the insertion for femoral adductor 1 that is absent from *Alectrosaurus*.

In caudal view, the distal condyles in *Alectrosaurus* are narrowly separated caudally by a gap that is less than half the width of the medial condyle (Fig. 2E). In other tyrannosauroids the gap is either slightly narrower than the medial condyle, as is seen in *Dryptosaurus* (ANSP 9995), *Bistahieversor* (NMMNH P-25049), *Daspletosaurus horneri* (MOR 590), and *Tyrannosaurus* (CM 12102, FMNH PR2081, PIN 551-2, PIN 552-2), or the gap is wider than the medial condyle, as in *Albertosaurus* (CMN 11315, TMP 1984.064.0001, TMP 1986.144.0001), *Alioramus* (IGM 100/1844), *D. torosus* (FMNH PR308), *T. bataar* (IVPP V4878, MgD-I/9), and in a subadult *T. rex* (BMRP 2002.4.1). Individual variation is seen in the holotype of *T. rex* (CM 9380) where the gap is narrow, indicating that this character may turn out to be taxonomically uninformative with a greater sampling. However, it is notable that a narrow or wide gap is independent of the size of the individual.

The condyles are separated cranially by a shallow intercondylar groove in *Alectrosaurus* (Fig. 2E), which is also seen in *Dryptosaurus* (ANSP 9995), *Teratophoneus* (BYU 13719), and cf. *T. rex* (CM 12102). A deep cleft separates the condyles in *Appalachiosaurus* (RMM 6670), *Albertosaurus* (CMN 2120, CMN 11315, TMP 1991.036.0500), *Alioramus* (IGM 100/1844), *Daspletosaurus* (CMN 350, FMNH PR308, MOR 590), and *Tyrannosaurus* (BMRP 2002.4.1, CM 9380, FMNH PR2081, MgD-I/9, MgD-1/29, PIN 551-2). The groove was probably for guiding the knee extensor tendon of Mm. femorotibialis + extensor digitorum longus femoris (Carrano and Hutchinson, 2002).

TABLE 1. Measurements (in millimeters) of the right hindlimb of the lectotype (AMNH FARB 6554) of *Alectrosaurus olseni*; where two measurements appear on one line, they correspond to left and right, respectively. Symbols: ~, approximate measurement at regions of damage; +, underestimate due to missing portions of bone.

Femur	
Length fragment through lateral condyle	647
Circumference at midlength	219.3~
Midshaft width	65.4
Midshaft length	72.1
Ratio midshaft width/midshaft length	0.91
Fourth trochanter width	19.3
Oval scar depth	44.6
Oval scar width	28.8
Width across distal condyles	141.4
Medial distal condyle length	111.3
Medial distal condyle width	52.9
Lateral distal condyle length	119.6
Lateral distal condyle width	62.8
Medial distal condyle depth	89.6+
Depth through process of lateral distal condyle	67.9+
Tibia	
Proximal length	165.3
Proximal length through lateral condyle	82.3
Maximum proximal width	109.5
Total length of bone through medial proximal condyle	732
Circumference at midlength	22.3
Length at midlength	55.4
Width at midlength	69.2
Ratio of midlength length/midlength width	0.80
Depth of fibular crest	138.4
Length of fibular crest	18.1
Caudal depth of lateral proximal condyle	51.3
Cranial depth of lateral proximal condyle	43.2
Proximal width across cranial end of lateral condyle	90.8
Fibula	
Proximal length	119.0
Proximal width, cranial	31.2
Proximal width, midlength	34.8
Total length	530+
Height of oval scar	44.1
Width of oval scar	24.6
Width ventral to oval scar	24.5
Length through midheight of oval scar	34.8
Width through midheight of the oval scar	23.4
Astragalus	
Height through lateral condyle	185.6
Ventral length through lateral condyle	81.2
Depth of lateral condyle	60.0
Height of ascending process	129.4
Calcaneum	
Cranial height	63.9
Caudal height	55.2
Maximum length	66.3
Dorsal width	22.2
Cranial width	26.8
Ventral width	16.1
Metatarsal I	
Maximum depth	62.8~
Maximum length	26.5
Minimum length	20.9
Maximum distal length	24.9
Maximum distal depth	22.1
Maximum distal width	17.3
Ratio distal width:distal length	0.80
Pedal phalanx I-1	
Maximum length	61.3
Minimum height	16.1
Minimum width	16.8
Ratio minimum height:minimum width	0.96
Proximal height	23.6
Proximal width	21.5
Ratio proximal width:proximal height	0.91
Distal height	18.4

(Continued)

TABLE 1. Continued.

Distal width	18.7
Ratio distal height:distal width	0.98
Ratio minimum height:length	0.26
Ratio minimum width:length	0.27
Ratio proximal height:length	0.39
Ratio proximal width:length	0.35
Ratio distal height:length	0.30
Ratio distal width:length	0.31
Phalanx I-2	
Maximum length	43.4+
Maximum height	25.2
Maximum width	14.4
Ratio width:height	0.57
Metatarsal II	
Maximum length	460.7, 470.7
Circumference at midlength	150, 154.3
Proximal width	83.3, -
Proximal length	-, 97.7
Length at midlength	56.2, 56.0
Width at midlength	34.5, 35.1
Ratio width midlength/length midlength	0.61, 0.63
Distal length	50.3, 49.7
Distal width	52.7, 54.0
Ratio distal length/distal width	0.96, 0.92
Phalanx II-1	
Proximal height	59.3~
Proximal width	50.6
Ratio proximal width:proximal height	0.85
Distal height	38.5
Distal width	47.6
Minimum depth	25.8
Minimum width	29.2
Maximum length	114.0
Ratio width:length	0.26
Ratio minimum height:length	0.23
Ratio minimum width:length	0.26
Ratio proximal height:length	0.52
Ratio proximal width:length	0.44
Ratio distal height:length	0.34
Ratio distal width:length	0.42
Phalanx II-2	
Proximal height	39.6
Proximal width	42.8
Ratio proximal height:proximal width	0.93
Distal height	38.1
Distal width	38.1
Ratio distal height:distal width	1.0
Minimum depth	24.0
Minimum width	26.8~
Ratio minimum height:minimum width	0.90
Maximum length	88.2
Ratio width:length	0.30
Ratio minimum height:length	0.27
Ratio minimum width:length	0.30
Ratio proximal height:length	0.49
Ratio proximal width:length	0.49
Ratio distal height:length	0.43
Ratio distal width:length	0.43
Phalanx II-3	
Maximum length	35.2+
Maximum height	24.3+
Maximum width	27.6
Metatarsal III	
Maximum width of shaft	43.5, 41.4
Minimum width above distal condyle	40.9, 41.5
Ratio of minimum/maximum shaft width	0.94, 1.00
Distal length	58.3, 56.7
Distal width	60.1, 61.2
Ratio distal length/distal width	0.97, 0.93
Ratio maximum shaft width/distal width	0.72, 0.68
Phalanx III-1	
Proximal height	57.9

(*Continued*)

TABLE 1. Continued.

Proximal width	65.3
Ratio proximal height:proximal width	0.89
Distal height	39.2
Distal width	51.0
Ratio distal height:distal width	0.77
Minimum height	24.4
Minimum width	31.3
Ratio minimum height:minimum width	0.78
Maximum length	109.5
Ratio width:length	0.29
Ratio minimum height:length	0.22
Ratio minimum width:length	0.29
Ratio proximal height:length	0.53
Ratio proximal width:length	0.60
Ratio distal height:length	0.36
Ratio distal width:length	0.47
Phalanx III-2	
Proximal height	42.1~
Proximal width	50.9
Ratio proximal height:proximal width	0.83
Distal height	29.5
Distal width	41.9
Ratio distal height:distal width	0.66
Minimum height	21.1
Minimum width	26.2
Ratio minimum height:minimum width	0.81
Maximum length	83.2
Ratio width:length	0.32
Ratio minimum height:length	0.25
Ratio minimum width:length	0.32
Ratio proximal height:length	0.51
Ratio proximal width:length	0.61
Ratio distal height:length	0.36
Ratio distal width:length	0.50
Phalanx III-3	
Proximal height	30.3
Proximal width	39.3
Ratio proximal height:proximal width	0.77
Distal height	25.1
Distal width	35.6
Ratio distal height:distal width	0.71
Minimum depth	16.9
Minimum width	25.9
Ratio minimum height:minimum width	0.65
Maximum length	67.5
Ratio width:length	0.38
Ratio minimum height:length	0.25
Ratio minimum width:length	0.38
Ratio proximal height:length	0.45
Ratio proximal width:length	0.58
Ratio distal height:length	0.37
Ratio distal width:length	0.53
Phalanx III-4	
Proximal height	28.0
Proximal width	24.0
Maximum length	-
Ratio proximal width:proximal height	0.90
Metatarsal IV	
Maximum length	33.5+, 478.2
Circumference at midlength	-, 136
Length at midlength	-, 50.6
Width at midlength	-, 27.0
Ratio width midlength/length midlength	-, 0.53
Proximal width	-, 66.4
Proximal length	-, 68.3
Ratio proximal width/proximal length	-, 0.97
Distal length	50.7, 54.4
Distal width	40.3, 40.9
Ratio distal width/distal length	0.80, 0.75
Phalanx IV-1	
Proximal height	52.4
Proximal width	43.7
Ratio proximal height:proximal width	0.83
Distal height	37.2

(*Continued*)

TABLE 1. Continued.

Distal width	47.6~
Ratio distal height:distal width	0.78
Minimum height	23.5
Minimum width	31.1
Ratio minimum height:minimum width	0.76
Maximum length	79.6~
Ratio minimum height:length	0.30
Ratio minimum width:length	0.39
Ratio proximal height:length	0.66
Ratio proximal width:length	0.55
Ratio distal height:length	0.47
Ratio distal width:length	0.60
Phalanx IV-2	
Proximal height	42.4
Proximal width	43.9
Ratio proximal height:proximal width	0.97
Distal height	27.5~
Distal width	-
Ratio distal height:distal width	-
Minimum height	19.7
Minimum width	31.9~
Ratio minimum height:minimum width	0.62
Maximum length	67.0~
Ratio minimum height:length	0.29
Ratio minimum width:length	0.48
Ratio proximal height:length	0.63
Ratio proximal width:length	0.66
Ratio distal height:length	0.41
Ratio distal width:length	-
Phalanx IV-3	
Proximal height	-
Proximal width	38.9~
Ratio proximal height:proximal width	-
Distal height	-
Distal width	-
Ratio distal height:distal width	-
Minimum depth	18.7~
Minimum width	-
Ratio minimum height:minimum width	-
Maximum length	52.5
Ratio minimum height:length	0.36
Ratio minimum width:length	-
Ratio proximal height:length	-
Ratio proximal width:length	0.62
Ratio distal height:length	-
Ratio distal width:length	-
Phalanx IV-4	
Proximal height	27.2
Proximal width	31.6
Ratio proximal height:proximal width	0.86
Distal height	25.7
Distal width	30.2
Ratio distal height:distal width	0.85
Minimum height	19.0
Minimum width	27.2
Ratio minimum height:minimum width	0.70
Maximum length	38.9
Ratio width:length	0.70
Ratio minimum height:length	0.49
Ratio minimum width:length	0.70
Ratio proximal height:length	0.69
Ratio proximal width:length	0.81
Ratio distal height:length	0.66
Ratio distal width:length	0.78
Phalanx IV-5	
Maximum length	38.0
Maximum height (excluding tubercle)	25.8
Maximum width	25.0
Ratio width:height	1.0
Ratio height:length	0.64
Ratio width:length	0.69
Metatarsal V	
Maximum depth fragment	109.9+
Length joint surface at expansion	20.9
Width bone at expansion	14.1

Tibia

In proximal view, the cranial process of the lateral cnemial process is not apparent in *Alectrosaurus*, where it is only visible in lateral view (Fig. 3D, H); this condition is also seen in juvenile *T. bataar* (IVPP V4878). The process is completely absent in *Dryptosaurus* (ANSP 9995), which is presumably the plesiomorphic state for Tyrannosauroidea. The process is seen in proximal view in *Appalachiosaurus* (RMM 6670), *Bistahieversor* (NMMNH P-25049), *Albertosaurus* (AMNH FARB 5227, AMNH FARB 5255, AMNH FARB 5458, CMN 11593, ROM 1247, TMP 1984.064.001; Fig. 3I), *Daspletosaurus horneri* (MOR 590), and in *Tyrannosaurus* (BMRP 2002.4.1, CM 9380, FMNH PR2081, LACM 23845, MgD-I/88, PIN 551-2, PIN 552-2, RSM 2523.8; Maleev, 1974:fig. 61). Individual variation is present in *Albertosaurus*, where some specimens (CMN 2120, CMN 11315, ROM 807) have a process that is not evident in proximal view. Measurements of the tibia are given in Table 1; polymorphic and ontogenetic characters are listed in Table S2 and Table S3, respectively.

In proximal view, the lateral margin of the bone in *Alectrosaurus* is uniformly convex (Fig. 3H); this condition is seen in *Dryptosaurus* (ANSP 9995) and *Daspletosaurus horneri* (MOR 590). In contrast, the margin is indented in *Albertosaurus* (AMNH FARB 5227, AMNH FARB 5255, CMN 11315, CMN 11593, ROM 1247; Fig. 3I), *D. torosus* (CMN 350), and in *Tyrannosaurus* (CM 9380, FMNH PR2081, IVPP V4878, LACM 23845, MgD-I/88, PIN 551-2, PIN 552-2, RSM 2523.8; Maleev, 1974:fig. 61). Individual variation is evident in *Albertosaurus* (AMNH FARB 5458, ROM 807) where the lateral margin is not indented.

In *Tyrannosaurus* (FMNH PR2081, LACM 23845, PIN 551-2, PIN 552-2; Maleev, 1974:fig. 61) and in *A. libratus* (CMN 11593), the indentation is positioned cranial to the midlength of the lateral condyle. However, this feature is variable in *A. sarcophagus* (CMN 11315) in which the indentation is cranial or caudal to the midlength of the lateral margin. Variation is also seen in *T. bataar*, where the indentation is positioned caudal to the midlength in one adult (MgD-I/88).

The transverse width across the cranial margin of the lateral cnemial process in *Alectrosaurus* is wide (Fig. 3H), as is seen in *Appalachiosaurus* (RMM 6670), *Bistahieversor* (NMMNH P-25049), *D. horneri* (MOR 590), and in *T. rex* (BMRP 2002.4.1, FMNH PR2081, LACM 23845, RSM 2523.8). This region is narrow in *Dryptosaurus* (ANSP 9995), *Albertosaurus* (AMNH FARB 5227, AMNH FARB 5255, AMNH FARB 5458, CMN 11593, ROM 1247; Fig. 3I), and *T. bataar* (MgD-I/88, PIN 551-2, PIN 552-2; Maleev, 1974:fig. 61). Individual variation is seen in *A. sarcophagus* (ROM 807), where the cranial margin is wide.

The lateral margin of the lateral cnemial process in *Alectrosaurus* extends subtly craniomedially in proximal view (Fig. 3H); this condition is seen in *Dryptosaurus* (ANSP 9995) and *T. bataar* (PIN 551-2, PIN 552-2; Maleev, 1974:fig. 61). In contrast, the margin extends craniomedially at an abrupt angle in *Appalachiosaurus* (RMM 6670), *Bistahieversor* (NMMNH P-25049), *Albertosaurus* (AMNH FARB 5227, AMNH FARB 5255, AMNH FARB 5458, CMN 11315, CMN 11593; Fig. 3I), *Daspletosaurus horneri* (MOR 590), and in *T. rex* (FMNH PR2081, LACM 23845, RSM 2523.8). Variation is seen in one *A. sarcophagus* (ROM 807), where the margin extends subtly craniomedially.

In lateral view, the lateral cnemial process is craniocaudally short in *Alectrosaurus* (Figs. 1B, 3D), *Dryptosaurus* (ANSP 9995), *Appalachiosaurus* (RMM 6670), *Bistahieversor* (NMMNH P-25049), *Daspletosaurus horneri* (MOR 590), and subadult *T. rex* (BMRP 2002.4.1). In contrast, the process is long in *Albertosaurus* (AMNH FARB 5227, AMNH FARB 5255, CMN 11315, CMN 11593, ROM 1247; Fig. 3E) and *Tyrannosaurus* (FMNH PR2081, LACM 23845, MgD-I/88, PIN 551-2).
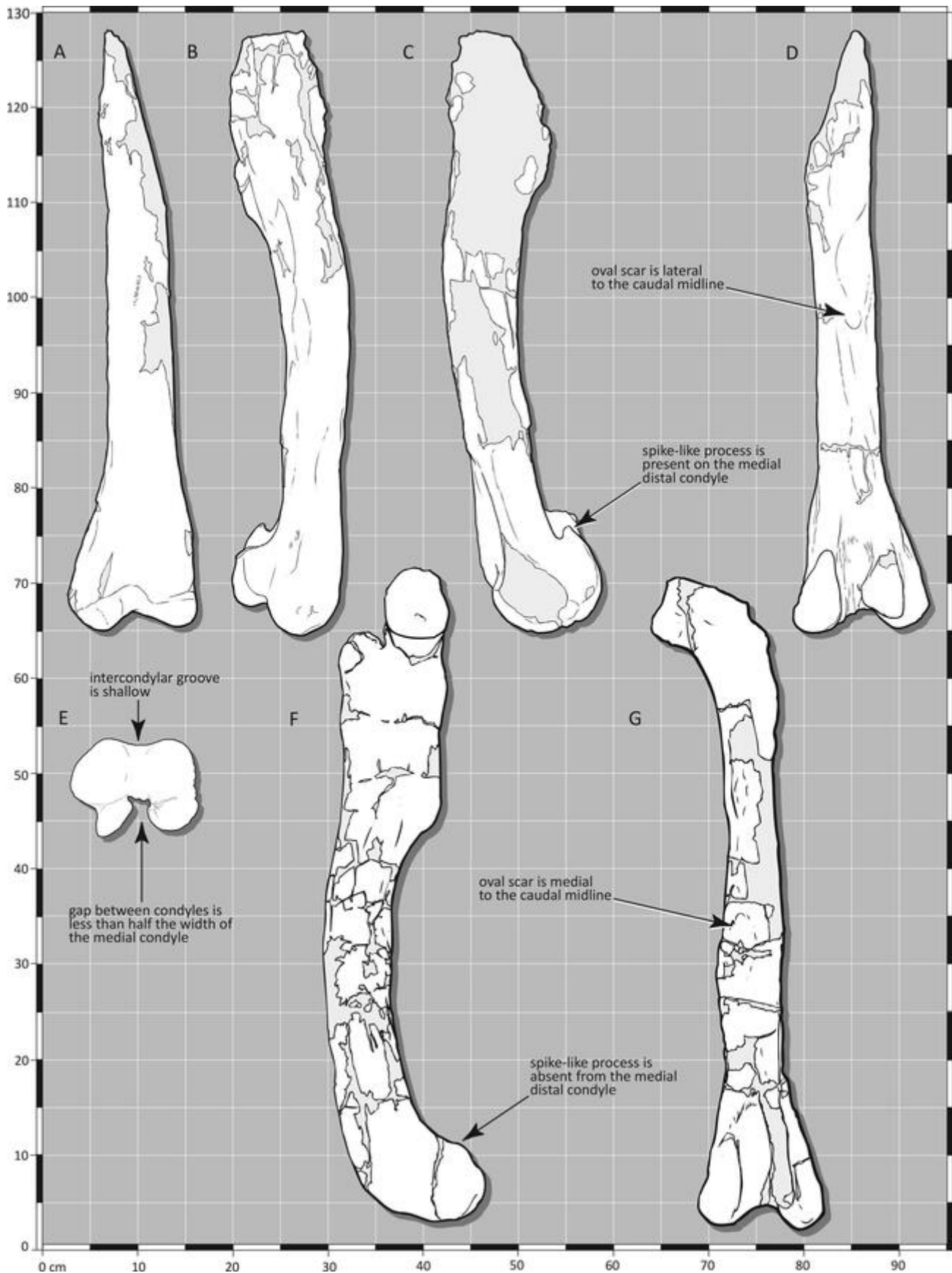
FIGURE 2. The right femur of the lectotype (AMNH FARB 6554) of *Alectrosaurus olseni* in **A**, cranial; **B**, lateral; **C**, medial; **D**, caudal; and **E**, distal views. The left (reversed) femur of *Albertosaurus sarcophagus* (CMN 11315) in **F**, medial; and **G**, caudal views for comparison.
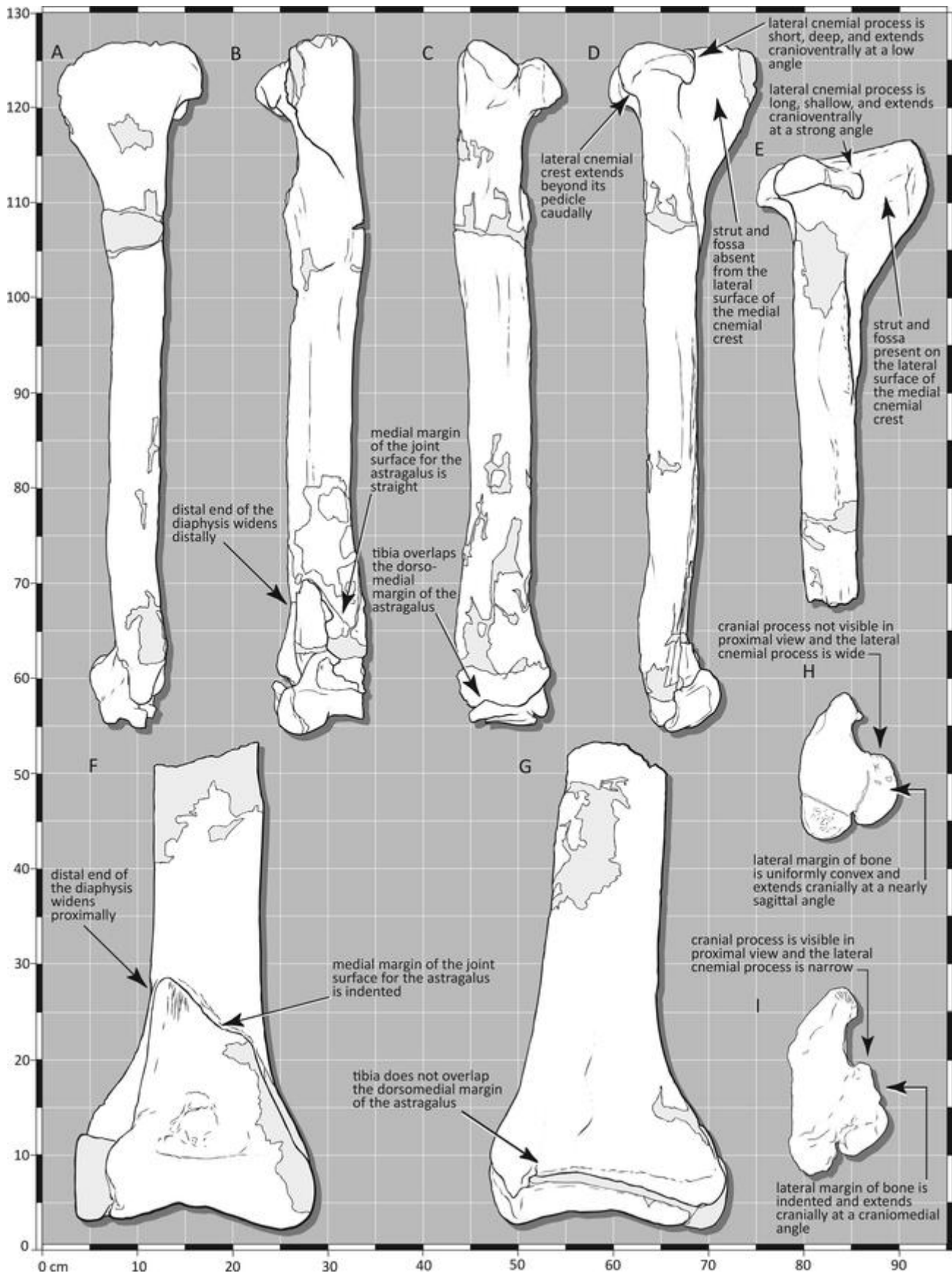
FIGURE 3. The right tibia of the lectotype (AMNH FARB 6554) of *Alectrosaurus olseni* in **A**, medial; **B**, cranial; **C**, caudal; **D**, lateral; and **H**, proximal views. Comparative illustrations of *Albertosaurus sarcophagus* in **E**, lateral (AMNH FARB 5255); **F**, cranial (AMNH FARB 5227); and **G**, caudal (AMNH FARB 5227) views; **I**, proximal (AMNH FARB 5255).

There is variation in *A. libratus*, where the process is short in large adults (AMNH FARB 5458, CMN 2120).

In *Alectrosaurus*, the lateral cnemial process is dorsoventrally deep (Figs. 1B, 3D); this condition is seen in *Appalachiosaurus* (RMM 6670). In contrast, the process is shallow in *Albertosaurus* (AMNH FARB 5227, AMNH FARB 5255, AMNH FARB 5458, CMN 11315, CMN 11593; Fig. 3E), *D. horneri* (MOR 590), and in *Tyrannosaurus* (BMRP 2002.4.1, FMNH PR2081 associated subadult, FMNH PR2081, LACM 23845, MgD-I/88, PIN 551-2).

The joint surface for the fibula is on the lateral surface of the lateral cnemial process in *Alectrosaurus* (Fig. 1B); this condition is also seen in *Dryptosaurus* (ANSP 9995), *Albertosaurus libratus* (CMN 11593), and in *Tyrannosaurus* (FMNH PR2081, PIN 551-2). In contrast, the joint surface is on the ventrolateral surface of the process in *A. sarcophagus* (AMNH FARB 5227), *Daspletosaurus horneri* (MOR 590), and subadult *T. rex* (BMRP 2002.4.1). Both conditions are seen in one specimen of *A. sarcophagus* (CMN 11315).

In lateral view, the dorsal margin of the lateral cnemial process extends cranioventrally at a low angle in *Alectrosaurus* (Figs. 1B, 3D); this condition is also seen in *Bistahieversor* (NMMNH P-25049), *Appalachiosaurus* (RMM 6670), *Dryptosaurus* (ANSP 9995), *Daspletosaurus horneri* (MOR 590), and in *Tyrannosaurus* (FMNH PR2081, LACM 23845, MgD-I/88, PIN 551-2). In contrast, the margin extends steeply cranioventrally in *Albertosaurus* (AMNH FARB 5227, AMNH FARB 5255, AMNH FARB 5458, CMN 11315, CMN 11593, ROM 1247; Fig. 3E) and in subadult *T. rex* (BMRP 2002.4.1).

The lateral cnemial process extends caudal to its pedicle in *Alectrosaurus* (Figs. 1B, 3D); this condition is also seen in *Albertosaurus* (AMNH FARB 5227, AMNH FARB 5255, AMNH FARB 5458, CMN 11315, CMN 11593, ROM 1247; Fig. 3E), *D. horneri* (MOR 590), and *Tyrannosaurus* (BMRP 2002.4.1, FMNH PR2081 associated subadult, FMNH PR2081, LACM 23845, MgD-I/88). In contrast, the process does not extend beyond the pedicle in *Dryptosaurus* (ANSP 9995) or *Appalachiosaurus* (RMM 6670), possibly indicating the plesiomorphic condition relative to Tyrannosauridae.

In *Alectrosaurus*, the lateral surface of the medial cnemial crest is not crossed by a strut and fossa (Figs. 1B, 3D); this condition is also seen in *Dryptosaurus* (ANSP 9995). In contrast, the strut and fossa are seen in *Albertosaurus* (AMNH FARB 5227, AMNH FARB 5255, AMNH FARB 5458, CMN 2120, CMN 11315, CMN 11593, ROM 1247, TMP 1984.064.0001; Fig. 3E), *Bistahieversor* (NMMNH P-25049), *Daspletosaurus* (CMN 350, MOR 590), and in *Tyrannosaurus* (BMRP 2002.4.1, CM 9380, FMNH PR2081 associated subadult, FMNH PR2081, MgD-I/88, PIN 551-2). These structures may be osteological correlates of M. extensor digitorum longus tibialis (Carrano and Hutchinson, 2002).

In cranial view, the medial margin of the joint surface for the astragalus in *Alectrosaurus* extends at a steep angle dorsolaterally (Fig. 3B). This condition is also seen in *Alioramus* (IGM 100/1844) and subadult *T. rex* (BMRP 20024.1). In contrast, the margin is steep distally before abruptly extending dorsolaterally at a low angle in *Appalachiosaurus* (RMM 6670), *Bistahieversor* (NMMNH P-25049, OMNH 10131), *Albertosaurus* (AMNH FARB 5458, CMN 2120, CMN 11315, CMN 11593, ROM 1247, TMP 1984.064.0001; Fig. 3F), *Daspletosaurus torosus* (CMN 350), and in *Tyrannosaurus* (CM 9380, DMNH 2827, FMNH PR2081, MOR 555, PIN 551-2).

In cranial view, in *Alectrosaurus* the shaft widens distally (below the dorsal tip of the ascending process of the astragalus) (Fig. 3B); this condition is also seen in *Tyrannosaurus bataar* (PIN 551-2) and subadult *T. rex* (BMRP 2002.4.1). In contrast, the shaft widens proximally (at approximately the same level as the tip of the astragalus) in *Appalachiosaurus* (RMM 6670), *Bistahieversor* (NMMNH P-25049, OMNH 10131), *Albertosaurus libratus* (CMN 11593), *Daspletosaurus torosus* (CMN 350), *T. rex*

(FMNH PR2081), and possibly also in *A. sarcophagus* (AMNH FARB 5227, AMNH FARB 5255, CMN 11315; Fig. 3F). Variation is seen in *A. sarcophagus* (TMP 1984.064.001) and *T. rex* (DMNH 2827), in which the tibia widens distally.

In caudal view, the tibia overlaps the dorsomedial margin of the astragalus in *Alectrosaurus* (Fig. 3C); this condition is also seen in *Dryptosaurus* (ANSP 9995), *Appalachiosaurus* (RMM 6670), *Bistahieversor* (NMMNH P-25049), and in one specimen of *T. rex* (DMNH 2827). In contrast, the tibia does not overlap the astragalus in *A. libratus* (CMN 11593, ROM 1247), two specimens of *A. sarcophagus* (AMNH FARB 5227, CMN 11315; Fig. 3G), *Alioramus* (IGM 100/1844), *T. bataar* (PIN 551-2), and subadult *T. rex* (BMRP 2002.4.1). Variation is present in *Albertosaurus sarcophagus* (AMNH FARB 5218) and in *T. rex* (FMNH PR2081), in which the astragalus is overlapped by the tibia.

Fibula

In proximal view, the caudal end of the medial margin of the fibula in *Alectrosaurus* is concave (Fig. 4A). This condition is also seen in subadult *Tyrannosaurus* (FMNH PR2081 associated subadult, PIN 552-2; Maleev, 1974:fig. 61). In contrast, the margin is straight or convex in *Appalachiosaurus* (RMM 6670), *Bistahieversor* (NMMNH P-25049), *Albertosaurus* (AMNH FARB 5227, AMNH FARB 5255, CMN 11315, TMP 1981.010.0001, TMP 1986.144.0001), *Daspletosaurus* (CMN 350, MOR 590), and *T. rex* (BMRP 2002.4.1, DMNH 2827, FMNH PR2081, LACM 23845; Fig. 4B). Variation is seen in *A. sarcophagus* (TMP 1984.064.0001), where the margin is concave. Measurements of the fibula are given in Table 1; polymorphic and ontogenetic characters are listed in Table S2 and Table S3, respectively.

The medial margin of the proximal end of the bone is concave at midlength in *Alectrosaurus*, when viewed from above (Fig. 4A); this condition is also seen in *Bistahieversor* (NMMNH P-25049). In contrast, the concavity is ahead of the midlength in *Albertosaurus* (AMNH FARB 5255, TMP 1986.144.0001), *D. torosus* (CMN 350), and in *Tyrannosaurus* (BMRP 2002.4.1, LACM 23845, PIN 551-2; Fig. 4B). Variation is seen in one specimen of *T. bataar* (MgD-I/88), where the concavity is at midlength.

In proximal view, the caudal end of the fibula in *Alectrosaurus* is pointed (Fig. 4A); this condition is also seen in *Tyrannosaurus* (DMNH 2827, MgD-I/88, PIN 551-2). In contrast, the caudal end is blunt in *Appalachiosaurus* (RMM 6670), *Bistahieversor* (NMMNH P-25049), and in *Albertosaurus* (AMNH FARB 5255, TMP 1986.144.0001). Variation is seen in *A. sarcophagus* where the caudal end is also pointed (CMN 11315, TMP 1984.064.0001).

In cranial view, the surface proximal to the bipartite scar (sensu Mader and Bradley, 1989), presumably for the insertion of M. iliofibularis (Carrano and Hutchinson, 2002), in *Alectrosaurus* is wide and convex (Fig. 4C). This condition is also seen in *Appalachiosaurus* (RMM 6670), *Albertosaurus* (ROM 1247, CMN 11315), and in *Tyrannosaurus* (DMNH 2827, FMNH PR2081 juvenile, MgD-I/88). In contrast, this surface is narrow in *Bistahieversor* (NMMNH P-25049) and *D. torosus* (CMN 350). Variation is seen in *Albertosaurus* (AMNH FARB 5227, AMNH FARB 5255, CMN 2120, CMN 11593, TMP 1981.010.0001, TMP 1984.064.0001) and *Tyrannosaurus* (BMRP 2002.4.1, FMNH PR2081, LACM 23845, PIN 551-2, RSM 2523.8; Fig. 4D), where the surface is narrow; this indicates the character is probably taxonomically uninformative. Ontogenetic variation is present in *D. horneri*, where the surface is wide and convex in subadults (MOR 590) whereas it is wide and flat in adults (MOR 1130).

In *Alectrosaurus* the cranial surface of the fibula that is distal to the bipartite scar is wide and flat (Fig. 4B), as is seen in *Appalachiosaurus* (RMM 6670), *Albertosaurus* (CMN 2120, CMN 11593, ROM 1247, TMP 1981.010.0001), and *D. torosus* (CMN 350). In contrast, this surface is narrow in *Bistahieversor* (NMMNH P-25049), some *A. libratus* (AMNH FARB 5458),
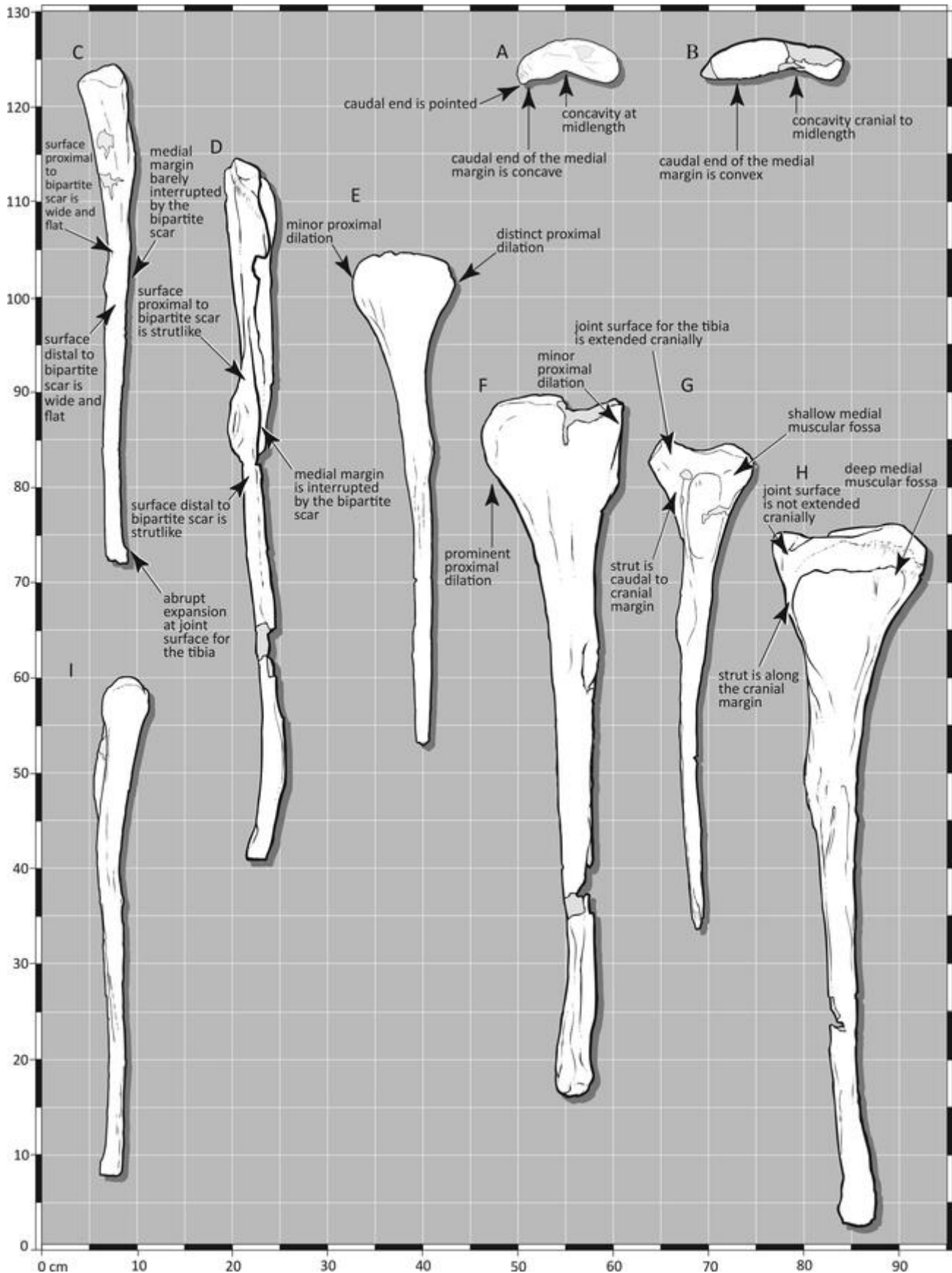
FIGURE 4. The fibula of the lectotype (AMNH FARB 6554) of *Alectrosaurus olseni* in **A**, proximal; **C**, cranial; **E**, lateral; **G**, medial; and **I**, caudal views. Comparative illustrations of *Tyrannosaurus rex* (LACM 23845) in **B**, proximal; **D**, cranial; **F**, lateral; and **H**, medial views.

A. sarcophagus (AMNH FARB 5227, CMN 11315, TMP 1984.064.0001), and in *Tyrannosaurus bataar* (MgD-I/88, PIN 551-2). Individual variation is seen in *T. rex*, where the surface is wide and flat (BMRP 2002.4.1, DMNH 2827) or narrow (LACM 23845; Fig. 4D). Ontogenetic variation is present in *D. horneri*, where the surface is wide and convex in subadults (MOR 590) whereas it is wide and flat in adults (MOR 1130).

The bipartite scar in *Alectrosaurus* barely interrupts the medial margin of the bone (Fig. 4B); this condition is also seen in *Bistahieversor* (NMMNH P-25049), *Albertosaurus* (CMN 2120, TMP 1986.144.001), *D. torosus* (CMN 350), and in *Tyrannosaurus bataar* (MgD-I/88, PIN 551-2, PIN 552-2; Maleev, 1974:fig. 71). In contrast, the scar strongly interrupts the medial margin of the bone in *Appalachiosaurus* (RMM 6670) and *Albertosaurus* (AMNH FARB 5227, AMNH FARB 5255, CMN 11315, CMN 11593, ROM 1247, TMP 1981.010.0001, TMP 1984.064.0001). Possible ontogenetic variation is present in *T. rex* where the margin is strongly interrupted in subadults (BMRP 2002.4.1, LACM 23845; Fig. 4D), whereas it is barely interrupted by the scar in adults (DMNH 2827, FMNH PR2081). In *D. horneri* the scar subtly interrupts the margin in subadults (MOR 590) whereas it distinctly interrupts the shaft in adults (MOR 1130).

In lateral view, the dorsal margin of the fibula in *Alectrosaurus* is horizontal (Figs. 1C, 4E), as is also seen in *Dryptosaurus* (ANSP 9995), *Appalachiosaurus* (RMM 6670), and subadult *T. rex* (BMRP 2002.4.1). In contrast, the cranial end of the dorsal margin is upturned (i.e., extends dorsally) in *Bistahieversor* (NMMNH P-25049), *Albertosaurus* (AMNH FARB 5227, AMNH FARB 5664, CMN 11315, CMN 11593, TMP 1981.010.0001), *Daspletosaurus horneri* (MOR 590, MOR 1130), and in *Tyrannosaurus* (FMNH PR2081, MgD-I/29, MgD-I/88, PIN 551-2, PIN 552-2).

In lateral view, the cranial margin of the shaft in *Alectrosaurus* dilates (widens) proximally toward the joint surface for the femur (Figs. 1C, 4E), this condition is also seen in *Dryptosaurus* (ANSP 9995), *Appalachiosaurus* (RMM 6670), *Albertosaurus* (AMNH FARB 5458, CMN 11593, CMN 2120, ROM 1247, TMP 1981.010.0001), and *Daspletosaurus horneri* (MOR 590, MOR 1130). In contrast, a minor dilation is seen in some *Albertosaurus* (AMNH FARB 5255, TMP 1986.144.0001), *D. torosus* (CMN 350), and *Tyrannosaurus* (BMRP 2002.4.01, FMNH PR2081, LACM 23845, MgD-I/29, MgD-I/88, PIN 551-2, PIN 552-2; Fig. 4F). A proximal dilation is absent in *Bistahieversor* (NMMNH P-25049). Individual variation is seen in *Albertosaurus*, where the dilation is absent from some specimens (AMNH FARB 5664, ROM 807; Parks, 1928).

In *Alectrosaurus*, only a minor proximal dilation is present in the caudal margin of the shaft (Figs. 1C, 4E), as is seen in *Bistahieversor* (NMMNH P-25049). In contrast, a prominent dilation is seen in *Appalachiosaurus* (RMM 6670), *Albertosaurus libratus* (AMNH FARB 5664, CMN 2120, CMN 11593, ROM 1247, TMP 1986.144.0001), *Daspletosaurus* (CMN 350, MOR 590, MOR 1130), and *Tyrannosaurus* (BMRP 2002.4.1, DMNH 2827, FMNH PR2081 associated subadult, FMNH PR2081, LACM 23845, MgD-I/29, MgD-I/88, PIN 551-2, PIN 552-2; Fig. 4F). Individual variation is seen in *A. sarcophagus*, where the margin has a minor dilation (AMNH FARB 5255) or a prominent dilation (AMNH FARB 5227, CMN 11315, ROM 807, TMP 1981.010.0001, TMP 1984.064.001; Parks, 1928).

In medial view, the fossa that extends caudally from the medial fossa in *Alectrosaurus* is shallow (Fig. 4G); this condition is also seen in one *Albertosaurus sarcophagus* (TMP 1981.010.001), *D. horneri* (MOR 590, MOR 1130), and in juvenile (DDM 2355.15) and subadult (BMRP 2002.4.1) *T. rex*. In contrast, the fossa is deep in *Dryptosaurus* (ANSP 9995), *Appalachiosaurus* (RMM 6670), *Bistahieversor* (NMMNH P-25049), *Albertosaurus* (AMNH FARB 5218, AMNH FARB 5227, AMNH FARB 5255,

CMN 2120, CMN 11315, CMN 11593, TMP 1986.144.0001), *Daspletosaurus torosus* (CMN 350), and in *Tyrannosaurus* (DMNH 2827, FMNH PR2081 associated subadult, FMNH PR2081, LACM 23845, PIN 551-2; Fig. 4H). The joint surface for the tibia above the medial pocket in *Alectrosaurus* is dorsoventrally deep, as is seen in most tyrannosauroids (Fig. 4G, H), except for two specimens of *Albertosaurus sarcophagus* (AMNH FARB 5227, CMN 11315), where it is shallow.

In medial view, a prominent strut bounds cranially the medial fossa in tyrannosauroids. In *Alectrosaurus* the proximal end of the strut is situated caudal to the cranial margin of the bone (Fig. 4G), as is seen in *Appalachiosaurus* (RMM 6670) and subadult *T. rex* (BMRP 2002.4.1). In contrast, the entire strut is situated along the cranial margin of the bone in *Dryptosaurus* (ANSP 9995), *Bistahieversor* (NMMNH P-25049), *Albertosaurus libratus* (CMN 11593, ROM 1247, TMP 1986.144.0001), *Daspletosaurus* (CMN 350, MOR 590, MOR 1130), and in *Tyrannosaurus* (DMNH 2827, FMNH PR2081 associated subadult, FMNH PR2081, LACM 23845, MgD-I/29, MgD-I/88, PIN 551-2; Fig. 4H). Variation is seen in *A. sarcophagus* where the strut is caudal to the anterior margin (AMNH FARB 5227, AMNH FARB 5255, CMN 11315) or it extends along the cranial margin (CMN 11315, TMP 1981.010.0001).

In *Alectrosaurus*, there is an abrupt expansion in the length of the cranial margin of the distal joint surface for the tibia, when seen in lateral or medial view (Fig. 4C). In contrast, this dilation is absent from *Appalachiosaurus* (RMM 6670), *Bistahieversor* (NMMNH P-25049), *Albertosaurus* (AMNH FARB 5432, AMNH FARB 5458, CMN 2120, CMN 11593, ROM 1247, TMP 1984.064.0001), *Daspletosaurus* (CMN 350, MOR 590, MOR 1130), and *Tyrannosaurus* (BMRP 2002.4.1, FMNH PR2081, LACM 23845, PIN 551-2; Fig. 4D, H).

Astragalus

In cranial view, the ventrolateral buttress for the fibula in *Alectrosaurus* is deeply undercut by the joint surface for the fibula distally such that the astragalus overlaps the fibula distally (Fig. 5A, C, G); this condition is also seen in *Appalachiosaurus* (RMM 6670) (Fig. 5B, D, H). In contrast, the joint surface is not undercut in *Dryptosaurus* (ANSP 9995), *Bistahieversor* (NMMNH P-25049), *Albertosaurus* (CMN 11315, CMN 11593, ROM 1247), or in *Tyrannosaurus* (BMRP 2002.4.1, DDM 2355.18, DMNH 2827, FMNH PR2081, LACM 23845, PIN 551-2). A laterally facing abutting surface is seen distally (ventrally) in *Daspletosaurus torosus* (CMN 350), but it cannot be considered undercut. Measurements of the astragalus are given in Table 1; polymorphic and ontogenetic characters are listed in Table S2 and Table S3, respectively.

The tendon pit adjacent to the buttress in *Alectrosaurus* undercuts the medial surface of the strut (Fig. 5A, G). In contrast, the pit does not undercut the strut in *Dryptosaurus* (ANSP 9995), *Appalachiosaurus* (RMM 6670) (Fig. 5B, H), *Bistahieversor* (NMMNH P-25049), *Albertosaurus sarcophagus* (CMN 11315), *Alioramus* (IGM 100/1844), *Daspletosaurus torosus* (CMN 350), or in *Tyrannosaurus* (BMRP 2002.4.1, DDM 2355.18, DMNH 2827, FMNH PR2081, LACM 23845, PIN 551-2). A slight undercut is seen in two adult *Albertosaurus libratus* (AMNH FARB 5458, CMN 11593).

The joint surface for the fibula marginally overlaps the astragalus (Fig. 5A); this condition is also seen in *Dryptosaurus* (ANSP 9995) and subadult *T. rex* (BMRP 2002.4.1). In contrast, the overlap is wide in *Appalachiosaurus* (RMM 6670) (Fig. 5B), *Bistahieversor* (NMMNH P-25049), *Albertosaurus libratus* (CMN 11593), and *Tyrannosaurus* (FMNH PR2081, PIN 551-2). Although its full width cannot be seen, this joint surface in *Daspletosaurus torosus* (CMN 350) is deeply excavated and a prominent vertical ridge bounds its medial edge.
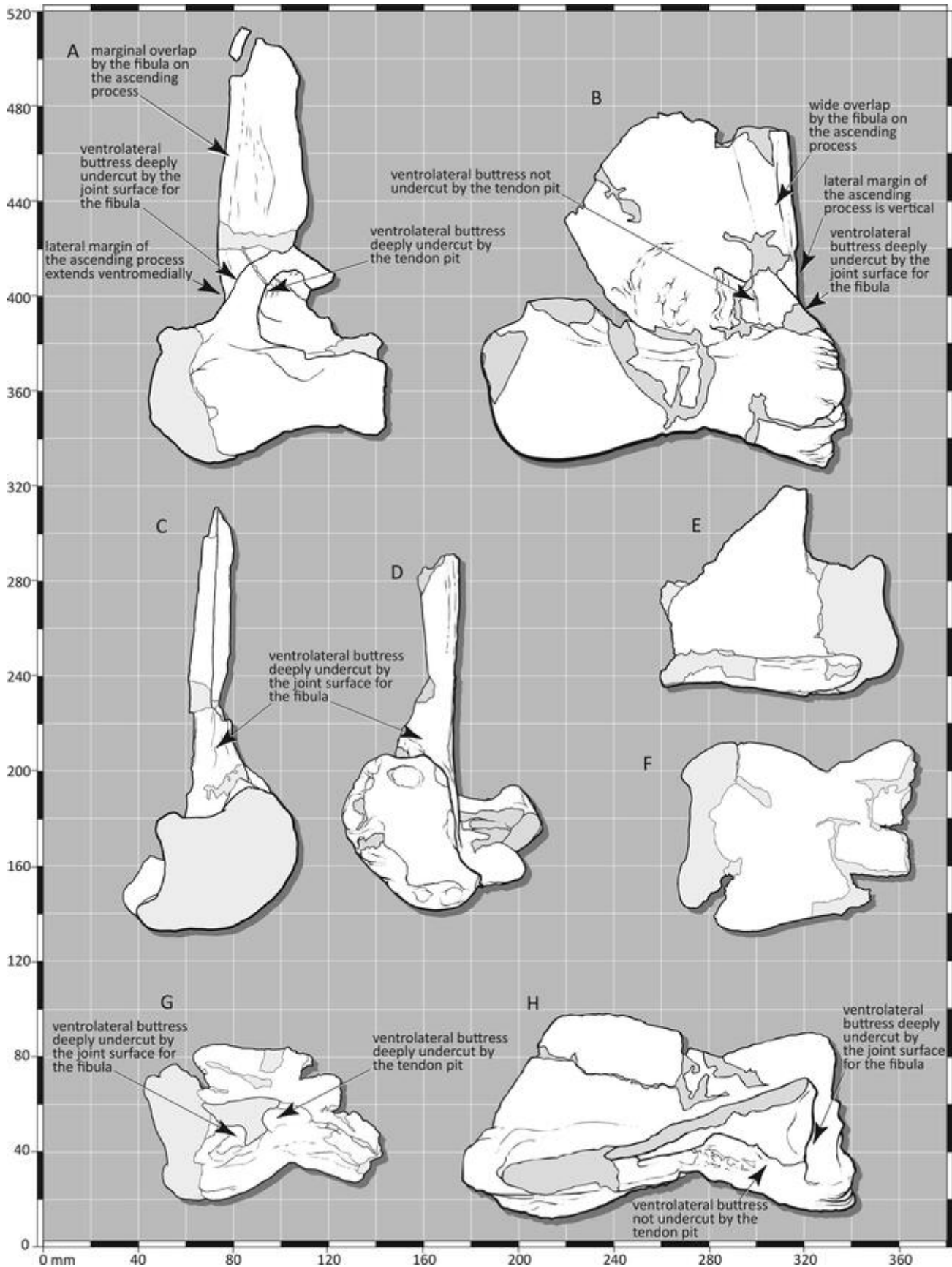
FIGURE 5. The astragalus of the lectotype (AMNH FARB 6554) of *Alectrosaurus olseni* in **A**, cranial; **C**, lateral; **E**, caudal; **F**, ventral; and **G**, dorsal views. Comparative illustrations of *Appalachiosaurus montgomeriensis* (RMM 6670) in **B**, cranial; **D**, lateral; and **H**, dorsal views. The *A. montgomeriensis* illustrations are modified after Carr, Williamson, and Schwimmer (2005).

The lateral margin of the ascending process extends ventromedially to the body of the bone in *Alectrosaurus* (Fig. 5A). This condition is also seen in *Albertosaurus libratus* (CMN 11593) and *T. rex* (BMRP 2002.4.1, FMNH PR2081). In contrast, the lateral margin is vertical in *Appalachiosaurus* (RMM 6670) (Fig. 5B); and the lateral margin extends ventrolaterally to the body of the bone in *Dryptosaurus* (ANSP 9995) and *Bistahieversor* (NMMNH P-25049). Individual variation is seen in *T. rex*, where the margin is vertical (FMNH PR2081) or extends ventrolaterally (DMNH 2827, LACM 23845) to the body of the bone.

The ascending process in *Alectrosaurus* does not extend proximal to the distal joint surface for the fibula on the tibia; this condition is also seen in *Alioramus* (IGM 100/1844) and *Tyrannosaurus* (FMNH PR2081, PIN 551-2). In contrast, the ascending process extends proximal to the joint surface in *Appalachiosaurus* (RMM 6670), *Albertosaurus libratus* (AMNH FARB 5458, CMN 11593), and subadult *T. rex* (BMRP 2002.4.1).

Calcaneum

In cranial view, the calcaneum in *Alectrosaurus* is narrow (w/h: 0.42; Fig. 6A, H); this condition is also seen in *Bistahieversor* (NMMNH P-25049), *Albertosaurus* (AMNH FARB 5458; CMN 2120, 0.37; CMN 11315, 0.41; ROM 1247, 0.42), *Daspletosaurus* (CMN 350, 0.40; MOR 1130, 0.29), and in *Tyrannosaurus bataar* (PIN 551-2, 0.44). In contrast, the bone is wide in *Appalachiosaurus* (RMM 6670, 0.53; Fig. 6B, I) and subadult *T. rex* (BMRP 2002.4.1, 0.66). Measurements of the calcaneum are given in Table 1; ontogenetic characters are listed in Table S3.

In lateral view, the medial half of the joint surface for the fibula in *Alectrosaurus* is not visible (Fig. 6E); this condition is also seen in *Albertosaurus sarcophagus* (CMN 11315), *D. horneri* (MOR 1130), and *Tyrannosaurus* (FMNH PR2081, PIN 551-2). In contrast, the medial half of the joint surface is exposed to view in *Appalachiosaurus* (RMM 6670) (Fig. 6F). The surface is marginally in view in subadult *T. rex* (BMRP 2002.4.1).

In lateral view, a prominent caudoventral 'heel' in *Alectrosaurus* is present (Fig. 6E); this condition is also seen in *Appalachiosaurus* (RMM 6670) (Fig. 6F) and *D. horneri* (MOR 1130). In contrast, this process is short in *Albertosaurus libratus* (CMN 2120) and *Tyrannosaurus rex* (BMRP 2002.4.1, FMNH PR2081); and the heel is absent from *A. sarcophagus* (CMN 11315) and *T. bataar* (PIN 551-2).

In *Alectrosaurus* the joint surface of the crurotarsal joint does not extend onto the caudoventral surface of the calcaneum. In contrast, the joint surface extends onto the caudoventral surface of the calcaneum in *Albertosaurus sarcophagus* (CMN 11315), *D. horneri* (MOR 1130), and *Tyrannosaurus* (BMRP 2002.4.1, PIN 551-2).

In ventral view, the caudal half of the bone is narrow in *Alectrosaurus* (Fig. 6H); this condition is also seen in *Albertosaurus libratus* (CMN 2120, ROM 1247), *Daspletosaurus* (CMN 350, MOR 1130), and *Tyrannosaurus* (BMRP 2002.4.1, FMNH PR2081, PIN 551-2). In contrast, the caudal half is wide in *Appalachiosaurus* (RMM 6670) (Fig. 6I) and *Albertosaurus sarcophagus* (CMN 11315).

A pyramid-shaped spur at the caudolateral edge of the joint surface for the fibula is seen in *Alectrosaurus* (Fig. 6C, E, G); this condition is also seen in *D. horneri* (MOR 1130), and *Tyrannosaurus* (FMNH PR2081, PIN 551-2). In contrast, the spur is absent from *Appalachiosaurus* and *Albertosaurus sarcophagus* (CMN 11315).

Metatarsal I

In distal view, the cranial margin of the joint surface in *Alectrosaurus* is blunt (Fig. 7F); this condition is also seen in *Albertosaurus* (AMNH FARB 5218, AMNH FARB 5255, AMNH

FARB 5458, AMNH FARB 5664, CMN 11593, ROM 1247, TMP 1981.010.0001, TMP 1986.144.0001), and *Daspletosaurus torosus* (CMN 350). In contrast, the margin is protuberant and narrow in *Bistahieversor* (NMMNH P-25049), *Alioramus* (IGM 100/1844), and subadult *Tyrannosaurus* (BMRP 2002.4.1, MgD-I/206). A unique condition is seen in one specimen of *Albertosaurus libratus* (CMN 11593), where the cranial extent of the joint surface is divided by a groove into a trochlea. Measurements of MTT I are given in Table 1; polymorphic and ontogenetic characters are listed in Table S2 and Table S3, respectively.

In medial view, the collateral ligament pit in *Alectrosaurus* is shallow (Fig. 7G). This condition is also seen in *Alioramus* (IGM 100/1844), *Daspletosaurus torosus* (CMN 350), and subadult *T. rex* (BMRP 2002.4.1). In contrast, the pit is deep in *Bistahieversor* (NMMNH P-25049) and *T. bataar* (MgD-I/206, PIN 551-2). The pit is absent from *Albertosaurus libratus* (CMN 11593, ROM 1247; Fig. 7H). This character may have limited taxonomic use, as variation is seen in *A. sarcophagus*, where the pit is shallow (AMNH FARB 5255, TMP 1981.010.0001) or absent (AMNH FARB 5218).

In medial view, the collateral ligament pit in *Alectrosaurus* lies in a deep groove (Fig. 7G). In contrast, the pit lies in a shallow groove in *Albertosaurus* (AMNH FARB 5458, AMNH FARB 5664, CMN 11593, ROM 1247, TMP 1981.010.0001; Fig. 7H). In *Alioramus* (IGM 100/1844) and subadult *T. rex* (BMRP 2002.4.1), the groove is vanishingly shallow.

In dorsal (extensor) view, the base of the lateral flange is triangular and lightly rugose (Fig. 7A). In contrast, a rugose tubercle is seen in this region in *Bistahieversor* (NMMNH P-25049), *Albertosaurus* (AMNH FARB 5218, AMNH FARB 5255, AMNH FARB 5458, AMNH FARB 5664, CMN 11593, ROM 1247, TMP 1981.010.0001, TMP 1986.144.0001; Fig. 7B), *Alioramus* (IGM 100/1844), and *T. rex* (BMRP 2002.4.1).

In *Alectrosaurus*, a ridge lies parallel and caudal to the proximal margin of the condyle (Figs. 1D, 7A, D). In contrast, the ridge is absent from *Bistahieversor* (NMMNH P-25049), *Alioramus* (IGM 100/1844), *Daspletosaurus torosus* (CMN 350), and *Tyrannosaurus* (BMRP 2002.4.1, PIN 551-2). Individual variation is seen in *Albertosaurus*, where the ridge is present (AMNH FARB 5218, CMN 11593) or absent (AMNH FARB 5255, AMNH FARB 5458, AMNH FARB 5664, ROM 1247, TMP 1981.010.0001, TMP 1986.144.0001; Fig. 7B).

The dorsal surface of the shaft in *Alectrosaurus* is almost flat (Fig. 7A). In contrast, the surface slopes plantomedially and it is convex in cross section in *Bistahieversor* (NMMNH P-25049), *Albertosaurus* (AMNH FARB 5218, AMNH FARB 5255, AMNH FARB 5664, CMN 11593, ROM 1247, 1981.010.0001, TMP 1986.144.0001; Fig. 7B), and *Tyrannosaurus* (BMRP 2002.4.1, MgD-I/206). In *Alioramus* (IGM 100/1844) the surface is flat, but it slopes plantomedially.

The apex of the dorsal margin of the distal joint surface in *Alectrosaurus* is situated medial to the midline of the bone (Fig. 7A). In contrast, the apex is at the lateral edge of the condyle in *Bistahieversor* (NMMNH P-25049), *Albertosaurus* (AMNH FARB 5218, AMNH FARB 5255, AMNH FARB 5458, AMNH FARB 5664, CMN 11593, ROM 1247, 1981.010.0001, TMP 1986.144.0001; Fig. 7B), *Alioramus* (IGM 100/1844), *Daspletosaurus torosus* (CMN 350), and *Tyrannosaurus* (BMRP 2002.4.1, MgD-I/206).

In lateral view, the collateral ligament pit in *Alectrosaurus* is proximodistally oval with a well-defined caudal margin (Figs. 1D, 7D); in addition, the pit does not extend proximally, and so it is positioned ventral to the level of the lateral tubercle. This condition is also seen in some *Albertosaurus libratus* (CMN 11593, TMP 1986.144.0001), and in *T. bataar* (MgD-I/206). The caudal edge is well-defined in *Daspletosaurus torosus* (CMN 350). In contrast, the pit extends further proximally, adjacent to the lateral tubercle, in *Albertosaurus* (AMNH FARB 5218,
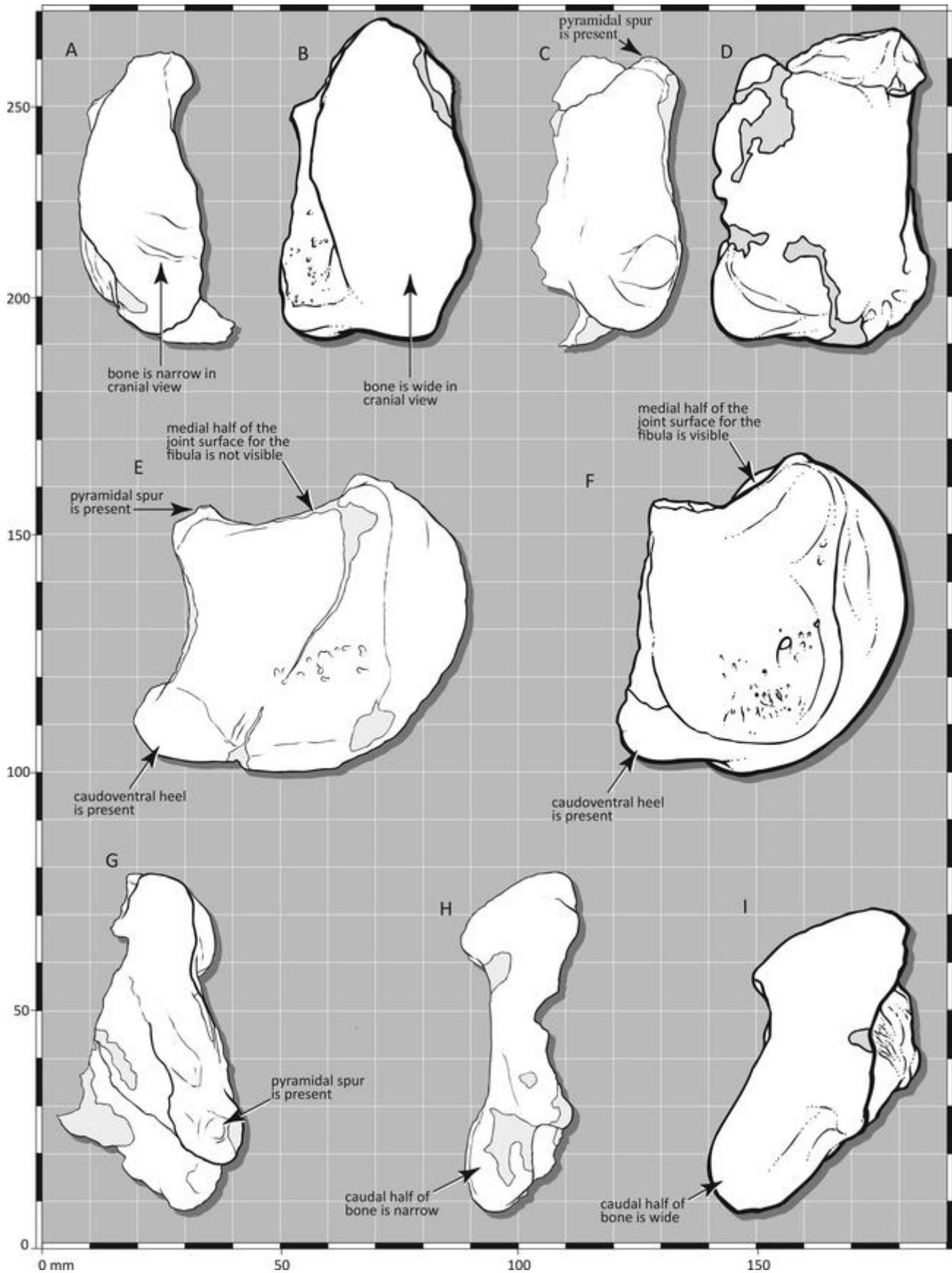
FIGURE 6. The calcaneum of the lectotype (AMNH FARB 6554) of *Alectrosaurus olseni* in **A**, cranial; **C**, caudal; **E**, lateral; **G**, dorsal; and **H**, ventral views. Comparative illustrations of *Appalachiosaurus montgomeriensis* (RMM 6670) in **B**, cranial; **D**, caudal; **F**, lateral; and **I**, ventral views. The *A. montgomeriensis* illustrations are modified after Carr, Williamson, and Schwimmer (2005).

AMNH FARB 5255, AMNH FARB 5458, CMN 11593, ROM 1247, TMP 1981.010.0001; Fig. 7E); also, it is bounded caudodistally by a ridge, and extends craniodistally adjacent to the apex of the joint surface (these conditions are also seen in TMP 1986.144.0001). The pit does not extend proximal to the tubercle, but it extends craniodistally adjacent to the apex of the joint surface in *Bistahieversor* (NMMNH P-25049). The pit of *T. rex* (BMRP 2002.4.1) is similar to that of *Alectrosaurus*, except the caudoproximal margin is poorly defined and it extends craniodistally. The pit extends craniodistally in *Daspletosaurus torosus* (CMN 350).

In lateral and medial views, the distal margin of the joint surface in *Alectrosaurus* is convex (Fig. 7D); this condition is also seen in *Albertosaurus libratus* (CMN 11593, ROM 1247; Fig. 7E) and *T. bataar* (MgD-I/206, PIN 551-2). In contrast, the margin is flat in *Bistahieversor* (NMMNH P-25049), *Albertosaurus* (AMNH FARB 5255, AMNH FARB 5458, TMP 1986.144.0001), and *T. rex* (BMRP 2002.4.1); and it is concave in one specimen of *A. libratus* (CMN 11593). In the trochleated *A. libratus* specimen (CMN 11593), the lateral condyle is concave, whereas the medial condyle is convex.

Digit I, Phalanx 1

In lateral view, the lateral condyle extends above the dorsal margin of the bone in *Alectrosaurus* (Fig. 1I, 8H; Table S4). In contrast, the lateral condyle is below the dorsal surface in *Alioramus* (IGM 100/1844) and some specimens of *Albertosaurus* (AMNH FARB 5218, AMNH FARB 5255, AMNH FARB 5664, TMP 1981.010.0001). Variation is seen in this character, where in some *Albertosaurus* it is level (AMNH FARB 5434, AMNH FARB 5458, CMN 2120, CMN 11593) with the dorsal surface. The level condition is also seen in *Tyrannosaurus* (BMRP 2002.4.1, PIN 551-2). For a taxonomic summary see Table S4. Measurements of I-1 are given in Table 1; polymorphic and ontogenetic characters are listed in Table S2 and Table S3, respectively.

In dorsal and plantar views, the phalanx in *Alectrosaurus* is narrow (w/l, 0.27; Fig. 8A, B); this condition is also seen in *Bistahieversor* (NMMNH P-25049, 0.26), *T. bataar* (PIN 551-2, 0.26), and subadult *T. rex* (BMRP 2002.4.1, 0.26). In contrast, the shaft is wide in *Albertosaurus sarcophagus* (AMNH FARB 5218, 0.33; TMP 1981.010.0001, 0.32), *Alioramus* (IGM 100/1844; 0.37), and adult *T. rex* (TMP 1981.012.0001, 0.32). Ontogenetic variation is seen in *Albertosaurus libratus* where the shaft is narrow (AMNH FARB 5664; ROM 1247, 0.27; Fig. 8C) or wide (AMNH FARB 5434, 0.33; CMN 11593, 0.32, 0.31).

In proximal view, the lateral and medial halves of the proximal joint surface in *Alectrosaurus* are not separated plantarly by a concavity (Fig. 8F); this condition is also seen in *Albertosaurus* (AMNH FARB 5218, AMNH FARB 5255, AMNH FARB 5434, CMN 11593, ROM 1247), *Alioramus* (IGM 100/1844), and subadult *T. rex* (BMRP 2002.4.1). In contrast, a concavity is seen in *Bistahieversor* (NMMNH P-25049) and in one specimen of *Albertosaurus sarcophagus* (TMP 1981.010.0001).

In distal view, the medial condyle in *Alectrosaurus* extends further dorsally than the lateral condyle (Fig. 8D). In contrast, the lateral condyle extends furthest dorsally in *Albertosaurus sarcophagus* (AMNH FARB 5218, AMNH FARB 5255) and *Tyrannosaurus* (BMRP 2002.4.1, PIN 551-2). Individual variation is seen in *Albertosaurus*, where the medial condyle extends furthest dorsally (AMNH FARB 5434, AMNH FARB 5458, CMN 11593) or the condyles are equal in height (AMNH FARB 5664; TMP 1981.010.0001).

In *Alectrosaurus* the groove in the distal joint surface is deepest dorsally (Fig. 8D); this condition is also seen in *T. bataar* (PIN 551-2). In contrast, the groove widens and fades dorsally in *Bistahieversor* (NMMNH P-25049), *Albertosaurus*

(AMNH FARB 5458, AMNH FARB 5664, CMN 11593, TMP 1981.010.0001), *Alioramus* (IGM 100/1844), and subadult *T. rex* (BMRP 2002.4.1).

In plantar view, the flexor groove in *Alectrosaurus* is deepest proximally (Fig. 8B); this condition is also seen in *T. bataar* (PIN 551-2). In contrast, the groove widens and fades proximally in *Bistahieversor* (NMMNH P-25049), *Albertosaurus* (AMNH FARB 5434, AMNH FARB 5458, AMNH FARB 5664, CMN 11593, ROM 1247, TMP 1981.010.0001; Fig. 8C), *Alioramus* (IGM 100/1844), and subadult *T. rex* (BMRP 2002.4.1).

The surface above the collateral ligament pit in *Alectrosaurus* is smooth (Figs. 1I, 8H); this condition is also seen in *Bistahieversor* (NMMNH P-25049) and in *Alioramus* (IGM 100/1844). In contrast, a rugosity is present in that location in *Albertosaurus* (AMNH FARB 5218, AMNH FARB 5218, AMNH FARB 5255, AMNH FARB 5434, AMNH FARB 5458, AMNH FARB 5664, CMN 2120, CMN 11593, TMP 1981.010.0001) and subadult *T. rex* (BMRP 2002.4.1).

In lateral view, the joint surface of the lateral condyle in *Alectrosaurus* does not extend past the midlength of the collateral pit plantarly (Figs. 1I, 8H); this condition is also seen in *Bistahieversor* (NMMNH P-25049), *Alioramus* (IGM 100/1844), *Albertosaurus libratus* (CMN 11593), and *T. bataar* (PIN 551-2). Variation is seen in *Albertosaurus* (AMNH FARB 5218, AMNH FARB 5255, AMNH FARB 5458, TMP 1981.010.0001), where the joint surface reaches or exceeds the caudal margin of the pit.

In dorsal, distal, and plantar views, the plantar lateral condyle in *Alectrosaurus* extends distinctly plantolaterally (Fig. 8A, B, D). In contrast, the condyle is nearly vertical with a slight plantolateral slope in *Bistahieversor* (NMMNH P-25049), *Albertosaurus* (AMNH FARB 5218, AMNH FARB 5255, AMNH FARB 5434, AMNH FARB 5458, CMN 11593, TMP 1981.010.0001), *Alioramus* (IGM 100/1844), and *Tyrannosaurus* (BMRP 2002.4.1, PIN 551-2).

In medial view, the collateral ligament pit in *Alectrosaurus* is small and circular (Fig. 8E); this condition is also seen in *Alioramus* (IGM 100/1844). In contrast, the pit is a large and long oval in *Bistahieversor* (NMMNH P-25049), *Albertosaurus* (AMNH FARB 5218, AMNH FARB 5255, AMNH FARB 5458, CMN 11593, ROM 1247, TMP 1981.010.0001; Figure 8G), and *Tyrannosaurus* (PIN 551-2).

The medial condyle in *Alectrosaurus* reaches the distal and dorsal surfaces of the bone (Fig. 8E); this condition is also seen in *Bistahieversor* (NMMNH P-25049). In contrast, the joint surface stops short of the dorsal surface in *Albertosaurus* (AMNH FARB 5218, AMNH FARB 5255, AMNH FARB 5434, AMNH FARB 5458, AMNH FARB 5664, CMN 2120, CMN 11593, TMP 1981.010.0001), *Alioramus* (IGM 100/1844), and *Tyrannosaurus bataar* (PIN 551-2).

Digit I, Phalanx 2

In lateral view, the proximodorsal lip in *Alectrosaurus* is long (Figs. 1I, 9C, D); this condition is also seen in *T. rex* (FMNH PR2081). In contrast, the lip is short in *Bistahieversor* (NMMNH P-25049) and *Albertosaurus* (CMN 2120, ROM 1247, TMP 1981.010.0001; Fig. 9F). Variation is seen in *T. bataar*, where both conditions are present in a single specimen (PIN 551-2), and the long condition is seen in another (MgD-I/29), indicating that this might not be a taxonomically informative character. Measurements of I-2 are given in Table 1; polymorphic characters are listed in Table S2.

In proximal view, the joint surface in *Alectrosaurus* is narrow (w/h, 0.57; Fig. 9E); this condition is also seen in *Bistahieversor* (NMMNH P-25049, 0.63) and in *Albertosaurus sarcophagus* (TMP 1981.010.0001, 0.58). In contrast, the joint surface is wide
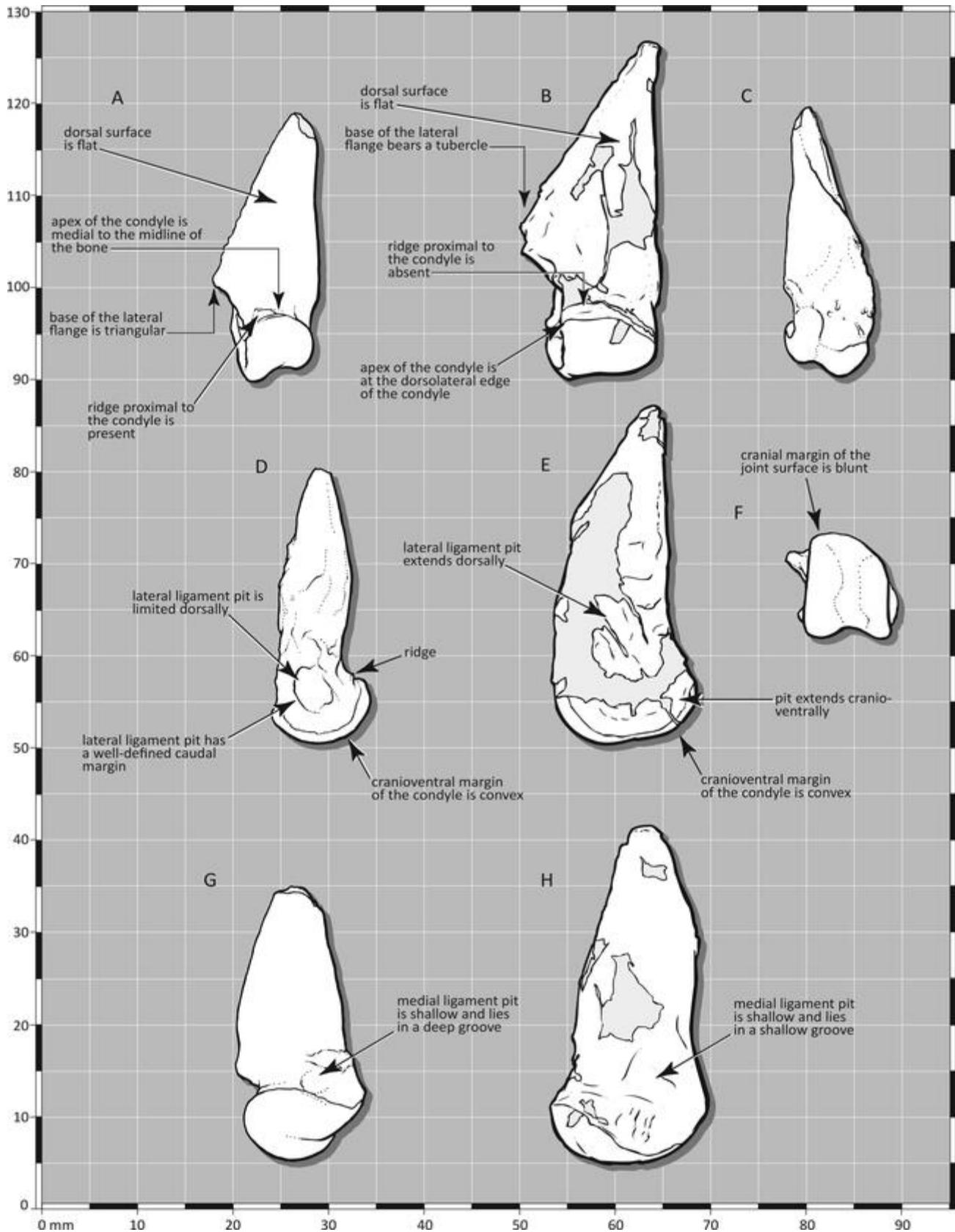
FIGURE 7. Metatarsal I of the lectotype (AMNH FARB 6554) of *Alectrosaurus olseni* in **A**, cranial; **C**, caudal; **D**, lateral; **F**, distal; and **G**, medial views. Comparative illustrations of *Albertosaurus libratus* (ROM 1247) in **B**, cranial; **E**, lateral; and **H**, medial views. Note the expanded distal end of the bone in *Alectrosaurus*.

in *A. libratus* (ROM 1247, 0.70; Fig. 9G) and *T. bataar* (PIN 551-2, 0.79, 0.66).

Metatarsal II

The dorsolateral condyle of the distal joint surface of metatarsal II in *Alectrosaurus* is on a pedicle, upon which the joint surface extends beyond the pedicle as a crest; the plantar condyles are elevated (Figs. 1E, 10E, H, J; Table S4). The dorsal and plantar condyles of the distal joint surface are elevated in *Appalachiosaurus* (RMM 6670), *Bistahieversor* (NMMNH P-25049, OMNH 10131), *Albertosaurus* (AMNH FARB 5233, AMNH FARB 5325, AMNH FARB 5255, AMNH FARB 5423, AMNH FARB 5432, CMN 11315, CMN 11593, ROM 807, ROM 1247, TMP 1986.144.0001), *Daspletosaurus* (AMNH FARB 5438, CMN 350, MOR 590, MOR 1130), and *Tyrannosaurus* (BMRP 2002.4.1, FMNH PR2081, LACM 23845, MgD-I/76, MgD-I/206, MOR 555, PIN 551-2; Fig. 10I). The plantar condyles are elevated in *Albertosaurus* at a low (AMNH FARB 5458, CMN 2120) or distinct (TMP 1981.010.0001, TMP 1984.064.0001, TMP 1994.012.0602) angle; in CMN 11593 the medial condyle is elevated at a distinct angle. A taxonomic summary is given in Table S4. Measurements of MTT II are given in Table 1; polymorphic and ontogenetic characters are listed in Table S2 and Table S3, respectively.

In dorsal view, the proximal rim of the bone in *Alectrosaurus* is flat (Fig. 10A); this condition is also seen in *Appalachiosaurus* (RMM 6670), *Bistahieversor* (NMMNH P-25049), *Daspletosaurus* (AMNH FARB 5346, CMN 350, MOR 590, MOR 1130), and in *T. bataar* (PIN 551-2). In contrast, the rim is ridge-like in *Albertosaurus libratus* (AMNH FARB 5432, CMN 11593, TMP 1984.144.0001), *Alioramus* (IGM 100/1844), and *T. rex* (BMRP 2002.4.1, CM 9380, FMNH PR2081). Individual variation is seen in *A. libratus*, where both states are present in one specimen (ROM 1247) and in another the lateral third is flat, whereas the remainder is a sharp ridge (TMP 1994.012.0602).

The distal joint surface in *Alectrosaurus* is separated from the lateral margin of the bone; this is, in part, an epiphenomenon of the presence of the pedicle (Fig. 10A). A gap is also seen in *Daspletosaurus* (CMN 350, MOR 590, MOR 1130) and *Tyrannosaurus* (BMRP 2002.4.1, CM 9380, FMNH PR2081, PIN 551-2). In contrast, the gap is absent from *Appalachiosaurus* (RMM 6670), *Albertosaurus* (AMNH FARB 5255, AMNH FARB 5423, AMNH FARB 5432, CMN 11315, CMN 11593, ROM 807, ROM 1247, TMP 1986.144.0001, TMP 1994.012.0602) and in *Alioramus* (Kurzanov, 1976). Individual variation is seen in *T. rex*, where a gap is absent from a subadult (LACM 23845; Fig. 10B).

In lateral view, the ligament pit in *Alectrosaurus* is situated close to the plantar edge of the shaft (Figs. 1E, 10H); this condition is also seen in *Daspletosaurus* (AMNH FARB 5438, CMN 350, MOR 590, MOR 1130) and in subadult *T. rex* (BMRP 2002.4.1). In contrast, the pit is not close to the plantar edge of the bone in *Appalachiosaurus* (RMM 6670), *Albertosaurus* (AMNH FARB 5228, AMNH FARB 5233, AMNH FARB 5234, AMNH FARB 5235, AMNH FARB 5255, AMNH FARB 5432, CMN 11315, CMN 11593, ROM 807, ROM 1247, TMP 1984.064.0001, TMP 1984.144.0001, TMP 1994.012.0602), and *Tyrannosaurus* (FMNH PR2081, LACM 23845, PIN 551-2; Fig. 10I). Variation is seen in *Bistahieversor*, where the pit is absent (OMNH 10131) or it is situated close to the plantar edge of the shaft (NMMNH P-25049).

In proximal view, the lateral process that contacts metatarsal IV in *Alectrosaurus* is craniocaudally short and transversely wide (Fig. 10C); this condition is also seen in *T. bataar* (MgD-I/76, PIN 552-1; Maleev, 1974:fig. 4A). In contrast, the process is craniocaudally long and transversely narrow in *Albertosaurus*

(AMNH FARB 5228, AMNH FARB 4234, AMNH FARB 5235, ROM 1247, TMP 1984.144.0001), *D. torosus* (AMNH FARB 5438), and in *T. rex* (BMRP 2002.4.1, LACM 23845; Fig. 10D). The process is long and wide in *D. horneri* (MOR 590, MOR 1130).

In proximal view, the lateral margin extends craniolaterally in *Alectrosaurus* (Fig. 10C); this condition is also seen in *Bistahieversor* (NMMNH P-25049), *Albertosaurus libratus* (CMN 11593, ROM 1247, TMP 1984.144.0001), *Daspletosaurus torosus* (CMN 350), and in *T. bataar* (MgD-I/76, PIN 551-2, PIN 552-1; Maleev, 1974:fig. 4A). In contrast, the margin is nearly parasagittally oriented in *Appalachiosaurus* (RMM 6670) and *T. rex* (BMRP 2002.4.1, FMNH PR2081, LACM 23845; Fig. 10D). Variation is seen in *Albertosaurus sarcophagus*, where the margin extends craniolaterally (CMN 11315) or parasagittally (AMNH FARB 5228). In *Alectrosaurus*, unlike other tyrannosaurids, the entire lateral margin extends craniolaterally; in contrast, the margin abruptly changes direction in all other tyrannosaurids except for one subadult *T. rex* (BMRP 2002.4.1). In subadult *D. horneri* the lateral margin extends parasagittally (MOR 590) and in adults it extends subtly craniolaterally (MOR 1130).

In plantar view, the medial edge of the medial condyle in *Alectrosaurus* is elevated beyond the shaft surface (Fig. 10E); this is also seen in *D. horneri* (MOR 590, MOR 1130). The condyle is elevated, but to a lesser degree, in subadult *Tyrannosaurus* (BMRP 2002.4.1, MgD-I/206). In contrast, the condyle is not elevated in *Appalachiosaurus* (RMM 6670), *Bistahieversor* (NMMNH P-25049), *Albertosaurus* (AMNH FARB 5255, AMNH FARB 5432, CMN 2120, CMN 11315, CMN 11593, ROM 807, ROM 1247, TMP 1981.010.0001, TMP 1984.064.0001, TMP 1984.144.0001, TMP 1994.012.0602), *D. torosus* (AMNH FARB 5438, CMN 350), or in *Tyrannosaurus* (LACM 23845, MgD-I/29, MOR 555; Fig. 10F).

The distal half of the plantomedial scar in *Alectrosaurus* is not deeply excavated (Fig. 10E); this condition is also seen in subadult *Albertosaurus libratus* (ROM 1247, TMP 1984.144.0001), *T. bataar* (MgD-I/206, PIN 551-2), and subadult *T. rex* (BMRP 2002.4.1). The scar is deeply excavated in large specimens of *A. libratus* (CMN 2120, CMN 11593, TMP 1994.012.0602), *Daspletosaurus* (CMN 350, MOR 590, MOR 1130), and large specimens of *T. rex* (FMNH PR2081, LACM 23845). Variation is seen in *A. sarcophagus* where the scar is shallow (AMNH FARB 5218, AMNH FARB 5225, AMNH FARB 5233, AMNH FARB 5234, AMNH FARB 5235, AMNH FARB 5255, TMP 1984.064.0001) or deep (CMN 11315, ROM 807, TMP 1981.010.0001). Variation is also seen in *Bistahieversor*, where a shallow scar is present in a juvenile (NMMNH P-25049) and is deep in an adult (OMNH 10131).

Finally, in *Alectrosaurus* a spur is present on the plantolateral edge of the bone above the distal articular process (Fig. 10E). A spur is also seen in juvenile *Albertosaurus libratus* (TMP 1984.144.0001), and a low coarse spur is seen in one adult *A. sarcophagus* (TMP 1981.010.0001). This spur is absent from all other tyrannosauroids (Fig. 10F); in some specimens of *Albertosaurus* (CMN 2120, CMN 11315, CMN 11593, ROM 1247, TMP 1994.012.0602), and *Daspletosaurus* (CMN 350, MOR 590, MOR 1130) a low rugosity is in the same position instead of the spur.

Digit II, Phalanx 1

The dorsolateral condyle in *Alectrosaurus* is elevated (Figs. 1J, 11C), this condition is also seen in *Albertosaurus libratus* (CMN 2120, CMN 11593, ROM 1247; Fig. 11D) *D. horneri* (MOR 590), and subadult *T. rex* (BMRP 2002.4.1). In contrast, the condyle is pediculate in *D. torosus* (CMN 350) and *T. bataar* (PIN 551-2).

The dorsomedial condyle in *Alectrosaurus* is elevated (Fig. 11E); this condition is also seen in *Albertosaurus libratus*
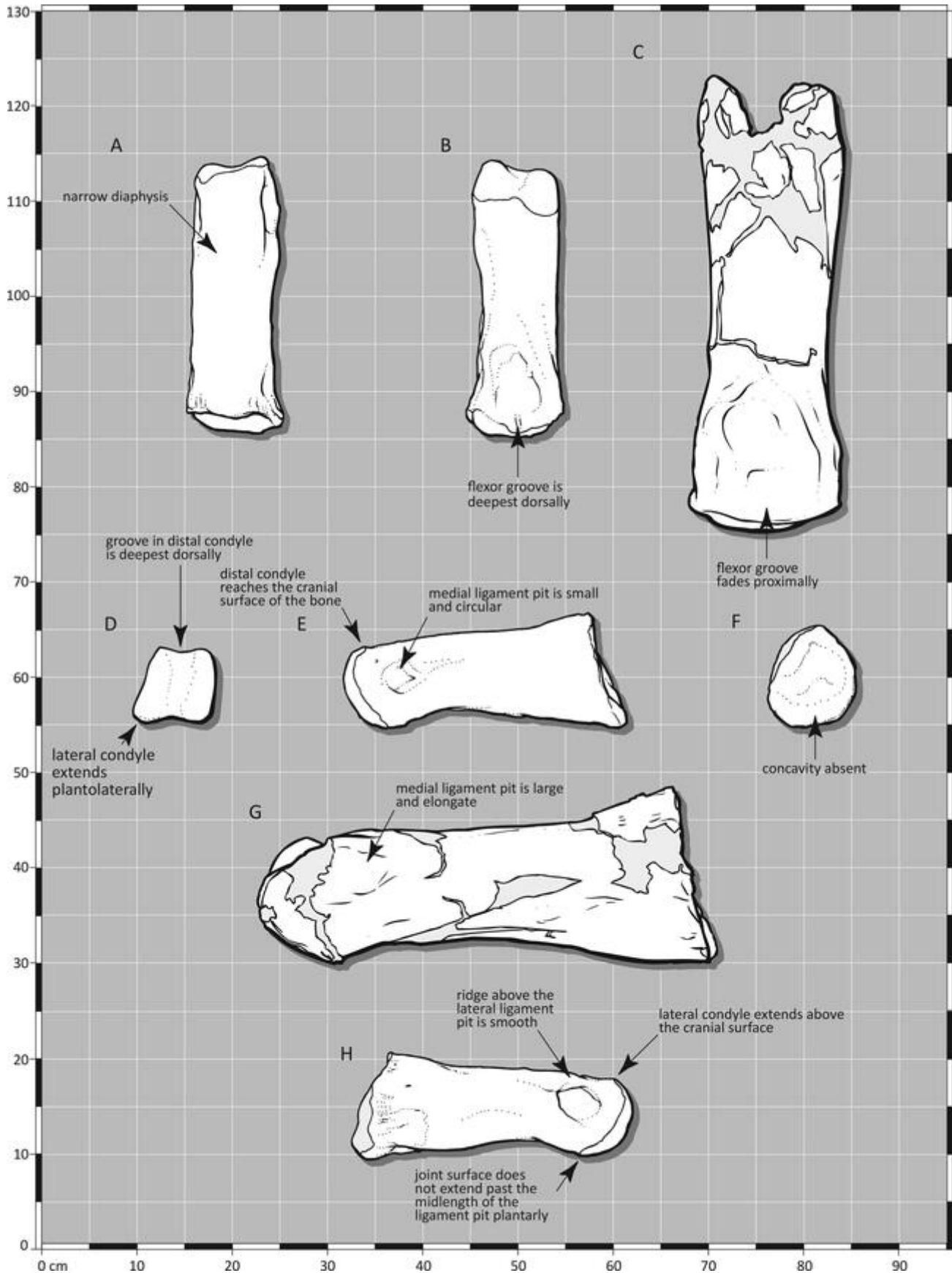
FIGURE 8. The phalanx I-1 of the lectotype of *Alectrosaurus olseni* (AMNH FARB 6554) in **A**, cranial; **B**, caudal; **D**, distal; **E**, medial; **F**, proximal; and **H**, medial views. Comparative illustrations of *Albertosaurus libratus* (ROM 1247) in **C**, caudal and **G**, medial views.
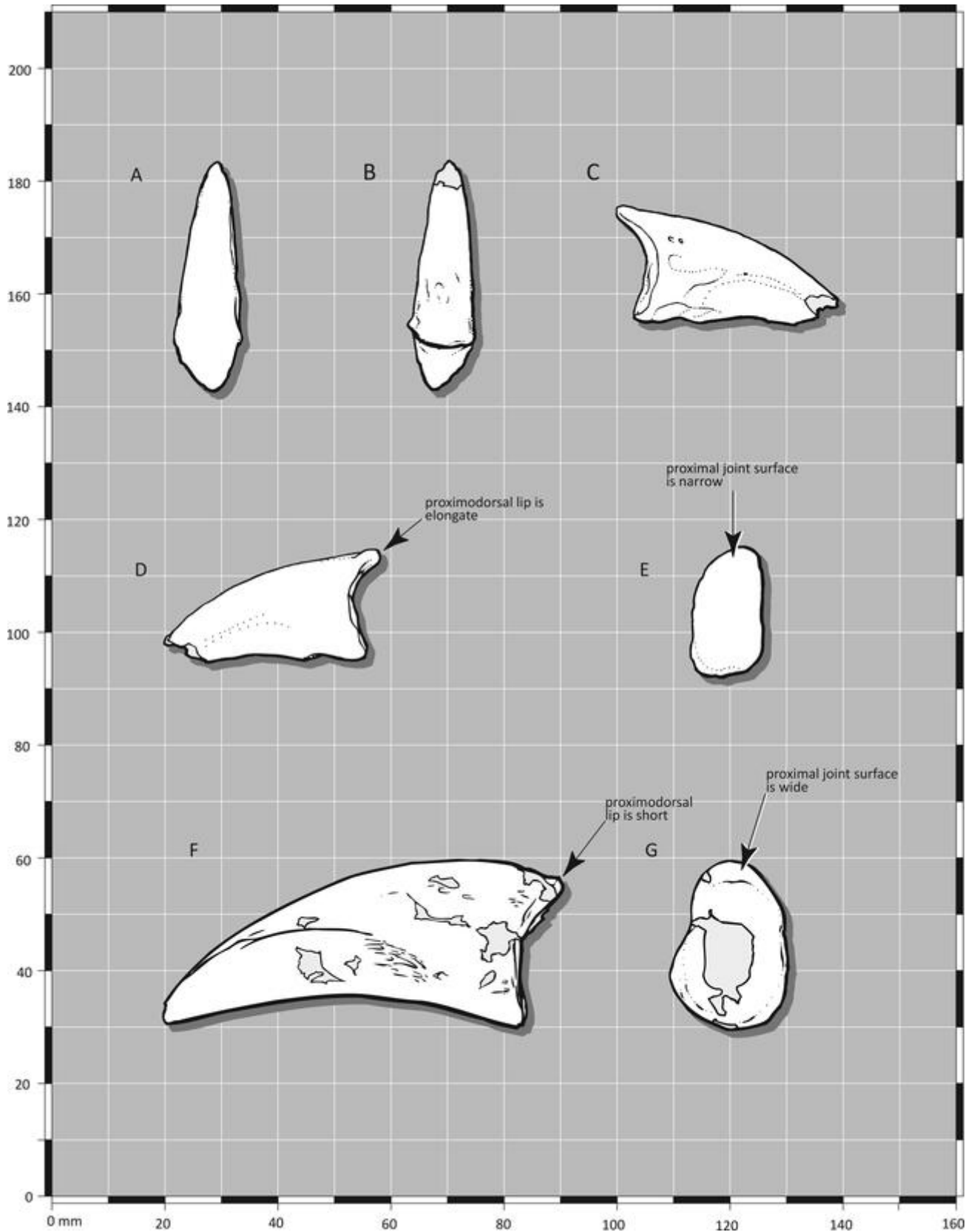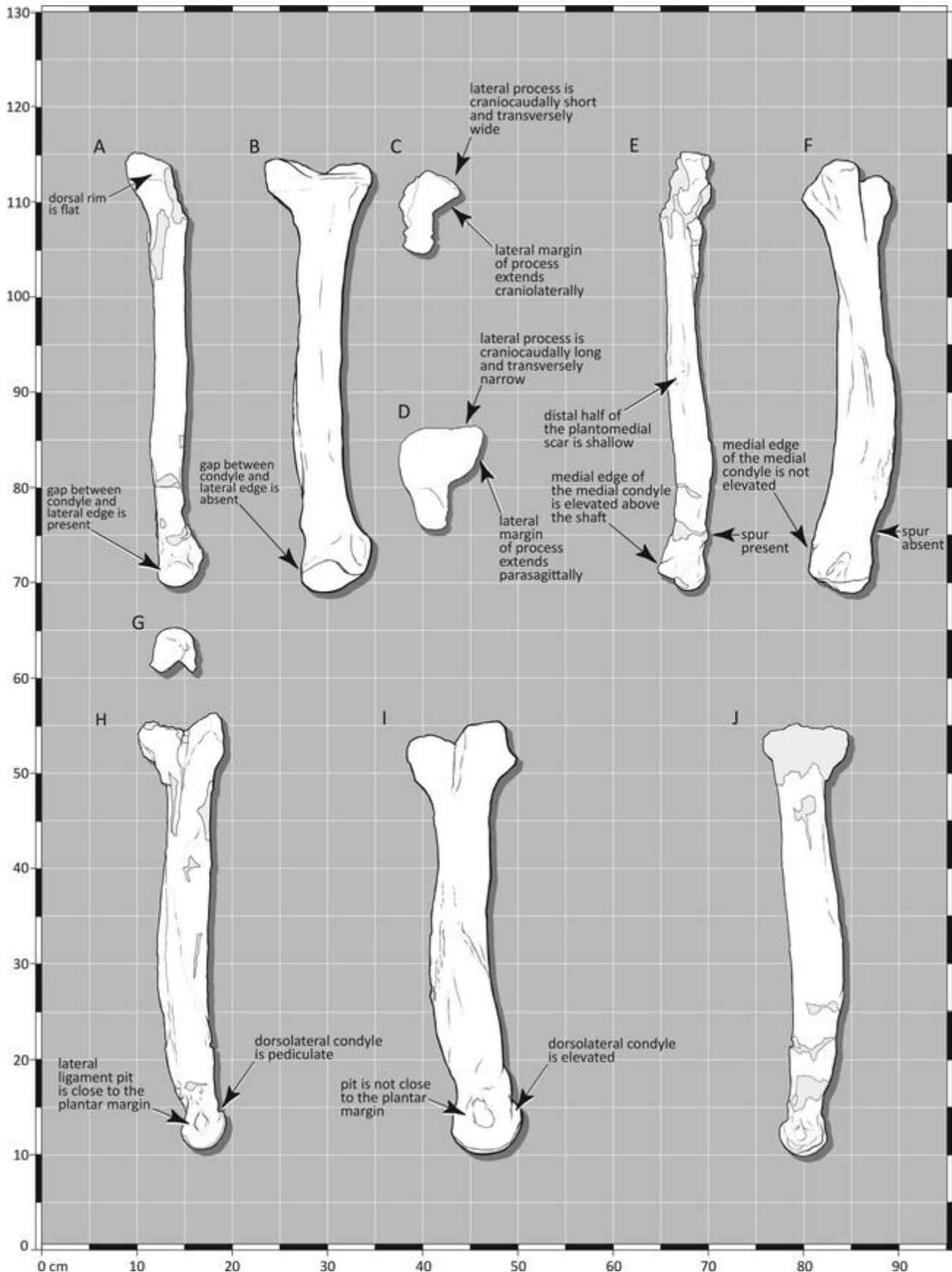
FIGURE 9. The phalanx I-2 of the lectotype (AMNH FARB 6554) of *Alectrosaurus olseni* in **A**, cranial; **B**, caudal; **C**, lateral; **D**, medial; and **E**, proximal views. Comparative illustration of *Albertosaurus libratus* (ROM 1247) in **F**, medial, and **G**, proximal views.

FIGURE 10. The right metatarsal II of the lectotype (AMNH FARB 6554) of *Alectrosaurus olseni* in **A**, cranial; **C**, proximal; **E**, plantar; **G**, distal; **H**, lateral; and **J**, medial views. Comparative illustrations of *Tyrannosaurus rex* (LACM 23845) in **B**, cranial; **D**, proximal; **F**, plantar; and **I**, lateral views.

(CMN 2120, CMN 11593, ROM 1247; Fig. 11F), *D. horneri* (MOR 590), and subadult *T. rex* (BMRP 2002.4.1). The condyle is on a low pedicle in *A. sarcophagus* (AMNH FARB 5218), *Bistahieversor* (NMMNH P-25049), *D. torosus* (CMN 350), and *T. rex* (FMNH PR2081). Individual variation is seen in *T. bataar* (PIN 551-2), where the condyle is elevated or level with the dorsal surface.

Unfortunately, the base of the plantolateral condyle in *Alectrosaurus* is missing; regardless, the plantomedial condyle is elevated (Fig. 11E). This condition is seen in adult *Albertosaurus libratus* (CMN 2120, CMN 11593) and *D. horneri* (MOR 590). In contrast, the plantomedial condyle of subadult *A. libratus* (ROM 1247; Fig. 11F) and subadult *T. rex* (BMRP 2002.4.1) is not elevated. This condyle is elevated in *Daspletosaurus* (CMN 350, MOR 590). Taxonomic comparisons are in Table S4; measurements of II-1 are given in Table 1; polymorphic and ontogenetic characters are listed in Table S2 and Table S3, respectively.

In proximal view, the flexor groove in *Alectrosaurus* is deeply incised into the phalanx (Fig. 11G). This condition is also seen in adult *Albertosaurus libratus* (CMN 2120, CMN 11593). In contrast, the groove is shallow in *Appalachiosaurus* (RMM 6670), *Bistahieversor* (NMMNH P-25049), *Albertosaurus libratus* (ROM 1247; Fig. 11H), *Daspletosaurus* (CMN 350, MOR 590), and *T. rex* (BMRP 2002.4.1, FMNH PR2081, LACM 23845). Both conditions are seen in *T. bataar* (PIN 551-2), whereas the groove is intermediate in depth in some *Albertosaurus* (AMNH FARB 5218, CMN 11593).

The joint surface for metatarsal II in *Alectrosaurus* is concave (Fig. 11G); this condition is also seen in *Appalachiosaurus* (RMM 6670), *Bistahieversor* (NMMNH P-25049), *Daspletosaurus* (CMN 350, MOR 590), and *T. rex* (BMRP 2002.4.1, FMNH PR2081). In contrast, the joint surface is centrally flat in *Albertosaurus sarcophagus* (AMNH FARB 5218). In *T. bataar* (PIN 551-2), the joint surface is concave with a midline vertical ridge that presumably stabilized the joint from mediolateral displacement. Individual variation is seen in *A. libratus*, where the joint surface is centrally flat (AMNH FARB 5434) or concave (CMN 2120, CMN 11593, ROM 1247; Fig. 11H).

In distal view, the dorsal margins of the distal condyles in *Alectrosaurus* are of equal height (Fig. 11I). In contrast, the lateral condyle is tallest in *Appalachiosaurus* (RMM 6670), *Bistahieversor* (NMMNH P-25049), *Albertosaurus* (AMNH FARB 5218, CMN 2120, CMN 11593, ROM 1247; Fig. 11J), *D. horneri* (MOR 590), and in *T. rex* (BMRP 2002.4.1, FMNH PR2081). This character may not be taxonomically informative, as both states are seen in *T. bataar* (PIN 551-2) and in *T. rex*.

In lateral view, the plantar extent of the distal joint surface in *Alectrosaurus* is visible (Figs. 1J, 11C), as is seen in *Appalachiosaurus* (RMM 6670), *Albertosaurus libratus* (ROM 1247; Fig. 11D), and *T. rex* (BMRP 2002.4.1, FMNH PR2081, LACM 23845). In contrast, the joint surface is only marginally visible in *Albertosaurus* (AMNH FARB 5218, CMN 2120, CMN 11593) and *D. horneri* (MOR 590). Both states are seen in *T. bataar* (PIN 551-2).

The lateral ligament pit in *Alectrosaurus* is small (Figs. 1J, 11C); this condition is also seen in *Appalachiosaurus* (RMM 6670) and subadult *T. rex* (BMRP 2002.4.1). In contrast, it is large in *Bistahieversor* (NMMNH P-25049), *Albertosaurus* (AMNH FARB 5218, ROM 1247; Fig. 11D), *Daspletosaurus* (CMN 350, MOR 590), and adult *Tyrannosaurus* (FMNH PR2081, MgD-I/76, PIN 551-2). Both conditions are seen in *A. libratus* (AMNH FARB 5434, ROM 1247), and the size of the pit is intermediate in some specimens (CMN 2120, CMN 11593).

The lateral ligament pit in *Alectrosaurus* does not approach the distal end of the bone (Figs. 1J, 11C); this condition is also seen in

Appalachiosaurus (RMM 6670), *Albertosaurus libratus* (CMN 2120, ROM 1247; Fig. 11D), *D. torosus* (CMN 350), and *Tyrannosaurus* (BMRP 2002.4.1, FMNH PR2081, LACM 23845, PIN 551-2). Variation is seen in *Albertosaurus* (AMNH FARB 5218, CMN 11593), *D. horneri* (MOR 590), and *T. bataar* (MgD-I/6), where the pit approaches the distal end of the bone. In addition, both states are present in one *A. libratus* (AMNH FARB 5434).

In medial view, the dorsal extent of the joint surface of the medial condyle approaches the midlength of the collateral ligament pit (Fig. 11E); this condition is also seen in *Appalachiosaurus* (RMM 6670), *Bistahieversor* (NMMNH P-25049), some specimens of *Albertosaurus libratus* (AMNH FARB 5664, CMN 11593, ROM 1247; Fig. 11F), and in *T. rex* (BMRP 2002.4.1, FMNH PR2081). In contrast, the joint surface extends past the midlength of the pit in *Albertosaurus* (AMNH FARB 5218, CMN 2120) and *Daspletosaurus* (CMN 350, MOR 590); both conditions are seen in *T. bataar* (PIN 551-2).

Digit II, Phalanx 2

The dorsolateral condyle in *Alectrosaurus* is pediculate (Figs. 1J, 12D), whereas the condyle is on a low pedicle in *Albertosaurus* (AMNH FARB 5218, CMN 11593) and subadult *T. rex* (BMRP 2002.4.1). The lateral edge of the condyle is pediculate in *T. rex* (FMNH PR2081). Variation is seen in *T. bataar* (PIN 551-2), where the condyle is on a low pedicle or it is elevated. The condyle is not pediculate in *Albertosaurus libratus* (CMN 2120, ROM 1247; Fig. 12E). The condyle is elevated in *D. horneri* (MOR 590).

The dorsomedial condyle in *Alectrosaurus* is pediculate (Fig. 12F), whereas the medial edge of the condyle is pediculate in *T. rex* (FMNH PR2081). A low pedicle is seen in subadult *T. rex* (BMRP 2002.4.1) In contrast, the condyle is elevated in *Appalachiosaurus* (RMM 6670) and *Albertosaurus libratus* (CMN 2120, CMN 11593, ROM 1247; Fig. 12G). Variation is seen in *A. sarcophagus* (AMNH FARB 5218) and *T. bataar* (PIN 551-2), where the condyle is level with the dorsal surface or it is on a low pedicle.

The plantolateral condyle in *Alectrosaurus* is elevated (Fig. 12D). In contrast, the joint surface is level with the plantar surface of the bone in *T. bataar* (PIN 551-2). Variation is seen in *Albertosaurus libratus* where it is level (ROM 1247; Fig. 12E) or elevated (CMN 2120, CMN 11593). The condyle is subtly pediculate in *D. horneri* (MOR 590) and subadult *T. rex* (BMRP 2002.4.1).

The plantomedial condyle in *Alectrosaurus* juts below the plantar margin of the bone (Fig. 12F). In contrast, the condyle is level with the plantar margin in *Albertosaurus libratus* (CMN 2120, CMN 11593, ROM 1247; Fig. 12G) and *Tyrannosaurus* (BMRP 2002.4.1, FMNH PR2081, PIN 551-2). The condyle extends at a low angle in *D. horneri* (MOR 590). See Table S4 for a taxonomic summary. Measurements of II-2 are given in Table 1; polymorphic and ontogenetic characters are listed in Table S2 and Table S3, respectively.

In dorsal and proximal views, the proximodorsal margin of the phalanx in *Alectrosaurus* is pointed (Fig. 12A, H). In contrast, the margin is convex in *Appalachiosaurus* (RMM 6670), *Bistahieversor* (NMMNH P-25049), *Albertosaurus* (AMNH FARB 5218, CMN 11593), and in *Tyrannosaurus* (BMRP 2002.4.1, Mg-D-I/36, PIN 551-2). The dorsal margin in adult *T. rex* is intermediate in shape (FMNH PR2081).

In lateral view, the lateral dorsal condyle of *Alectrosaurus* reaches the midlength of the collateral ligament pit (Figs. 1J, 12D). In contrast, neither of the condyles (lateral or medial) extend far past the cranial margin of the collateral ligament pits in *Appalachiosaurus* (RMM 6670), *D. horneri* (MOR 590), and *T. rex* (FMNH PR2081). In *Albertosaurus* (AMNH FARB 5218, ROM 1247; Fig. 12E, G), the lateral distal condyle does
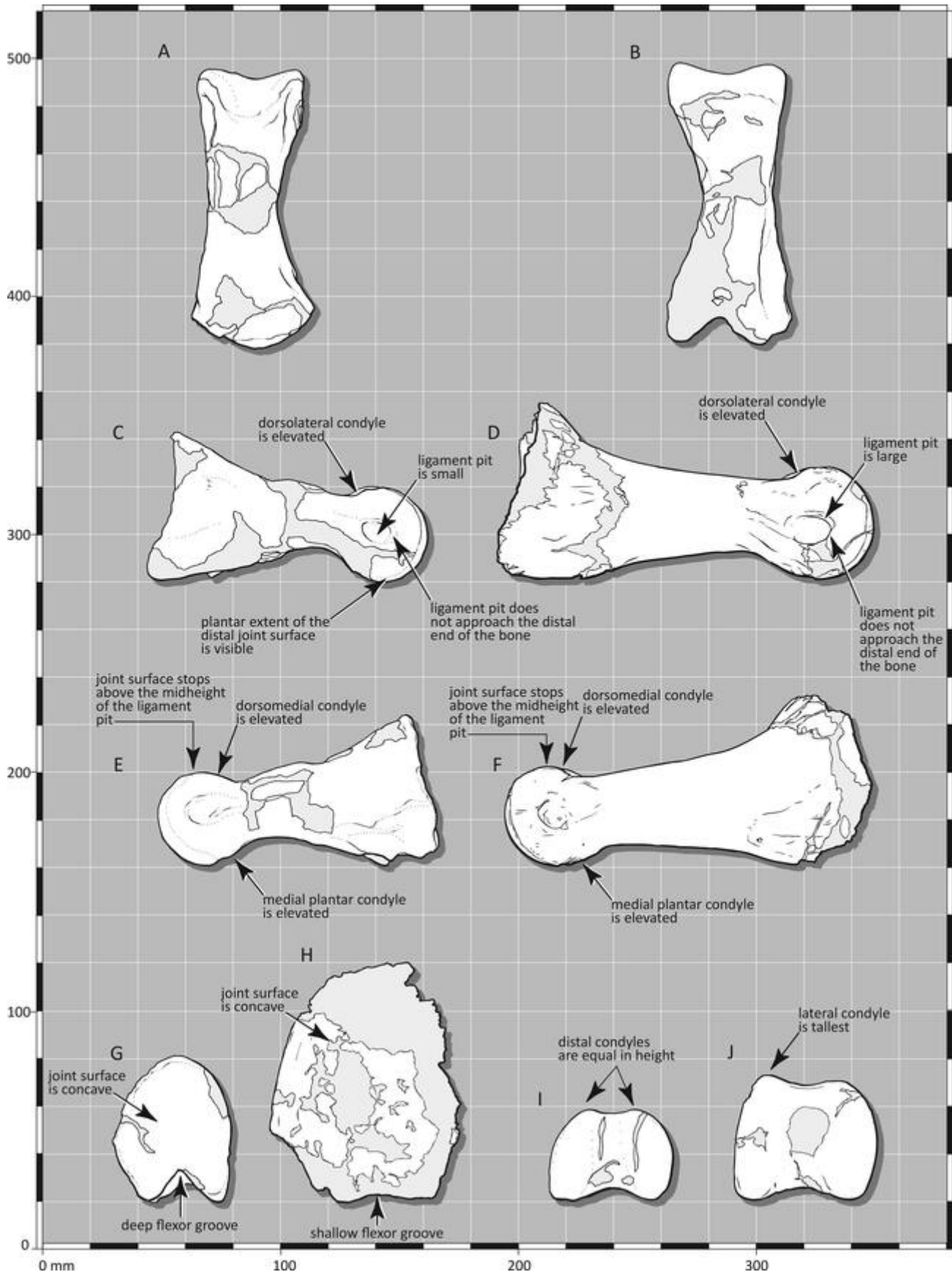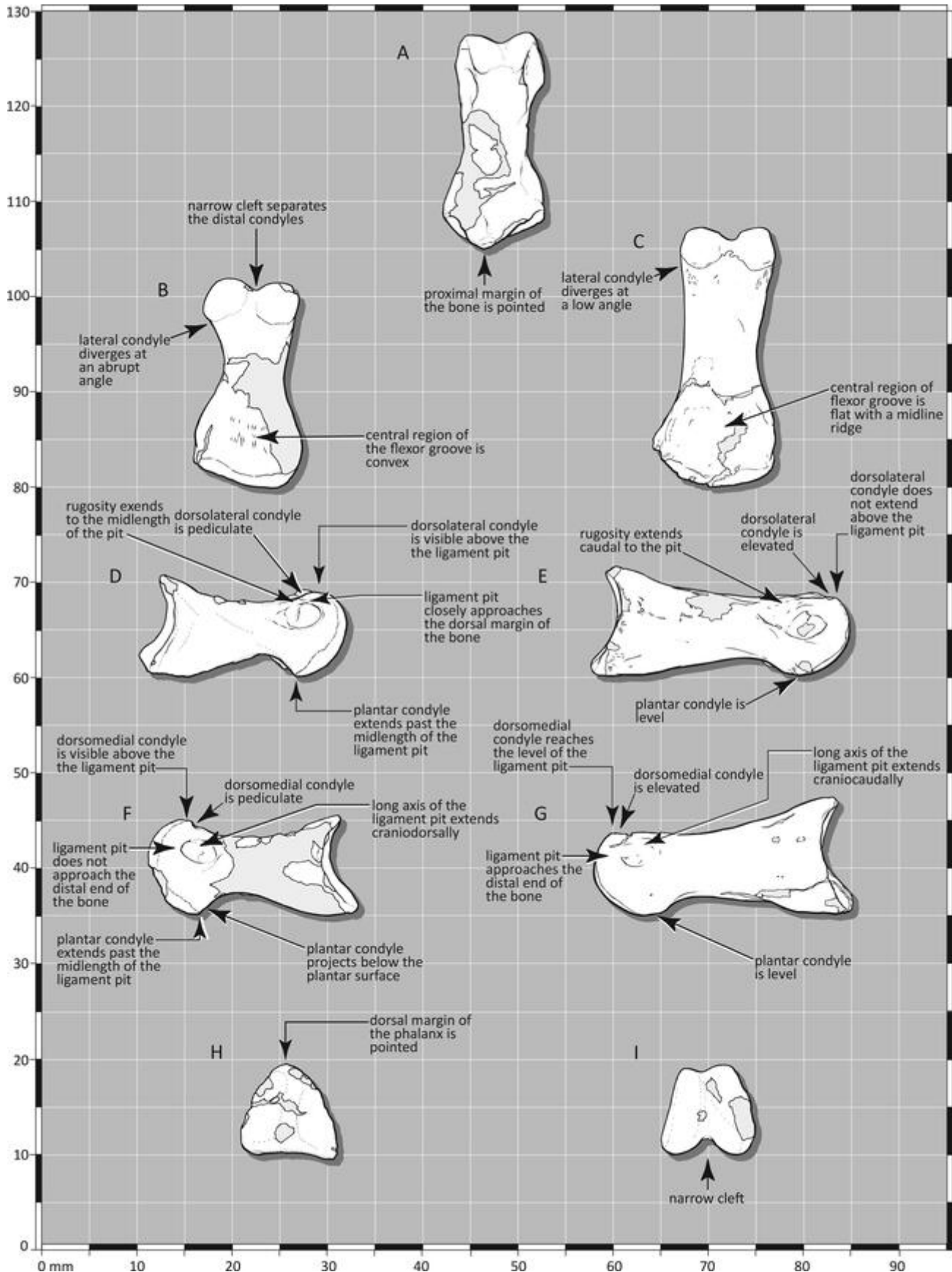
FIGURE 11. The phalanx II-1 of the lectotype (AMNH FARB 6554) of *Alectrosaurus olseni* in **A**, dorsal; **B**, plantar; **C**, lateral; **E**, medial; **G**, proximal; and **I**, distal views. Comparative illustrations of *Albertosaurus libratus* (ROM 1247) in **D**, lateral; **F**, medial; **H**, proximal; and **J**, distal views. Note the generally dilated distal end of *Alectrosaurus* in contrast to *Albertosaurus*.

FIGURE 12. The phalanx II-2 of the lectotype (AMNH FARB 6554) of *Alectrosaurus olseni* in **A**, dorsal; **B**, plantar; **D**, lateral; **F**, medial; **H**, proximal; and **I**, distal views. Comparative illustrations of *Albertosaurus libratus* (ROM 1247) in **C**, plantar; **E**, lateral; and **G**, medial views. Note the greatly dilated distal end of *Alectrosaurus* in contrast to *Albertosaurus*.

not reach the cranial margin of the pit, but the medial distal condyle reaches the margin. The condyles of each side reach the cranial margin in some specimens of *A. libratus* (CMN 2120, CMN 11593) and in subadult *T. rex* (BMRP 2002.4.1).

In medial view, the dorsal extent of the distal joint surface extends past the cranial margin of the medial collateral ligament pit in *Alectrosaurus* (Fig. 12F); this condition is also seen in *Tyrannosaurus* (FMNH PR2081, MgD-I/76, PIN 551-2). In contrast, the joint surface in *A. libratus* does not reach (CMN 2120, ROM 1247; Fig. 12G), reaches (CMN 2120, CMN 11593), or it marginally extends past the cranial margin of the medial pit (CMN 11593). In subadult *T. rex* (BMRP 2002.4.1) the joint surfaces reaches the cranial margin of the pit.

In *Alectrosaurus*, a deep and narrow cleft separates the distal condyles (Fig. 12B, I). In contrast, a shallow and wide cleft separates the distal condyles in *Appalachiosaurus* (RMM 6670), *Albertosaurus* (AMNH FARB 5218, CMN 2120, CMN 11593, ROM 1247), *D. horneri* (MOR 590), and *T. rex* (FMNH PR2081). The groove is deep and wide in subadult *T. rex* (BMRP 2002.4.1).

In *Alectrosaurus*, the rugosity above the lateral ligament pit extends to its midlength and partly roofs the pit (Figs. 1J, 12D); this condition is also seen in *D. horneri* (MOR 590) and *T. rex* (FMNH PR2081). A rugosity is only developed on the lateral side in *Albertosaurus libratus* (CMN 2120, CMN 11593, ROM 1247; Fig. 12E), which extends caudal to the ligament pit. A similar ridge is seen in *T. bataar* (MgD-I/29). The rugosity is low and does not extend laterally in *A. sarcophagus* (AMNH FARB 5218) and subadult *T. rex* (BMRP 2002.4.1).

In plantar view the lateral condyle in *Alectrosaurus* extends craniolaterally at a distinct angle (Fig. 12B); this condition is also seen in *Tyrannosaurus* (FMNH PR2081, MgD-I/29, MgD-I/76). In contrast, the lateral condyle extends craniolaterally at a low angle in *Appalachiosaurus* (RMM 6670), *Albertosaurus* (AMNH FARB 5218, CMN 2120, CMN 11593, ROM 1247; Fig. 12C), *D. horneri* (MOR 590), and subadult *T. rex* (BMRP 2002.4.1).

In plantar view, the central region of the flexor groove in *Alectrosaurus* is convex (Fig. 12B); this is also seen in subadult *T. rex* (BMRP 2002.4.1). The surface is convex medially and concave laterally in *D. horneri* (MOR 590). In contrast, the central region of the flexor groove is concave in *Albertosaurus sarcophagus* (AMNH FARB 5218) and *Tyrannosaurus* (FMNH PR2081, PIN 551-2); this surface is flat, with a midline ridge, in *A. libratus* (CMN 11593, ROM 1247; Fig. 12C).

In lateral view, the plantar extent of the distal joint surface in *Alectrosaurus* extends past the midlength of the collateral ligament pit (Figs. 1J, 12D); this condition is also seen in *Appalachiosaurus* (RMM 6670), *A. libratus* (CMN 2120, CMN 11593, ROM 1247; Fig. 12E), *D. horneri* (MOR 590), and *Tyrannosaurus* (BMRP 2002.4.1, FMNH PR2081, MgD-I/76). There is variation in this character, where in *T. bataar* (PIN 551-2) the joint surface is restricted cranially in lateral view, and in one specimen of *A. libratus* (CMN 11593) it reaches the midlength of the pit.

In medial view, the plantar extent of the distal joint surface in *Alectrosaurus* extends past the midlength of the collateral ligament pit (Fig. 12F); this condition is also seen in *Albertosaurus libratus* (AMNH FARB 5458, CMN 2120, ROM 1247; Fig. 12G), *D. horneri* (MOR 590), and *Tyrannosaurus* (BMRP 2002.4.1, FMNH PR2081, PIN 551-2). In contrast, the joint surface reaches the midlength in *Appalachiosaurus* (RMM 6670), and one specimen of *Albertosaurus libratus* (CMN 11593).

In medial view, the medial ligament pit in *Alectrosaurus* does not approach the cranial margin of the bone (Fig. 12F). In contrast, the pit approaches the cranial margin of the bone in *Albertosaurus libratus* (AMNH FARB 5458, AMNH FARB 5664, CMN 11593, ROM 1247; Fig. 12G), *D. horneri* (MOR 590), and *Tyrannosaurus* (BMRP 2002.4.1, FMNH PR2081, MgD-I/76, PIN 551-2). Variation is seen in *T. bataar* (MgD-I/29), where the pit does not approach the cranial end of the bone.

The long axis of the medial ligament pit in *Alectrosaurus* is craniodorsally oriented (Fig. 12F); this condition is also seen in *Tyrannosaurus* (FMNH PR2081, PIN 551-2). In contrast, the long axis is craniocaudally oriented in *Appalachiosaurus* (RMM 6670), *Albertosaurus* (AMNH FARB 5218, AMNH FARB 5458, AMNH FARB 5664, CMN 2120, CMN 11593, ROM 1247; Fig. 12G), *D. horneri* (MOR 590), and subadult *T. rex* (BMRP 2002.4.1). Variation is seen in *T. bataar* (MgD-I/29, MgD-I/76), where it is also craniocaudally oriented.

The lateral ligament pit in *Alectrosaurus* closely approaches the dorsal margin of the bone (Fig. 1J, 12D); this condition is also seen in *Albertosaurus libratus* (CMN 2120, CMN 11593, ROM 1247; Fig. 12G), *T. bataar* (PIN 551-2), and subadult *T. rex* (BMRP 2002.4.1). In contrast, the lateral ligament pit is positioned far below the dorsal margin of the bone in *D. horneri* (MOR 590) and *T. rex* (FMNH PR2081).

Digit II, Phalanx 3

In side view, the flexor tubercle in *Alectrosaurus* is hypertrophied and it reaches the level of the proximal joint surface (Figs. 1J, 13A, B; Mader and Bradley, 1989). The flexor tubercle in the specimen (IGM 100/50), which Perle (1977: fig. 3) referred to *Alectrosaurus*, is hypertrophied, but it does not reach the proximal margin of the bone; this condition is also seen in *T. bataar* (MgD-I/29, PIN 551-2). In contrast, the flexor tubercle is low and far cranial to the joint surface in *Appalachiosaurus* (RMM 6670), *Bistahieversor* (NMMNH P-25049), *Albertosaurus libratus* (CMN 11593, ROM 1247), *D. horneri* (MOR 590), and in *T. rex* (FMNH PR2081). In one specimen of *A. libratus* (CMN 2120), the tubercle is low and approaches, but does not reach, the proximal joint surface. Measurements of II-3 are given in Table 1; ontogenetic characters are listed in Table S3.

In *Alectrosaurus* an indentation is present in the dorsal margin between the dorsal surface and lip of the proximal joint surface (Figs. 1J, 13A, B); this condition is also seen in *Bistahieversor* (NMMNH P-25049), *A. libratus* (CMN 11593, ROM 1247), and in *Tyrannosaurus* (FMNH PR2081, PIN 551-2). In contrast, the indentation is far rostral to the joint surface in *Appalachiosaurus* (RMM 6670).

In all of the unguals in *Alectrosaurus*, the proximal joint surface bears a low vertical ridge at the midline to stabilize the interphalangeal joint (Fig. 13D). In contrast, a ridge is absent from *Bistahieversor* (NMMNH P-25049), *D. horneri* (MOR 590), *Tyrannosaurus* (FMNH PR2081, PIN 551-2), and possibly also *Albertosaurus libratus* (ROM 1247).

In medial view, the proximal joint surface in *Alectrosaurus* laps onto the dorsal surface of the bone (Fig. 13B); this condition is also seen in *Bistahieversor* (NMMNH P-25049; D II, IV), *Albertosaurus libratus* (CMN 11593), and *T. rex* (FMNH PR2081). In contrast, the joint surface does not extend onto the dorsal surface of the bone in a subadult *A. libratus* (ROM 1247).

Metatarsal III

The dorsolateral condyle in *Alectrosaurus* is pediculate (Figs. 1F, 14F). In contrast, the condyle is elevated in *Albertosaurus* (CMN 11593, ROM 807, ROM 1247, TMP 1984.064.0001, TMP 1984.144.0001, TMP 1994.012.0602) and *Daspletosaurus torosus* (CMN 350). The joint surface is level with the dorsal surface in an adult *Albertosaurus sarcophagus* (TMP 1981.010.0001) and in *T. rex* (BMRP 2002.4.1, MOR 555). The dorsomedial condyle in *Alectrosaurus* is pediculate (Fig. 14H). In contrast, the condyle in *T. rex* is elevated (BMRP 2002.4.1), level (LACM 23845; Fig 14I), or it is on a low pedicle (MOR 555), which is also seen in *Daspletosaurus torosus* (CMN 350); in *Albertosaurus* (CMN 11593, ROM 807, ROM 1247, TMP 1984.144.0001) and *D. horneri* (MOR 590), the condyle is
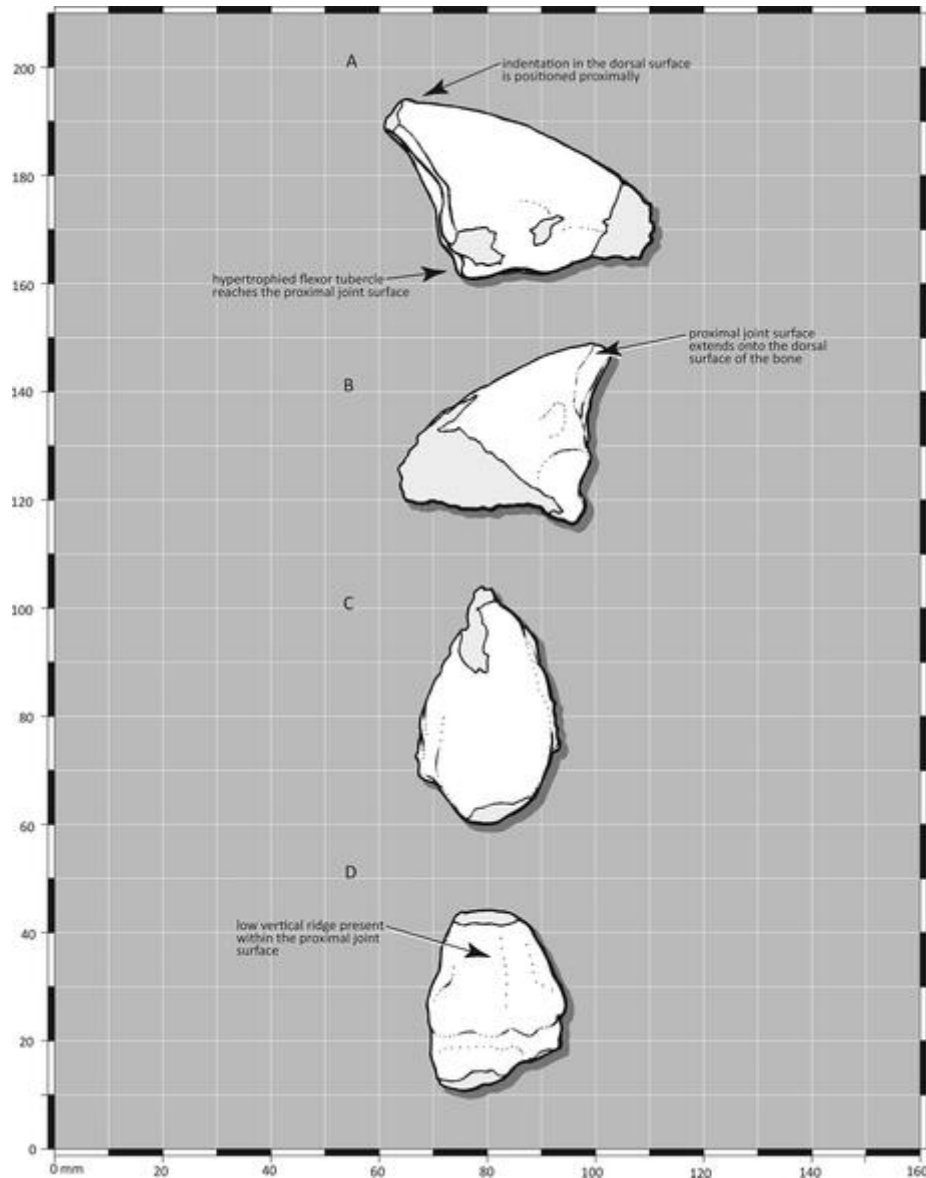
FIGURE 13. The phalanx II-3 of the lectotype (AMNH FARB 6554) of *Alectrosaurus olseni* in **A**, lateral; **B**, medial; **C**, dorsal; and **D**, proximal views.

elevated and in a subadult *A. sarcophagus* (TMP 1984.064.0001) it is level with the dorsal surface of the bone. In one adult *A. libratus* (TMP 1994.012.0602), the medial extent of the condyle is elevated, whereas it is pediculate along the deeply inset supracondylar pit.

The plantolateral condyle in *Alectrosaurus* is on a low pedicle (Figs. 1F, 14F). In *Albertosaurus* (CMN 2120, CMN 11593, ROM 807, ROM 1247, TMP 1981.010.0001, TMP 1984.064.0001, TMP 1984.144.0001, TMP 1994.012.0602), the condyle is elevated, whereas it is level with the plantar surface in *Daspletosaurus* (CMN 350, MOR 590) and *T. rex* (BMRP 2002.4.1, LACM 23845; Fig. 14G). The plantomedial condyle is elevated in *Albertosaurus* (CMN 2120, CMN 11593, ROM 807, ROM 1247, TMP 1981.010.0001, TMP 1984.064.0001, TMP 1984.144.0001, TMP 1994.012.0602). In contrast, it is level in *Daspletosaurus* (CMN 350, MOR 590) and *T. rex* (LACM 23845; Fig. 14I). See Table S4 for a taxonomic summary. Measurements of metatarsal III

are given in Table 1; polymorphic and ontogenetic characters are listed in Table S2 and Table S3, respectively.

In dorsal view, the dorsal margin of the distal condyle in *Alectrosaurus* extends dorsolaterally at a low angle such that it is nearly oriented horizontally (Fig. 14A). In contrast, the dorsal margin slopes dorsomedially such that it is convex in *Appalachiosaurus* (RMM 6670), *Bistahieversor* (NMMNH P-25049, OMNH 10131), *Albertosaurus* (AMNH FARB 5218, AMNH FARB 5228, AMNH FARB 5233, AMNH FARB 5234, AMNH FARB 5235, AMNH FARB 5255, AMNH FARB 5423, AMNH FARB 5423, AMNH FARB 5458, AMNH FARB 5664, CMN 11315, CMN 11593, ROM 807, ROM 1247, TMP 1981.010.0001, TMP 1984.064.0001, TMP 1984.144.0001, TMP 1994.012.0602), *Bistahieversor* (OMNH 10131), *Daspletosaurus torosus* (CMN 350), *Alioramus* (Kurzanov, 1976), and in *Tyrannosaurus* (BMRP 2002.4.1, CM 9380, FMNH PR2081, LACM 23845, MgD-I/29, PIN 551-2; Fig. 14B).
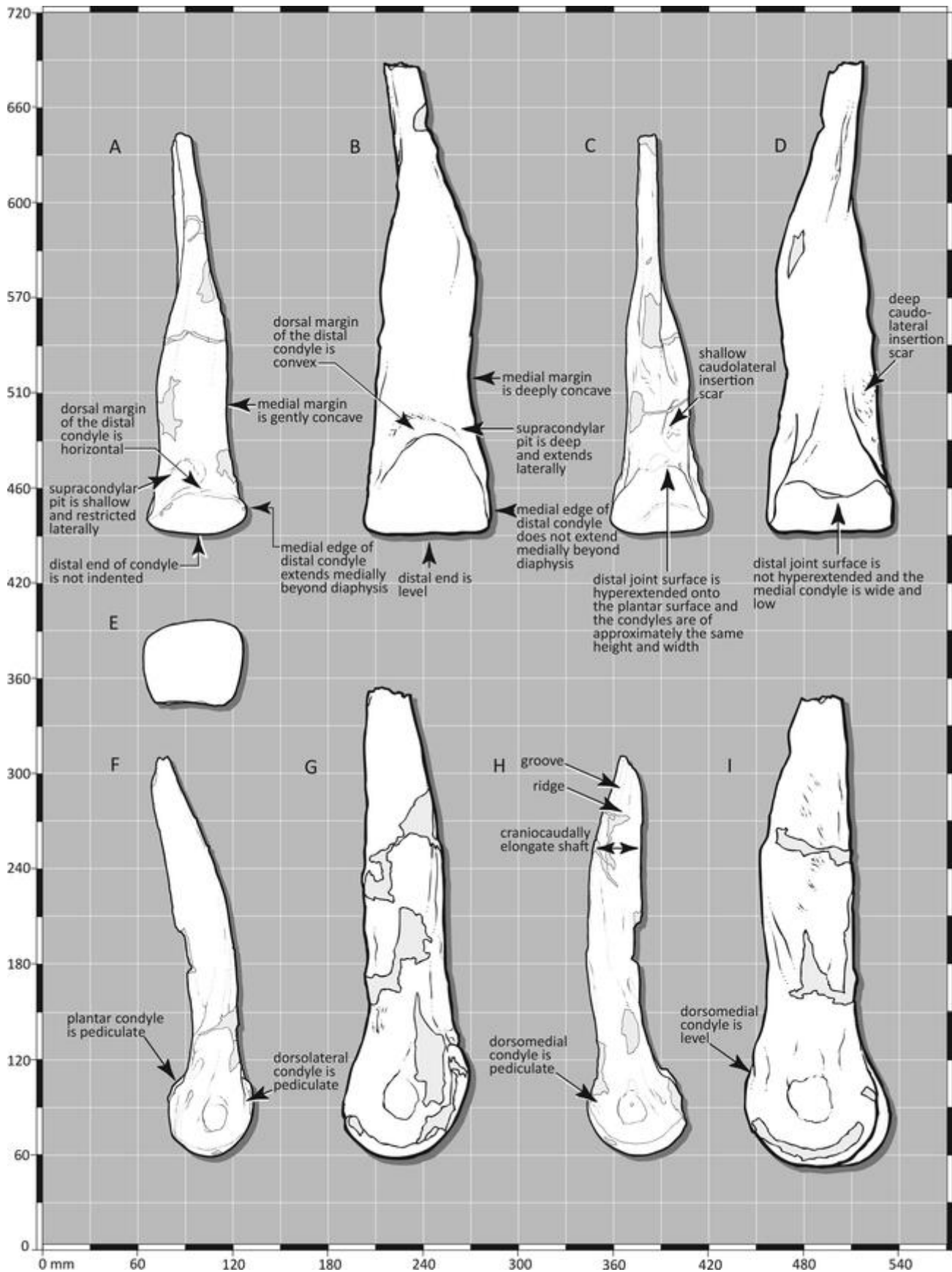
FIGURE 14. Metatarsal III of the lectotype (AMNH FARB 6554) of *Alectrosaurus olseni* in **A**, dorsal; **C**, plantar; **E**, distal; **F**, lateral; and **H**, medial views. Comparative illustrations of *Tyrannosaurus rex* (LACM 23845) in **B**, dorsal; **D**, plantar; **G**, lateral; and **I**, medial views. Note the greatly dilated distal end of *Alectrosaurus* in contrast to *T. rex*.
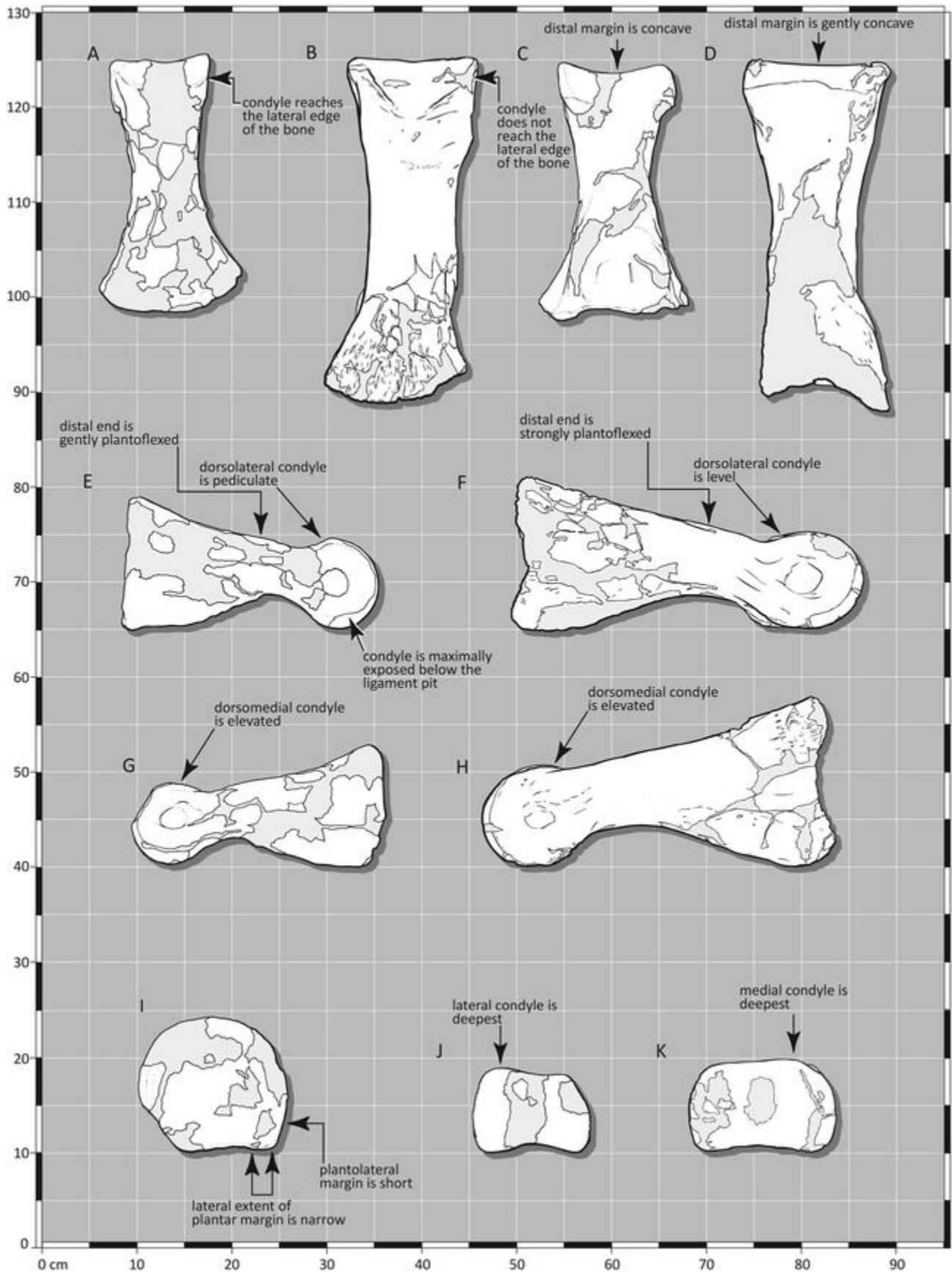
FIGURE 15. The phalanx III-1 of the lectotype (AMNH FARB 6554) of *Alectrosaurus olseni* in **A**, dorsal; **C**, plantar; **E**, lateral; **G**, medial; **I**, proximal; and **J**, distal views. Comparative illustrations of *Albertosaurus libratus* (ROM 1247) in **B**, dorsal; **D**, plantar; **F**, lateral; **H**, medial; and **K**, distal views. Note the generally dilated distal end of *Alectrosaurus* in contrast to *Albertosaurus*.

The medial edge of the distal joint surface in *Alectrosaurus* extends beyond the medial edge of the shaft (Fig. 14A). In contrast, the joint surface is as wide as the shaft in *Bistahieversor* (NMMNH P-25049), *Albertosaurus* (AMNH FARB 5255, AMNH FARB 5458, AMNH FARB 5664, CMN 11315, CMN 11593, ROM 807, ROM 1247, TMP 1984.144.0001, TMP 1994.012.0602), *Alioramus* (Kurzanov, 1976), *Daspletosaurus torosus* (CMN 350), and *Tyrannosaurus* (LACM 23845, MgD-I/29, PIN 551-2, PIN 552-2; Fig. 14B; Maleev, 1974: fig. 62). The medial edge of the bone is widened beyond the shaft in one specimen of *T. rex* (FMNH PR2081), but the joint surface does not extend beyond it, and in others (BMRP 2002.4.1) the condyle extends marginally past the edge of the shaft; this condition is also seen in some specimens of *Albertosaurus sarcophagus* (TMP 1981.010.0001, TMP 1984.064.0001) and *D. horneri* (MOR 590). In *Appalachiosaurus* (RMM 6670) and the specimen referred by Perle (GIN 100/51; 1977:fig. 5) to *Alectrosaurus*, both sides of the distal end are widened relative to the shaft, but the joint surface does not appear to extend beyond it.

The supracondylar pit in *Alectrosaurus* is shallow (Fig. 14A); this condition is also seen in *Alioramus* (IGM 100/1844). In contrast, it is deep in *Appalachiosaurus* (RMM 6670), *Bistahieversor* (NMMNH P-25049, OMNH 10131), *Albertosaurus* (AMNH FARB 5255, AMNH FARB 5423, AMNH FARB 5432, AMNH FARB 5458, AMNH FARB 5664, CMN 11315, CMN 11593, ROM 807, ROM 1247, TMP 1981.010.0001, TMP 1984.064.0001, TMP 1984.144.0001, TMP 1994.012.0602), *Daspletosaurus* (CMN 350, MOR 590), and in *Tyrannosaurus* (BMRP 2002.4.1, CM 9380, LACM 23845, MgD-I/29, FMNH PR2081, MOR 555, PIN 551-2; Fig. 14B).

In *Alectrosaurus*, the pit is restricted to the lateral half of the shaft (Fig. 14A). In contrast, the pit extends medially in *Appalachiosaurus* (RMM 6670), *Bistahieversor* (NMMNH P-25049, OMNH 10131), *Albertosaurus* (AMNH FARB 5255, CMN 11315, CMN 11593, ROM 807, ROM 1247, TMP 1984.144.0001, TMP 1994.012.0602), *Alioramus* (Kurzanov, 1976), *Daspletosaurus* (CMN 350, MOR 590), and *T. bataar* (MgD-I/29, PIN 551-2). Variation is seen in *T. rex*, where the pit is limited laterally in some adults (CM 9380, FMNH PR2081), whereas it extends medially in subadults (BMRP 2002.4.1, LACM 23845; Fig. 14B). In *Albertosaurus libratus* (CMN 11593), *Alioramus* (IGM 100/1844), and *Daspletosaurus* (CMN 350, MOR 590) the deepest part of the pit is lateral in position.

In dorsal view, the distal surface of the distal condyle in *Alectrosaurus* is convex (Fig. 14A); this condition is also seen in *Daspletosaurus* (CMN 350, MOR 590). In contrast, this surface is indented in *Appalachiosaurus* (RMM 6670), *Bistahieversor* (NMMNH P-25049, OMNH 10131), *Albertosaurus* (AMNH FARB 5218, AMNH FARB 5228, AMNH FARB 5233, AMNH FARB 5235, AMNH FARB 5255, CMN 11315, CMN 11593, ROM 807, TMP 1981.010.0001, TMP 1984.064.0001, TMP 1984.144.0001, TMP 1994.012.0602), *Alioramus* (Kurzanov, 1976), and in *Tyrannosaurus bataar* (MgD-I/29, PIN 551-2). Variation is present in *A. libratus*, where the condyle is convex (ROM 1247) or indented (AMNH FARB 5432, ROM 1247). Possible ontogenetic variation is present in *T. rex*, where the condyle is convex in relatively small subadults (BMRP 2002.4.1), level in large subadults (LACM 23845; Fig. 14B), and is indented in adults (CM 9380, FMNH PR2081). A similar condition is also seen in *T. bataar*, where the indentation is very shallow in subadults (MgD-I/29).

The medial margin of the bone in *Alectrosaurus* is gently concave above the distal joint surface (Fig. 14A); this condition is also seen in *Appalachiosaurus* (RMM 6670) and in a juvenile *Albertosaurus libratus* (TMP 1984.144.0001). In contrast, the margin is deeply concave in *Bistahieversor* (NMMNH P-25049, OMNH 10131), *Albertosaurus* (AMNH FARB 5218, AMNH

FARB 5228, AMNH FARB 5233, AMNH FARB 5234, AMNH FARB 5235, AMNH FARB 5255, AMNH FARB 5423, AMNH FARB 5397, AMNH FARB 5458, AMNH FARB 5664, CMN 11315, CMN 11593, ROM 807, ROM 1247, TMP 1981.010.0001, TMP 1984.064.0001, TMP 1994.012.0602), *Alioramus* (IGM 100/1844), *Daspletosaurus* (CMN 350, MOR 590), and in *Tyrannosaurus* (BMRP 2002.4.1, CM 9380, FMNH PR2081, LACM 23845, MOR 555, PIN 551-2, PIN 552-2; Fig. 14B; Maleev, 1974: fig. 62).

In plantar view, the distal joint surface in *Alectrosaurus* is hyperextended onto the plantar surface of the shaft (Fig. 14C, F; Mader and Bradley, 1989). In contrast, the joint surface is not hyperextended in *Appalachiosaurus* (RMM 6670), *Bistahieversor* (NMMNH P-25049), *Albertosaurus* (AMNH FARB 5255, CMN 2120, CMN 11315, CMN 11593, ROM 807, ROM 1247, TMP 1981.010.0001, TMP 1984.064.0001, TMP 1984.144.0001, TMP 1994.012.0602), *Alioramus* (IGM 100/1844), *Daspletosaurus* (CMN 350, MOR 590), nor in *Tyrannosaurus* (BMRP 2002.4.1, CM 9380, FMNH PR2081, LACM 23845, PIN 551-2, PIN 552-1; Fig. 14D, G, I; Maleev, 1974).

In plantar view, the distal condyles in *Alectrosaurus* appear to be of equal height and width (Fig. 14C); the condyles are of equal height in subadult *T. rex* (BMRP 2002.4.1). In *Albertosaurus* (AMNH FARB 5255, CMN 11315, ROM 807, TMP 1984.144.0001, TMP 1994.012.0602) and possibly also *T. bataar* (PIN 552-1; Maleev, 1974), the lateral condyle is lower and wider than the tall and narrow medial condyle. The medial condyle is tallest but they are the same width in *D. horneri* (MOR 590). In *Bistahieversor* (NMMNH P-25049, OMNH 10131), one *A. sarcophagus* (TMP 1984.064.0001), and *T. rex* (LACM 23845; Fig. 14D), the medial condyle is lower and wider than the lateral condyle.

The caudolateral insertion scar in *Alectrosaurus* is shallow (Fig. 14C); this condition is also seen in *Bistahieversor* (NMMNH P-25049, OMNH 10131), *Alioramus* (IGM 100/1844), *D. torosus* (CMN 350), and *Tyrannosaurus bataar* (PIN 551-2). The scar is deep in *Appalachiosaurus* (RMM 6670) and *D. horneri* (MOR 590). However, this character is probably not taxonomically informative, as both conditions are present in *Albertosaurus* (shallow: AMNH FARB 5397, CMN 2120, CMN 11315, CMN 11593, ROM 807, ROM 1247, TMP 1981.010.0001; deep: AMNH FARB 5218, AMNH FARB 5228, AMNH FARB 5233, AMNH FARB 5234, AMNH FARB 5235, AMNH FARB 5255, AMNH FARB 5432, AMNH FARB 5458, TMP 1984.064.0001, TMP 1984.144.0001, TMP 1994.012.0602) and *T. rex* (shallow: CM 9380, FMNH PR2081; deep: BMRP 2002.4.1, LACM 23845; Fig. 14D).

In medial view, the proximal shaft contact with metatarsal II in *Alectrosaurus* is reinforced by a groove and ridge (Fig. 14H); this condition is also seen in *T. rex* (FMNH PR2081). These structures are absent from subadult *T. rex* (BMRP 2002.4.1). Only the ridge is present in *Bistahieversor* (NMMNH P-25049), *Albertosaurus* (AMNH FARB 5233, AMNH FARB 5235, AMNH FARB 5255, CMN 11315, CMN 11593, ROM 1247, TMP 1984.064.0001, TMP 1984.144.0001), and *Daspletosaurus torosus* (CMN 350). Ontogenetic variation is seen in *D. horneri* where the ridge and groove are absent from subadults (MOR 590) whereas they are present in adults (MOR 1130).

Finally, the shaft of the bone is anteroposteriorly (from dorsal to the plantar surface) long in *Alectrosaurus* (Fig. 14H) and *D. horneri* (MOR 590), whereas it is narrow in *Bistahieversor* (NMMNH P-25049), *Albertosaurus* (AMNH FARB 5255, CMN 11315, ROM 1247, TMP 1984.144.0001), and *D. torosus* (CMN 350).

Digit III, Phalanx 1

The dorsolateral condyle in *Alectrosaurus* is pediculate (Figs. 1K, 15E); this condition is also seen in *T. rex* (FMNH PR2081).

In contrast, the condyle is elevated in *Bistahieversor* (NMMNH P-25049), *Albertosaurus libratus* (CMN 11593, ROM 1247; [Fig. 15F](#)), *Daspletosaurus* (CMN 350, MOR 590), *T. bataar* (PIN 551-2), and subadult *T. rex* (BMRP 2002.4.1). The condyle is level with the dorsal surface in *Appalachiosaurus* (RMM 6670) and *Albertosaurus sarcophagus* (AMNH FARB 5218, AMNH FARB 5233, AMNH FARB 5234, AMNH FARB 5255).

The dorsomedial condyle in *Alectrosaurus* is elevated ([Fig. 15G](#)); this condition is also seen in *Albertosaurus libratus* (CMN 11593, ROM 1247; [Fig. 15H](#)), *Daspletosaurus* (CMN 350, MOR 590), and subadult *T. rex* (BMRP 2002.4.1). In contrast, the condyle is level with the dorsal surface in *Bistahieversor* (NMMNH P-25049), *A. sarcophagus* (AMNH FARB 5218, AMNH FARB 5233, AMNH FARB 5234, AMNH FARB 5255), and adult *T. rex* (FMNH PR2081). Variation is seen in *T. bataar* (PIN 551-2), where the condyle is on a low pedicle or it is elevated. In *A. libratus* (ROM 1247) the distal joint surface is pediculate across the midline between the distal condyles ([Fig. 15B](#)).

The plantolateral condyle in *Alectrosaurus* is elevated ([Figs. 1K, 15E](#)); this condition is also seen in *Bistahieversor* (NMMNH P-25049), *Albertosaurus libratus* (CMN 2120, CMN 11593, ROM 1247; [Fig. 15F](#)), *D. horneri* (MOR 590), and in *Tyrannosaurus* (BMRP 2002.4.1, PIN 551-2). Unfortunately, the plantomedial condyle is damaged; see Table S4 for a taxonomic summary. Measurements of III-1 are given in [Table 1](#); polymorphic and ontogenetic characters are listed in Table S2 and Table S3, respectively.

In proximal view, the plantolateral margin of the bone in *Alectrosaurus* is short ([Fig. 15I](#)); this condition is also seen in *Albertosaurus libratus* (ROM 1247), *D. horneri* (MOR 590), and *Tyrannosaurus* (BMRP 2002.4.1, FMNH PR2081, PIN 551-2). In contrast, the margin is tall in *Appalachiosaurus* (RMM 6670), *Bistahieversor* (NMMNH P-25049), and in *Albertosaurus sarcophagus* (AMNH FARB 5218, AMNH FARB 5255). Variation is seen in *A. libratus* (CMN 2120, CMN 11593), where the margin is also tall.

The lateral extent of the plantar margin in *Alectrosaurus* is narrow ([Fig. 15I](#)); this is also seen in *Appalachiosaurus* (RMM 6670), *Bistahieversor* (NMMNH P-25049), *Albertosaurus libratus* (ROM 1247), and *T. bataar* (PIN 551-2). In contrast, the lateral extent is wide in *D. horneri* (MOR 590) and *T. rex* (LACM 23845). Variation is seen in *A. sarcophagus*, where the lateral extent is narrow (ROM 807) or wide (AMNH FARB 5218, AMNH FARB 5255). In adult *A. libratus* the lateral extent is wide (CMN 2120, CMN 11593).

In distal view, the lateral condyle in *Alectrosaurus* is deeper than the medial condyle ([Fig. 15J](#)). In contrast, the medial condyle is deepest in *Bistahieversor* (NMMNH P-25049), *Albertosaurus libratus* (CMN 11593, ROM 1247; [Fig. 15K](#)), *Daspletosaurus* (CMN 350, MOR 590), and *T. rex* (BMRP 2002.4.1, LACM 23845). In *A. sarcophagus* (AMNH FARB 5218, AMNH FARB 5255, ROM 807) the condyles are equal in height.

In dorsal view, the condylar surface in *Alectrosaurus* closely approaches the lateral margin of the bone on a pedicle ([Fig. 15A](#)). In contrast, the condyle does not approach the lateral margin in *Appalachiosaurus* (RMM 6670), *Bistahieversor* (NMMNH P-25049), *Albertosaurus* (AMNH FARB 5218, AMNH FARB 5255, CMN 11593, ROM 1247; [Fig. 15B](#)), *Daspletosaurus* (CMN 350, MOR 590), and *T. rex* (BMRP 2002.4.1, FMNH PR2081, LACM 23845). Both conditions are seen in *T. bataar* (PIN 551-2).

In plantar view, the cranial margin of the bone in *Alectrosaurus* is deeply concave ([Fig. 15C](#)). This condition is also seen in *Albertosaurus libratus* (CMN 11593) and in subadult *T. rex* (BMRP 2002.4.1). In contrast, the cranial margin is gently concave in *Bistahieversor* (NMMNH P-25049), *Albertosaurus* (AMNH FARB 5218, AMNH FARB 5255, CMN

11593, ROM 807, ROM 1247; [Fig. 15D](#)), *D. horneri* (MOR 590), and in *Tyrannosaurus* (FMNH PR2081, LACM 23845, MgD-I/29, PIN 551-2). The margin is convex in *Appalachiosaurus* (RMM 6670).

In plantar view, the lateral condyle in *Alectrosaurus* is narrower than the medial condyle ([Fig. 15C](#)); this condition is also seen in *Albertosaurus libratus* (CMN 2120), *D. horneri* (MOR 590), and *T. rex* (FMNH PR2081, LACM 23845). In contrast, the lateral condyle is wider than the medial condyle in *A. libratus* (ROM 1247; [Fig. 15D](#)) and *T. bataar* (PIN 551-2). The condyles are undifferentiated in *Appalachiosaurus* (RMM 6670), *Bistahieversor* (NMMNH P-25049), *Albertosaurus sarcophagus* (AMNH FARB 5218, AMNH FARB 5255), and in subadult *T. rex* (BMRP 2002.4.1). Variation is seen in *A. libratus*, where the condyles are approximately the same width in one specimen (CMN 11593).

The caudal margin of the joint surface in *Alectrosaurus* is bowed (convex) caudally ([Fig. 15C](#)). In contrast, this margin is transverse (straight) in *Albertosaurus sarcophagus* (AMNH FARB 5218, AMNH FARB 5255); sinuous in *Bistahieversor* (NMMNH P-25049), *Albertosaurus libratus* (CMN 2120, ROM 1247; [Fig. 15D](#)), *D. torosus* (CMN 350), and *T. bataar* (MgD-I/29, PIN 551-2); the margin is concave (bowed cranially) in *Appalachiosaurus* (RMM 6670), *Albertosaurus libratus* (CMN 11593), *D. horneri* (MOR 590), and also in *T. rex* (BMRP 2002.4.1, FMNH PR2081, LACM 23845).

In lateral view, the distal end of the bone in *Alectrosaurus* is slightly plantoflexed ([Figs. 1K, 15E, G](#)). This condition is also seen in *D. horneri* (MOR 590) and subadult *T. rex* (LACM 23845). In contrast, this region is strongly plantoflexed in *Appalachiosaurus* (RMM 6670), *Albertosaurus* (AMNH FARB 5218, AMNH FARB 5255, CMN 11593, ROM 807, ROM 1247; [Fig. 15F](#)), *Bistahieversor* (NMMNH P-25049), *Daspletosaurus torosus* (CMN 350), and in *Tyrannosaurus bataar* (PIN 551-2). Variation is seen in *T. rex* where a distinct angle is present in subadults (BMRP 2002.4.1) and adults (FMNH PR2081).

The condylar surface in *Alectrosaurus* is maximally exposed below both collateral ligament pits ([Figs. 1K, 15E, G](#)); this condition is also seen in *Tyrannosaurus* (FMNH PR2081, LACM 23845, PIN 551-2), and on the lateral side of *Albertosaurus libratus* (CMN 11593, ROM 1247; [Fig. 15F](#)). The condyle is evenly exposed in *Appalachiosaurus* (RMM 6670) and *Albertosaurus sarcophagus* (AMNH FARB 5218, AMNH FARB 5255). In contrast, the condylar surface shallows below the pit in *Bistahieversor* (NMMNH P-25049), and medially in *A. libratus* (CMN 2120, CMN 11593, ROM 1247; [Fig. 15H](#)). In *D. horneri* (MOR 590) it is maximally exposed laterally but not medially.

Digit III, Phalanx 2

The dorsolateral condyle in *Alectrosaurus* is pediculate ([Figs. 1K, 16D](#)); this condition is also seen in *T. rex* (FMNH PR2081). In contrast, the condyle is level with the dorsal surface in *Albertosaurus libratus* (ROM 1247; [Fig. 16E](#)), although a shallow groove elevates it above the external surface. The condyle is level with or elevated above the dorsal surface in *Appalachiosaurus* (RMM 6670), *Bistahieversor* (NMMNH P-25049), *Albertosaurus* (AMNH FARB 5218, AMNH FARB 5255, AMNH FARB 5397, AMNH FARB 5434, CMN 11593, ROM 807), and in *T. rex* (BMRP 2002.4.1, LACM 23845). Variation is seen in *T. bataar* (PIN 551-2), where the condyle is level or elevated. The condyle is elevated in *D. horneri* (MOR 590).

The dorsomedial condyle in *Alectrosaurus* is pediculate ([Fig. 16F](#)); this condition is also seen in *T. rex* (FMNH PR2081). In contrast, the condyle is level with the dorsal surface in *Albertosaurus libratus* (ROM 1247; [Fig. 16G](#)), although a shallow groove elevates it above its external margin. The condyle is level with or elevated above the dorsal surface in
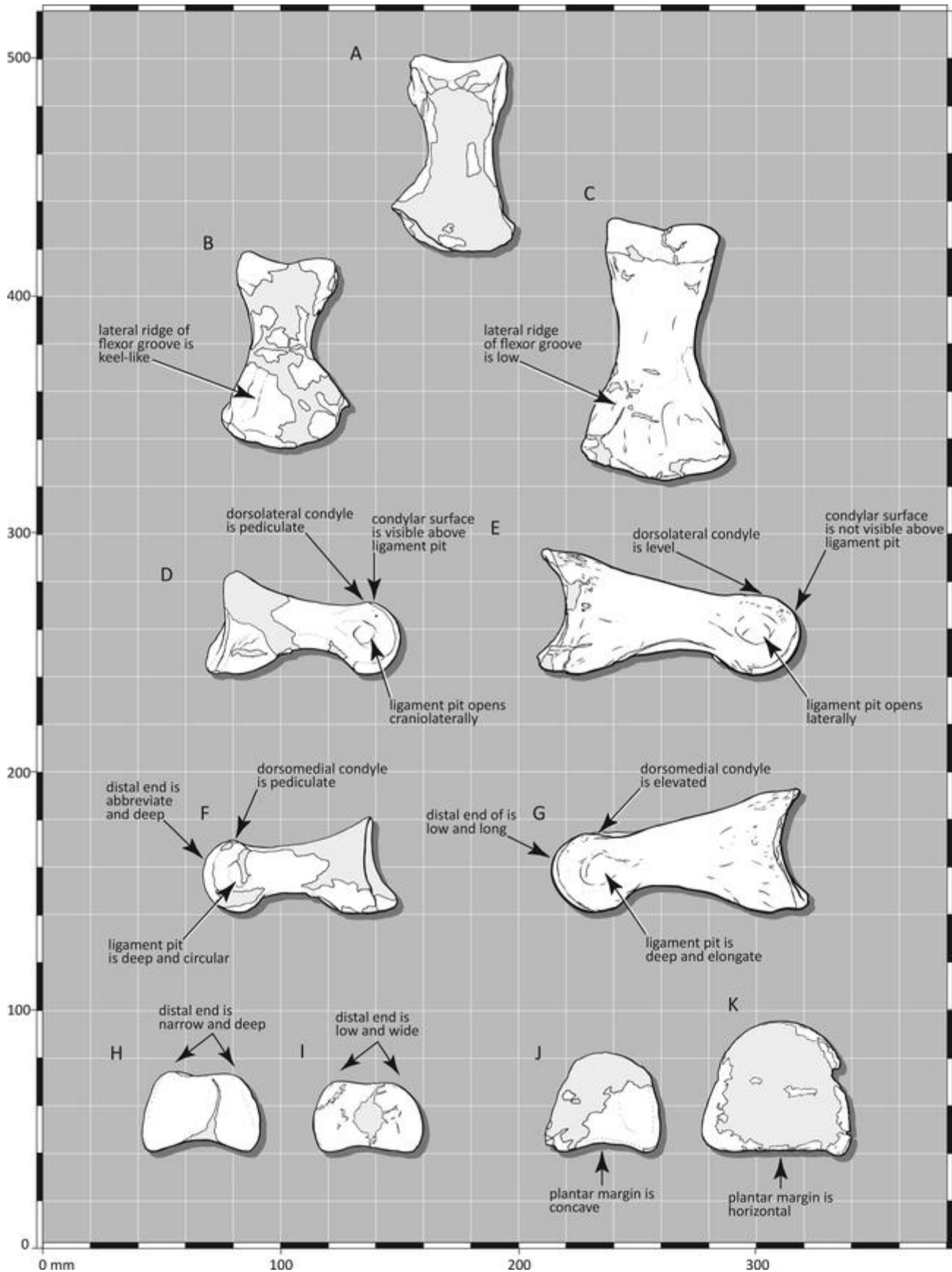
FIGURE 16. The phalanx III-2 of the lectotype (AMNH FARB 6554) of *Alectrosaurus olseni* in **A**, dorsal; **B**, plantar; **D**, lateral; **F**, medial; **H**, distal; and **J**, proximal views. Comparative illustrations of *Albertosaurus libratus* (ROM 1247) in **C**, plantar; **E**, lateral; **G**, medial; **I**, distal; and **K**, proximal views. Note the greatly dilated distal end of *Alectrosaurus* in contrast to *Albertosaurus*.

Appalachiosaurus (RMM 6670), *Bistahieversor* (NMMNH P-25049), *Albertosaurus* (AMNH FARB 5218, AMNH FARB 5255, AMNH FARB 5397, AMNH FARB 5434, CMN 11593, ROM 807), and in a subadult *T. rex* (BMRP 2002.4.1, LACM 23845). Individual variation is seen in *T. bataar* (PIN 551-2) where the condyle is level or elevated. The condyle is elevated in *D. horneri* (MOR 590).

The plantolateral condyle in *Alectrosaurus* is elevated (Figs. 1K, 16D); this condition is also seen in *Albertosaurus libratus* (CMN 2120, CMN 11593), *D. horneri* (MOR 590), and *T. rex* (BMRP 2002.4.1, FMNH PR2081). The plantomedial condyle in *Alectrosaurus* is elevated (Fig. 16F), which is also seen in *Albertosaurus libratus* (CMN 2120, CMN 11593), *D. horneri* (MOR 590), and in *T. rex* (BMRP 2002.4.1, FMNH PR2081). See taxonomic summary in Table S4. Measurements of III-2 are given in Table 1; polymorphic and ontogenetic characters are listed in Table S2 and Table S3, respectively.

In distal (=cranial) view, the distal condyles in *Alectrosaurus* are transversely narrow and relatively deep (h/w, 0.70; Fig. 16H); this is seen on one specimen of *A. libratus* (CMN 11593, 0.69). In contrast, the condyles are shallow and wide in *Appalachiosaurus* (RMM 6670, 0.63, 0.61), *Bistahieversor* (NMMNH P-25049, 0.66), *Albertosaurus* (AMNH FARB 5218; AMNH FARB 5255; AMNH FARB 5397; ROM 807; ROM 1247, 0.66; Fig. 16I), *D. horneri* (MOR 590: 0.64), and *Tyrannosaurus* (BMRP 2002.4.1, 0.63; FMNH PR2081, LACM 23845, PIN 551-2, 0.54).

In proximal view, the plantar margin in *Alectrosaurus* is concave (Fig. 16J); this condition is also seen in *Bistahieversor* (NMMNH P-25049), *D. horneri* (MOR 590), and *T. bataar* (PIN 551-2). In contrast, the plantar margin is trilobate in *Albertosaurus sarcophagus* (AMNH FARB 5218, AMNH FARB 5255, AMNH FARB 5397, CMN 2120, ROM 807) and *T. rex* (BMRP 2002.4.1, FMNH PR2081). Variation is seen in *A. libratus*, where the margin is trilobate (ROM 1247), horizontal (ROM 1247; Fig. 16K), or concave (CMN 11593).

In plantar view, the lateral-bounding ridge of the flexor groove in *Alectrosaurus* is keel-like (Fig. 16B). In contrast, the ridge is low in *Appalachiosaurus* (RMM 6670), *Bistahieversor* (NMMNH P-25049), *Albertosaurus* (AMNH FARB 5218, AMNH FARB 5255, AMNH FARB 5397, AMNH FARB 5434, CMN 11593, ROM 807, ROM 1247; Fig. 16C), and in *Tyrannosaurus* (BMRP 2002.4.1, FMNH PR2081, LACM 23845, PIN 551-2). An intermediate condition is seen in the type specimen of *A. libratus* (CMN 2120). The ridge is absent from *D. horneri* (MOR 590).

In lateral view, the condylar surface in *Alectrosaurus* is visible above the collateral ligament pit (Figs. 1K, 16D); this condition is also seen in *D. horneri* (MOR 590) and *T. rex* (BMRP 2002.4.1, FMNH PR2081). In contrast, the surface extends out of view craniodorsal to the pit in *Appalachiosaurus* (RMM 6670) and *Albertosaurus* (AMNH FARB 5218, AMNH FARB 5397, CMN 11593, ROM 1247; Fig. 16E). Both conditions are seen in *T. bataar* (PIN 551-2).

The lateral collateral ligament pit in *Alectrosaurus* opens craniolaterally (Figs. 1K, 16D); this is also seen in *T. rex* (BMRP 2002.4.1, FMNH PR2081, LACM 23845). In contrast, the pit opens laterally in *Appalachiosaurus* (RMM 6670), *Albertosaurus* (AMNH FARB 5218, AMNH FARB 5255, AMNH FARB 5397, AMNH FARB 5434, CMN 2120, CMN 11593, ROM 1247; Figure 16E), *D. horneri* (MOR 590), and in *T. bataar* (PIN 551-2).

In medial view, the collateral ligament pit in *Alectrosaurus* is deep (Fig. 16F); this condition is also seen in *Albertosaurus libratus* (AMNH FARB 5434, AMNH FARB 5458, AMNH FARB 5664, CMN 2120, CMN 11593, ROM 1247; Fig. 16G), *D. horneri* (MOR 590), *T. bataar* (PIN 551-2), and in subadult *T. rex* (BMRP 2002.4.1). In contrast, the pit is shallow in *Bistahieversor* (NMMNH P-25049), *A. sarcophagus* (AMNH FARB 5218, AMNH FARB 5255, AMNH FARB 5397), and in *T. rex* (FMNH PR2081, LACM 23845).

The medial collateral ligament pit in *Alectrosaurus* is craniocaudally abbreviate or circular (Fig. 16F); this condition is also seen in *Bistahieversor* (NMMNH P-25049) and in one specimen of *Albertosaurus libratus* (CMN 11593). In contrast, the pit is craniocaudally long in *Appalachiosaurus* (RMM 6670), *Albertosaurus* (AMNH FARB 5218, AMNH FARB 5255, AMNH FARB 5397, AMNH FARB 5434, AMNH FARB 5458, AMNH FARB 5664, CMN 2120, ROM 1247; Fig. 16G), *D. horneri* (MOR 590), and in *Tyrannosaurus* (BMRP 2002.4.1, FMNH PR2081, LACM 23845, PIN 551-2).

The distal (=cranial) end of the bone in *Alectrosaurus* is dorsoplantarly deep and craniocaudally short (Figs. 1K, 16D, F); this condition is also seen in *Appalachiosaurus* (RMM 6670), some *Albertosaurus libratus* (CMN 11593, ROM 1247), *D. horneri* (MOR 590), and in *T. bataar* (PIN 551-2). In contrast, the distal end is low and long in *Bistahieversor* (NMMNH P- 25049), and *Albertosaurus* (AMNH FARB 5218, AMNH FARB 5255, AMNH FARB 5397, AMNH FARB 5434, AMNH FARB 5458, AMNH FARB 5664, ROM 1247; Fig. 16E, G). Possible ontogenetic variation is present in *T. rex* where subadults (BMRP 2002.4.1, LACM 23845) have a low and long distal end whereas adults (FMNH PR2081) have a short and deep distal end.

Digit III, Phalanx 3

The dorsolateral condyle in *Alectrosaurus* is elevated (Figs. 1K, 17E); this condition is also seen in *Appalachiosaurus* (RMM 6670) and *D. horneri* (MOR 590). In contrast, the condyle is pediculate in *T. rex* (FMNH PR2081). Variation is seen in *T. bataar* (PIN 551-2), where the condyle is level or pediculate. Variation is also seen in *Albertosaurus sarcophagus*, where the condyle is on a low pedicle (AMNH FARB 5397) or it is level with the dorsal surface (AMNH FARB 5218, AMNH FARB 5255, ROM 807). Variation is seen in *A. libratus*, where the condyle is on a low pedicle (CMN 11593, ROM 1247; Fig. 17F) or it is elevated (AMNH FARB 5434, CMN 11593).

The dorsomedial condyle in *Alectrosaurus* is elevated; this condition is also seen in *Appalachiosaurus* (RMM 6670) and *D. horneri* (MOR 590). The condyle is on a low pedicle in *T. bataar* (PIN 551-2). Variation is seen in *Albertosaurus libratus*, where the condyle is on a low pedicle (CMN 11593, ROM 1247; Fig. 17H) or it is elevated (AMNH FARB 5434).

The plantar condyles in *Alectrosaurus* are elevated (Figs. 1K, 17E, G); this condition is also seen in *Albertosaurus libratus* (AMNH 5458, CMN 2120, CMN 11593, ROM 1247; Fig. 17F, H) and *D. horneri* (MOR 590). In contrast, the condyles are level in *T. bataar* (PIN 551-2). See Table S4 for taxonomic summary. Measurements of III-3 are given in Table 1; polymorphic and ontogenetic characters are listed in Table S2 and Table S3, respectively.

In proximal view, the phalanx in *Alectrosaurus* is narrow and deep (h/w: 0.77; Fig. 17I). In contrast, the proximal surface is low and wide in *Bistahieversor* (NMMNH P-25049, 0.66), *Albertosaurus* (AMNH FARB 5218; AMNH FARB 5255; AMNH FARB 5397; CMN 11593; ROM 807, 0.70), *D. horneri* (MOR 590: 0.72), and in *Tyrannosaurus* (FMNH PR2081; LACM 23845, 0.65; PIN 551-2, 0.61). Both states are seen in *A. libratus* (ROM 1247, 0.73, 0.80; Fig. 17J).

In distal view the bone in *Alectrosaurus* is low and wide (h/w, 0.71; Fig. 17K); this condition is also seen in *Appalachiosaurus* (RMM 6670), *Albertosaurus libratus* (CMN 11593, 0.72), *D. horneri* (MOR 590, 0.74), and *Tyrannosaurus* (FMNH PR2081; LACM 23845; PIN 551-2, 0.67). In contrast, the distal end is tall and narrow in some specimens of *A. libratus* (AMNH FARB 5434; ROM 1247, 0.78, 0.79; Fig. 17L). Variation is seen in *A. sarcophagus*, where the bone is low and wide (ROM 807, 0.67) or tall and narrow (AMNH FARB 5255, AMNH FARB 5397).
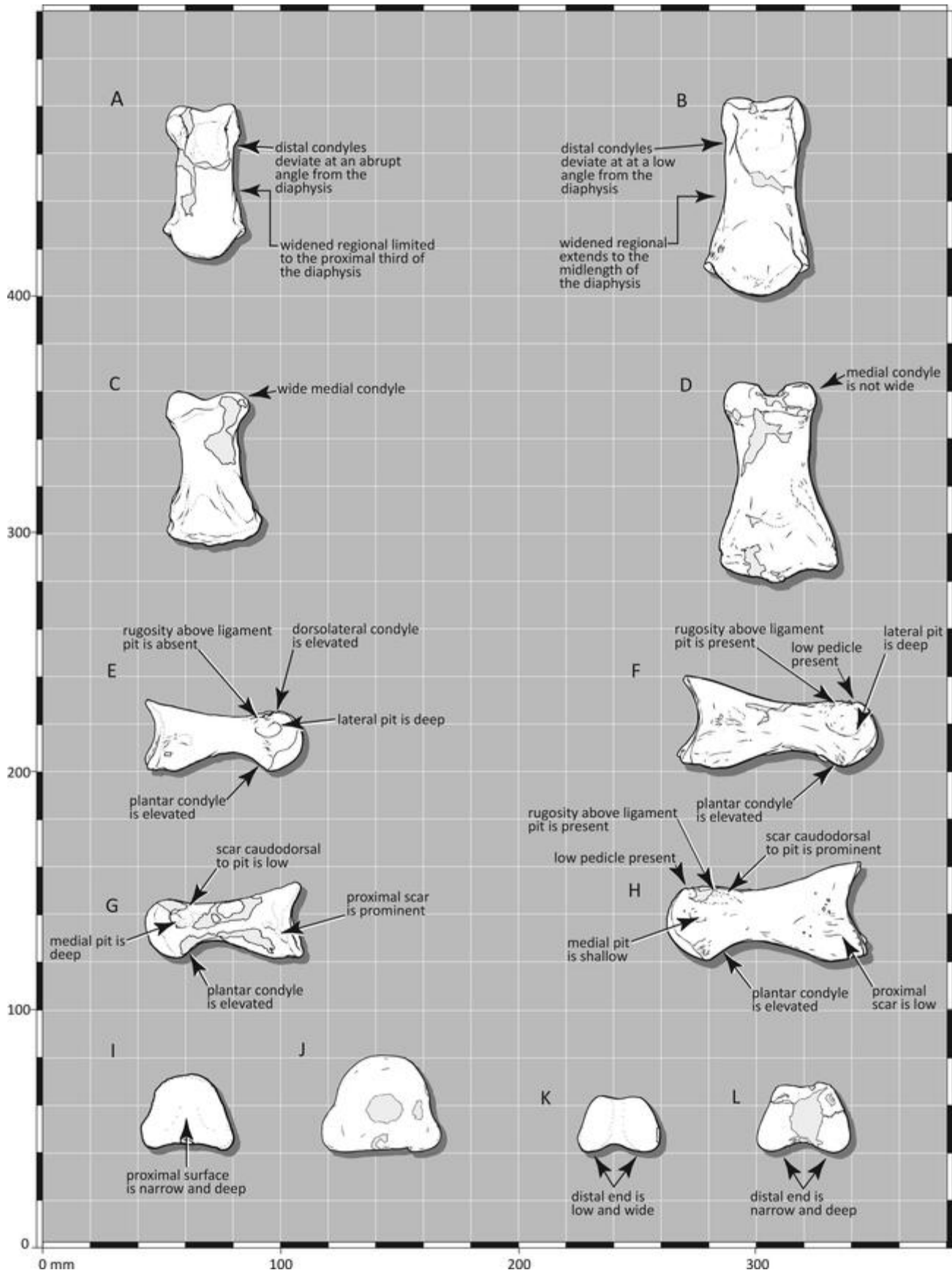
FIGURE 17. The phalanx III-3 of the lectotype (AMNH FARB 6554) of *Alectrosaurus olseni* in **A**, dorsal; **C**, plantar; **E**, lateral; **G**, medial; **I**, proximal; and **K**, distal views. Comparative illustrations of *Albertosaurus libratus* (ROM 1247) in **B**, dorsal; **D**, plantar; **F**, lateral; **H**, medial; **J**, proximal; and **L**, distal views. Note the generally dilated distal end of *Alectrosaurus* in contrast to *Albertosaurus*.

In dorsal and side views, rugosities above the collateral ligament pit in *Alectrosaurus* are absent (Figs. 1K, 17E, G). In contrast, rugosities are present in *Albertosaurus* (AMNH FARB 5218, AMNH FARB 5255, AMNH FARB 5397, AMNH FARB 5434, CMN 11593, ROM 807, ROM 1247; Fig. 17F, H), *D. horneri* (MOR 590), and *T. bataar* (PIN 551-2).

In dorsal view, the wide caudal region in *Alectrosaurus* is restricted to the caudal third of the shaft, producing a columnar and parallel-sided shaft (Fig. 17A). In contrast, the expanded caudal region extends to the shaft midlength to produce a stout shaft in *Appalachiosaurus* (RMM 6670), *Bistahieversor* (NMMNH P-25049), *Albertosaurus* (AMNH FARB 5218, AMNH FARB 5255, AMNH FARB 5397, AMNH FARB 5434, CMN 2120, CMN 11593, ROM 807, ROM 1247; Fig. 17B), *D. horneri* (MOR 590), and *Tyrannosaurus* (FMNH PR2081, LACM 23845, MgD-I/36, PIN 551-2).

In dorsal view, the distal condyles in *Alectrosaurus* deviate abruptly from the lateral margin of the bone such that the distal end of the phalanx is expanded transversely (Fig. 17A, C); this is also seen in *Appalachiosaurus* (RMM 6670) and in one specimen of *Albertosaurus libratus* (CMN 11593). In contrast, the condyles do not deviate abruptly in *Bistahieversor* (NMMNH P-25049), *Albertosaurus* (AMNH FARB 5218, AMNH FARB 5255, AMNH FARB 5397, AMNH FARB 5434, ROM 807, ROM 1247; Fig. 17B, D), *D. horneri* (MOR 590), and *T. bataar* (MgD-I/36, PIN 551-2). Variation is seen in *T. rex*, where in some specimens (LACM 23845) the condyles deviate at a shallow angle, whereas in others (FMNH PR2081) they deviate at an abrupt angle.

In plantar view, the cranioplantar surfaces of the condyles in *Alectrosaurus* are transversely strongly convex. In contrast, the condyles are weakly convex in *Appalachiosaurus* (RMM 6670), *Albertosaurus* (AMNH FARB 5218, AMNH FARB 5255, AMNH FARB 5397, AMNH FARB 5434, CMN 2120, CMN 11593, ROM 807), *D. horneri* (MOR 590), and *Tyrannosaurus* (FMNH PR2081, LACM 23845, PIN 551-2).

In plantar view, the condyles in *Alectrosaurus* are separated by a deep groove (Fig. 17C); this condition is also seen in *T. bataar* (PIN 551-2). In contrast, the groove is shallow in *Appalachiosaurus* (RMM 6670), *Albertosaurus* (AMNH FARB 5218, AMNH FARB 5255, AMNH FARB 5397, AMNH FARB 5434, CMN 2120, CMN 11593, ROM 807), *D. horneri* (MOR 590), and in *T. rex* (FMNH PR2081, LACM 23845). Variation is seen in *A. libratus*, where the groove is deep in a subadult (ROM 1247).

The collateral margins of the distal joint surface in *Alectrosaurus* diverge abruptly such that the medial condyle is widened (Fig. 17A, C); this condition is also seen in *Appalachiosaurus* (RMM 6670) and *Tyrannosaurus* (FMNH PR2081, LACM 23845, PIN 551-2). In contrast, the condyles are subparallel and the medial condyle is not greatly widened in *Bistahieversor* (NMMNH P-25049) and *D. horneri* (MOR 590). Variation is present in *Albertosaurus*, where the margins diverge abruptly (AMNH FARB 5397, AMNH FARB 5434, CMN 11593) or are subparallel (AMNH FARB 5255, ROM 1247; Fig. 17B, D). In one specimen of *A. libratus* (CMN 11593), the medial condyle is not widened.

The collateral ligament pits in *Alectrosaurus* are almost equally deep (Fig. 17E, G); this condition is also seen in *Bistahieversor* (NMMNH P-25049) and in *Tyrannosaurus* (FMNH PR2081, LACM 23845, PIN 551-2). In contrast, the lateral pit is shallow in *Appalachiosaurus* (RMM 6670). Variation is seen in *Albertosaurus* where the medial pit is shallow (ROM 807, ROM 1247; Fig. 17H) or deep (AMNH FARB 5255, AMNH FARB 5397, AMNH FARB 5434, CMN 11593). The medial pit is slightly shallower than the lateral pit in *D. horneri* (MOR 590).

In medial view, the scar caudodorsal to the collateral ligament pit in *Alectrosaurus* is low (Fig. 17G). In contrast, the scar is prominent in *Albertosaurus* (AMNH FARB 5255, AMNH FARB 5397, AMNH FARB 5434, CMN 11593, ROM 807, ROM 1247; Fig. 17H) and *Tyrannosaurus* (FMNH PR2081, PIN 551-2).

In *Alectrosaurus* a low ridge extends craniodorsally from the proximal joint surface above the plantar margin of the bone (Fig. 17G); this condition is also seen in *D. horneri* (MOR 590). In contrast, this scar is a low mound in *T. bataar* (PIN 551-2). The scar is low in some specimens of *Albertosaurus* (ROM 1247; Fig. 17H) or absent from *T. rex* (FMNH PR2081). Variation is seen in *A. sarcophagus*, where the scar is present (AMNH FARB 5397), absent (AMNH FARB 5255, ROM 807), or a mound is in that position (AMNH FARB 5218).

Digit III, Phalanx 4

In side view, the flexor tubercle in *Alectrosaurus* is hypertrophied and almost reaches the level of the proximal joint surface (Figs. 1L, 18D, F, G; Mader and Bradley, 1989). In contrast, the flexor tubercle is low and does not approach the caudal margin in *Albertosaurus libratus* (CMN 2120, ROM 1247; Fig. 18E), *D. horneri* (MOR 590), or *T. rex* (LACM 23845). Measurements of III-4 are given in Table 1.

In medial view, the proximodorsal surface in *Alectrosaurus* is concave above the joint surface (Fig. 18F); this condition is also seen in *Albertosaurus libratus* (ROM 1247). In dorsal view, the axis of the median ridge is medially offset from the midline proximally (Fig. 18A). Although there is damage to this region in AMNH FARB 6554, it does not seem to have affected the position of the ridge. In contrast, the ridge is on the midline in *A. libratus* (ROM 1247; Fig. 18B).

Metatarsal IV

The distal condyles in *Alectrosaurus* are pediculate, except for the plantomedial condyle (Figs. 1G, 19A, H, J). The condyles are not pediculate in other tyrannosauroid taxa (Fig. 19I, K), although the plantar condyles are subtly pediculate in adult *D. horneri* (MOR 1130). The plantomedial condyle in subadult *T. rex* (BMRP 2002.4.1) is level with the plantar surface of the bone. The plantolateral condyle is elevated in *Daspletosaurus torosus* (CMN 350). The plantar condyles are elevated in the type specimen of *Albertosaurus libratus* (CMN 2120). See taxonomic summary in Table S4. Measurements of metatarsal IV are given in Table 1; polymorphic and ontogenetic characters are listed in Table S2 and Table S3, respectively.

In plantar view, the bases of the distal condyles in *Alectrosaurus* are parallel with each other (Fig. 19D); this condition is also seen in *T. bataar* (PIN 551-2). In contrast, the bases diverge in *Bistahieversor* (NMMNH P-25049), *Appalachiosaurus* (Fig. 19E), *Albertosaurus* (AMNH FARB 5255, AMNH FARB 5432, CMN 2120, CMN 11315, CMN 11593, ROM 1247, TMP 1981.010.0001, TMP 1984.064.0001, TMP 1984.144.0001, TMP 1994.012.0602), *D. horneri* (MOR 590, MOR 1130), and *Tyrannosaurus* (BMRP 2002.4.1, FMNH PR2081, MgD-I/29, PIN 551-2).

The plantomedial heel in *Alectrosaurus* is massively developed and rugose (Fig. 19D); this condition is also seen in *Daspletosaurus* (CMN 350, MOR 590, MOR 1130) and *Tyrannosaurus* (CM 9380, FMNH PR2081, MgD-I/206, PIN 551-2; Maleev, 1974: fig. 4). In contrast, the heel of *Albertosaurus* (AMNH FARB 5255, AMNH FARB 5229, AMNH FARB 6554 CMN 11315, TMP 1981.010.0001, TMP 1984.064.0001, TMP 1984.144.0001) is not massive or rugose. The heel is moderately developed in *Bistahieversor* (NMMNH P-25049), *Appalachiosaurus* (RMM 6670) (Fig. 19E), and in subadult *T. rex* (BMRP 2002.4.1). A heel is absent from *Dryptosaurus* (AMNH FARB 2438). Variation is seen in *Albertosaurus libratus*, where the heel is reduced (CMN 2120, ROM 1247) or massive (AMNH FARB 5432, AMNH FARB 5423, CMN 2120, CMN 11593, TMP 1994.012.0602).
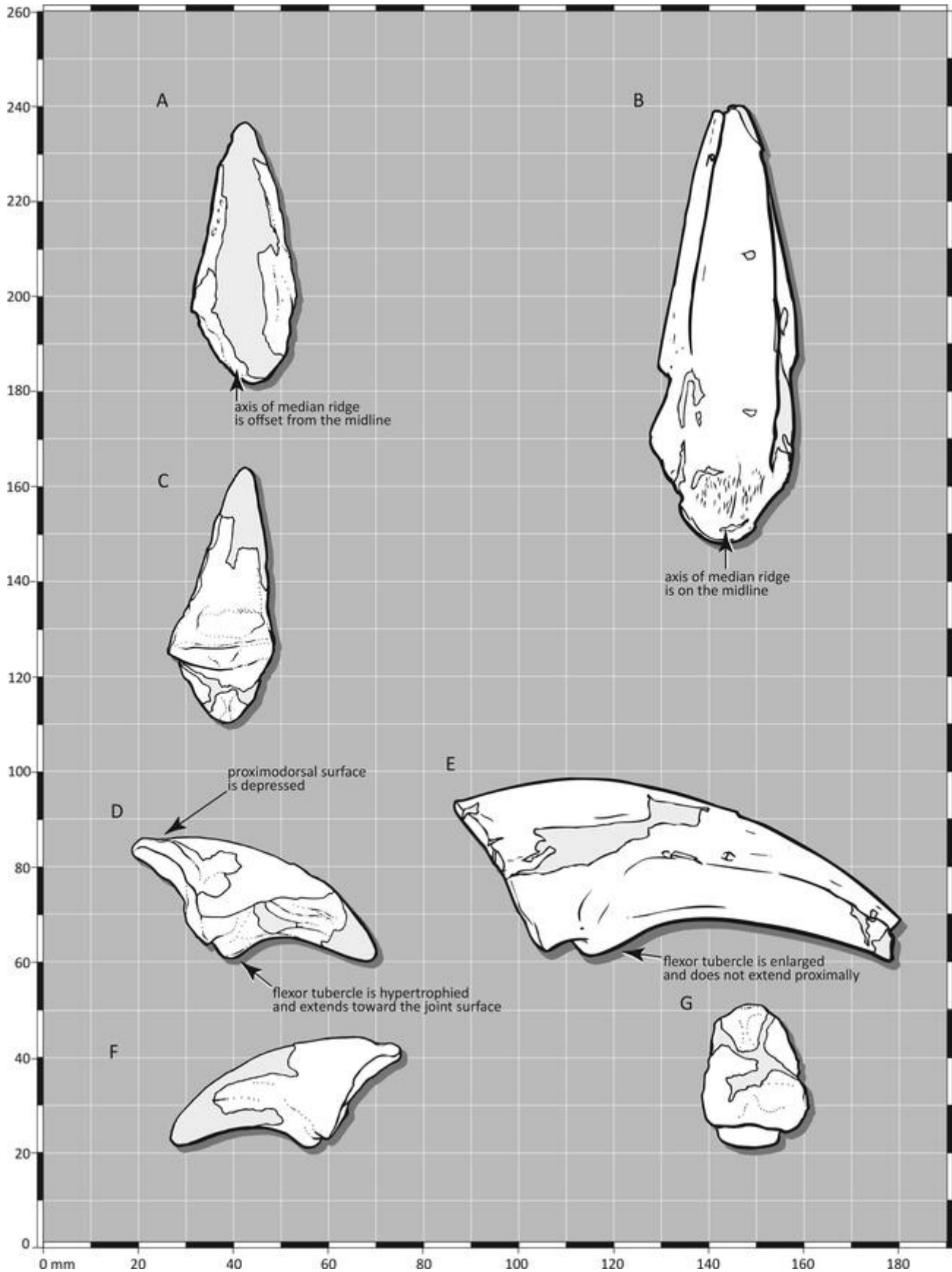
FIGURE 18. The phalanx III-4 of the lectotype (AMNH FARB 6554) of *Alectrosaurus olseni* in **A**, dorsal; **C**, plantar; **D**, lateral; **F**, medial; and **G**, proximal views. Comparative illustrations of *Albertosaurus libratus* (ROM 1247) in **B**, dorsal; and **E**, lateral views.
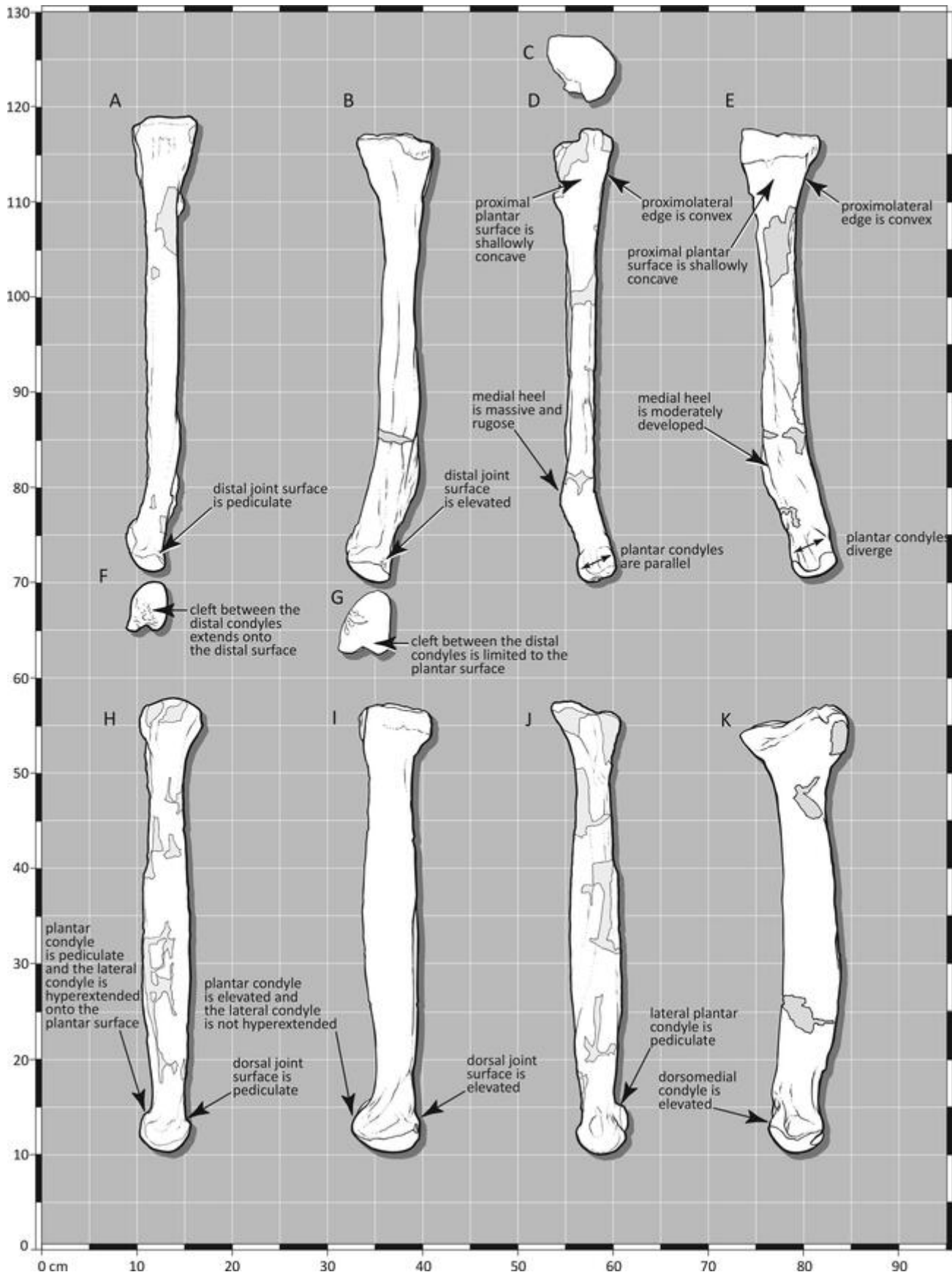
FIGURE 19. Metatarsal IV of the lectotype (AMNH FARB 6554) of *Alectrosaurus olseni* in **A**, dorsal; **C**, proximal; **D**, plantar; **F**, distal; **H**, lateral; and **J**, medial views. Comparative illustrations of *Appalachiosaurus montgomeriensis* (RMM 6670) in **B**, dorsal; **E**, plantar; **G**, distal; **I**, lateral; and **K**, medial views. The *A. montgomeriensis* illustrations are modified after Carr, Williamson, and Schwimmer (2005).

The plantar surface in *Alectrosaurus* is only slightly concave proximally (Fig. 19D); this condition is also in *Dryptosaurus aquilunguis* (AMNH FARB 2438), *Appalachiosaurus* (RMM 6670) (Fig. 19E), *Bistahieversor* (NMMNH P-25049), *Albertosaurus libratus* (AMNH FARB 5432), *Alioramus* (IGM 100/1844), and *T. bataar* (MgD-I/29, PIN 551-2). In contrast, the proximal fossa is deep in several specimens of *Albertosaurus* (CMN 11315, CMN 11593, ROM 807, TMP 1994.012.0602), *Daspletosaurus* (CMN 350, MOR 590), and in *T. rex* (BMRP 2002.4.1, CM 9380). Variation is seen in *T. bataar* (MgD-I/206), where the surface is deeply concave in some specimens.

The proximolateral edge of the bone in *Alectrosaurus* is convex in frontal section (Fig. 19D); this condition is seen in *Dryptosaurus* (AMNH FARB 2438), *Appalachiosaurus* (RMM 6670) (Fig. 19E), *Albertosaurus* (AMNH FARB 5432, TMP 1981.010.0001, TMP 1984.064.0001, TMP 1994.012.0602), *Alioramus* (IGM 100/1844), *Daspletosaurus torosus* (CMN 350), and in *Tyrannosaurus* (CM 9380, MgD-I/29, MgD-I/206). In contrast, the edge is a narrow strut in *Bistahieversor* (NMMNH P-25049), *A. libratus* (CMN 11593), and subadult *T. rex* (BMRP 2002.4.1). Variation is seen in *Albertosaurus sarcophagus*, where the edge is convex (CMN 11315) and narrow (CMN 11315, ROM 807); both conditions are also seen in *T. bataar* (MgD-I/76, PIN 551-2). Ontogenetic variation is seen in *D. horneri* where it is convex in subadults (MOR 590), whereas it is narrow in adults (MOR 1130).

The shaft of the bone in *Alectrosaurus* is transversely narrow (Fig. 19A, D; midlength w/l, 0.06); this condition is also seen in *Appalachiosaurus* (0.09), *Bistahieversor* (NMMNH P-25049), *Albertosaurus* (CMN 2120, 0.10; CMN 11593, 0.11; TMP 1984.064.0001, 0.09), *D. horneri* (MOR 590, 0.12; MOR 1130, 0.09), *T. bataar* (PIN 551-2), and in subadult *T. rex* (BMRP 2002.4.1, 0.08). The shaft is wide in other *A. sarcophagus* (ROM 807, 0.14), *Daspletosaurus torosus* (CMN 350, 0.13), and *T. rex* (CM 9380; FMNH PR2081, 0.20; Brochu, 2003). Variation is seen in *A. libratus* where the diaphysis is narrow (AMNH FARB 5423; ROM 1247, 0.09) or wide (AMNH FARB 5432).

The plantar lateral condyle in *Alectrosaurus* is hyperextended onto the plantar surface and in lateral view it extends almost vertically (Figs. 1F, 19D, H, J). This condition is also seen in *Albertosaurus libratus* (CMN 11593), where it extends caudodorsally at a steep angle, and also in *Daspletosaurus torosus* (CMN 350), where the condyle extends from caudoplantarly to craniodorsally. In contrast, the condyle is not hyperextended and it extends caudodorsally in *Appalachiosaurus* (RMM 6670) (Fig. 19E, I), *Bistahieversor* (NMMNH P-25049), *Albertosaurus* (AMNH FARB 5255, AMNH FARB 5664, AMNH FARB 5458, CMN 2120, CMN 11315, CMN 11593, ROM 807, ROM 1247, TMP 1981.010.0001, TMP 1984.064.0001, TMP 1984.144.0001, TMP 1994.012.0602), *D. horneri* (MOR 590, MOR 1130), and *Tyrannosaurus* (BMRP 2002.4.1, CM 9380, FMNH PR2081, MgD-I/29, MgD-I/206, PIN 551-2).

In *Alectrosaurus*, the cleft that separates the distal condyles in lateral view extends craniodistally between the distal condyles (Fig. 1G, 19F). In contrast, the cleft is restricted to the plantar surface in *Appalachiosaurus* (Fig. 19G), *Albertosaurus* (AMNH FARB 5255, CMN 2120, CMN 11315, CMN 11593, TMP 1984.064.0001, TMP 1984.144.0001, TMP 1994.012.0602), *Daspletosaurus* (CMN 350, MOR 590, MOR 1130), and in subadult *T. rex* (BMRP 2002.4.1).

Digit IV, Phalanx 1

The dorsolateral condyle in *Alectrosaurus* is pediculate (Figs. 1L, 20E). The external edge of the condyle is pediculate in *T. rex* (FMNH PR2081). The condylar region is pediculate across the midline in *D. horneri* (MOR 590) and the lateral condyle is elevated. In contrast, the condyle is level with the dorsal surface in *Bistahieversor* (NMMNH P-25049) and *Albertosaurus libratus* (CMN 11593, ROM 1247; Fig. 20F). Variation is seen in *A. libratus* (CMN 11593) and in *T. bataar* (PIN 551-2) where the condyle is elevated or pediculate. In subadult *T. rex* (BMRP 2002.4.1) the condyle is elevated.

The dorsomedial condyle in *Alectrosaurus* is pediculate (Fig. 20G). In contrast, the condyle is elevated in *Bistahieversor* (NMMNH P-25049), *Albertosaurus libratus* (CMN 11593, ROM 1247; Fig. 20H), and in subadult *T. rex* (BMRP 2002.4.1). The joint surface is level with the dorsal surface of the bone in *A. sarcophagus* (AMNH FARB 5218, AMNH FARB 5255). Variation is seen in *T. bataar* (PIN 551-2) where the condyle is elevated or pediculate.

The plantar condyles are elevated (Figs. 1L, 20E, G); this condition is seen in other tyrannosauroids. The plantomedial condyle is steeply elevated in one specimen of *A. libratus* (CMN 11593). See taxonomic summary in Table S4. Measurements of IV-1 are given in Table 1; polymorphic and ontogenetic characters are listed in Table S2 and Table S3, respectively.

In proximal view, the joint surface in *Alectrosaurus* is deeply concave (Fig. 20I); this condition is also seen in *Bistahieversor* (NMMNH P-25049) and in *D. horneri* (MOR 590). This surface is shallowly concave in *Albertosaurus sarcophagus* (AMNH FARB 5218, AMNH FARB 5255), *Tyrannosaurus* (FMNH PR2081, PIN 551-2), and in *A. libratus* (CMN 2120, ROM 1247; Fig. 20J). In subadult *T. rex* (BMRP 2002.4.1) the joint surface is shallowly concave laterally and deeply concave medially.

In proximal view, the lateral margin in *Alectrosaurus* is concave dorsolaterally and plantolaterally (Fig. 20I). In contrast, the margin in *Appalachiosaurus* (RMM 6670), *Albertosaurus sarcophagus* (AMNH FARB 5218, AMNH FARB 5255), and in *T. rex* (FMNH PR2081) is uniformly convex. Both conditions are seen in *T. bataar* (PIN 551-2). In *A. libratus* (CMN 11593, ROM 1247; Fig. 20J) and subadult *T. rex* (BMRP 2002.4.1), the margin is convex plantolaterally and gently concave dorsolaterally above midheight, thereafter it is convex. The plantolateral margin is convex in the type specimen of *A. libratus* (CMN 2120). In *D. horneri* the dorsolateral margin is strongly convex and the plantolateral margin is subtly convex (MOR 590).

The medial margin in *Alectrosaurus* is gently convex at midheight (Fig. 20I); this condition is also seen in *Bistahieversor* (NMMNH P-25049) and *T. rex* (FMNH PR2081). In contrast, the medial margin is strongly convex in *Appalachiosaurus* (RMM 6670) and *Albertosaurus* (AMNH FARB 5218, CMN 11593, ROM 1247; Fig. 20J), *D. horneri* (MOR 590), and in *T. rex* (BMRP 2002.4.1, FMNH PR2081). In *T. bataar* (PIN 551-2), the margin is concave on the left.

In distal view, the medial condyle in *Alectrosaurus* is slightly deeper than the lateral condyle (Fig. 20K). In contrast, the medial condyle is significantly deeper than the lateral condyle in *Appalachiosaurus*, *Bistahieversor* (NMMNH P-25049), *Albertosaurus* (AMNH FARB 5218, AMNH FARB 5255, CMN 11593), *D. horneri* (MOR 590), and in *Tyrannosaurus* (BMRP 2002.4.1, FMNH PR2081, LACM 23845, PIN 551-2).

In lateral view, the collateral ligament pit in *Alectrosaurus* is shallow, but the circumference is well defined (Figs. 1L, 20E); this condition is also seen in *Appalachiosaurus* (RMM 6670) and *Bistahieversor* (NMMNH P-25049). In contrast, the pit is shallow and the circumference is poorly defined in *Albertosaurus* (AMNH FARB 5255, AMNH FARB 5458, CMN 11593, ROM 1247; Fig. 20F), *D. horneri* (MOR 590), and *T. rex* (BMRP 2002.41.1, FMNH PR2081, LACM 23845). In *T. bataar* (PIN 551-2), the pit is well defined, but it is shallow on the left. In contrast, the pit is deep and well defined in large *A. libratus* (CMN 2120, CMN 11593).
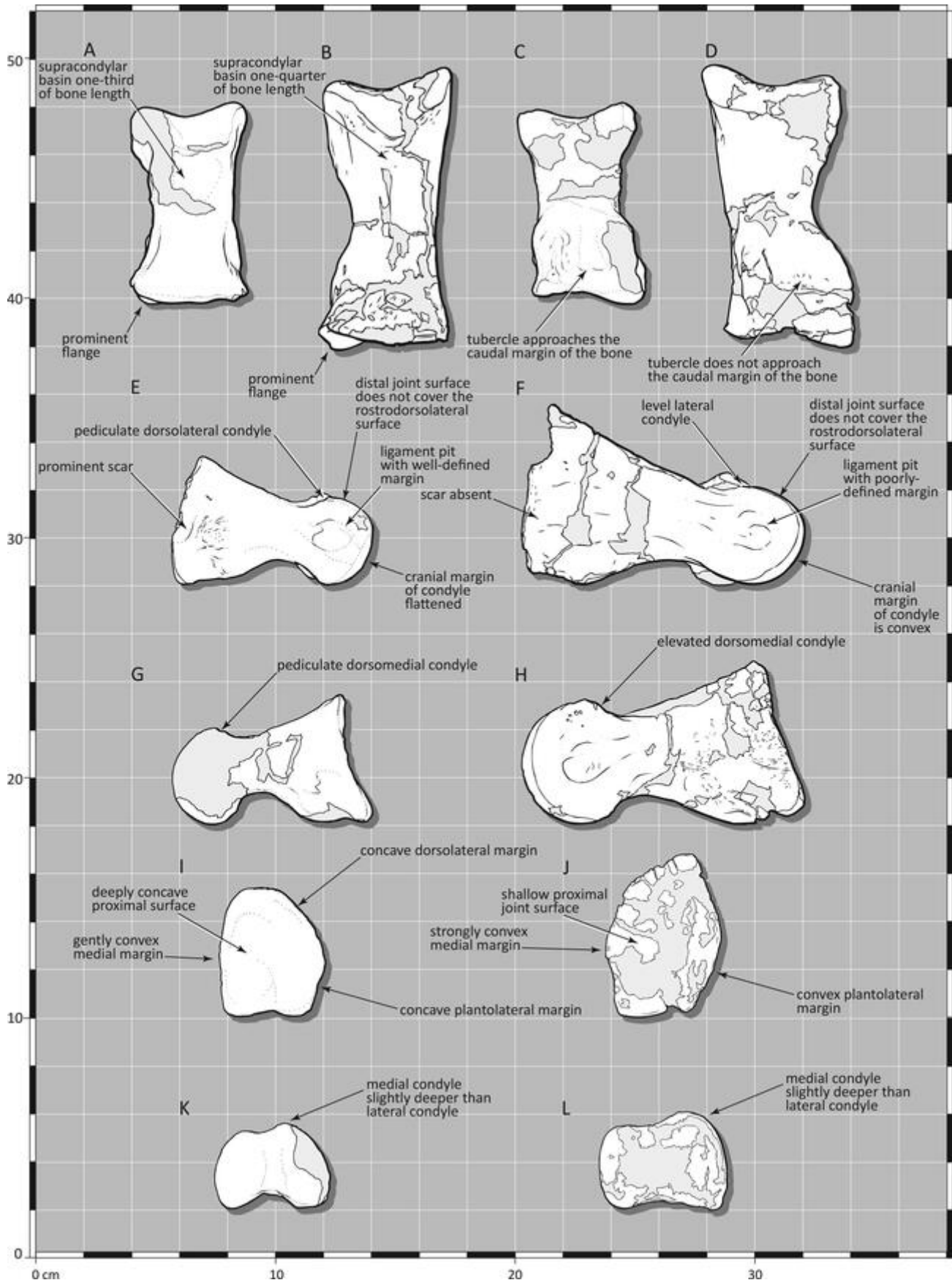
FIGURE 20. The phalanx IV-1 of the lectotype (AMNH FARB 6554) of *Alectrosaurus olseni* in **A**, dorsal; **C**, plantar; **E**, lateral; **G**, medial; **I**, proximal; and **K**, distal views. Comparative illustrations of *Albertosaurus libratus* (ROM 1247) in **B**, dorsal; **D**, plantar; **F**, lateral; **H**, medial; **J**, proximal; and **L**, distal views. Note the generally dilated distal end of *Alectrosaurus* in contrast to *Albertosaurus*.
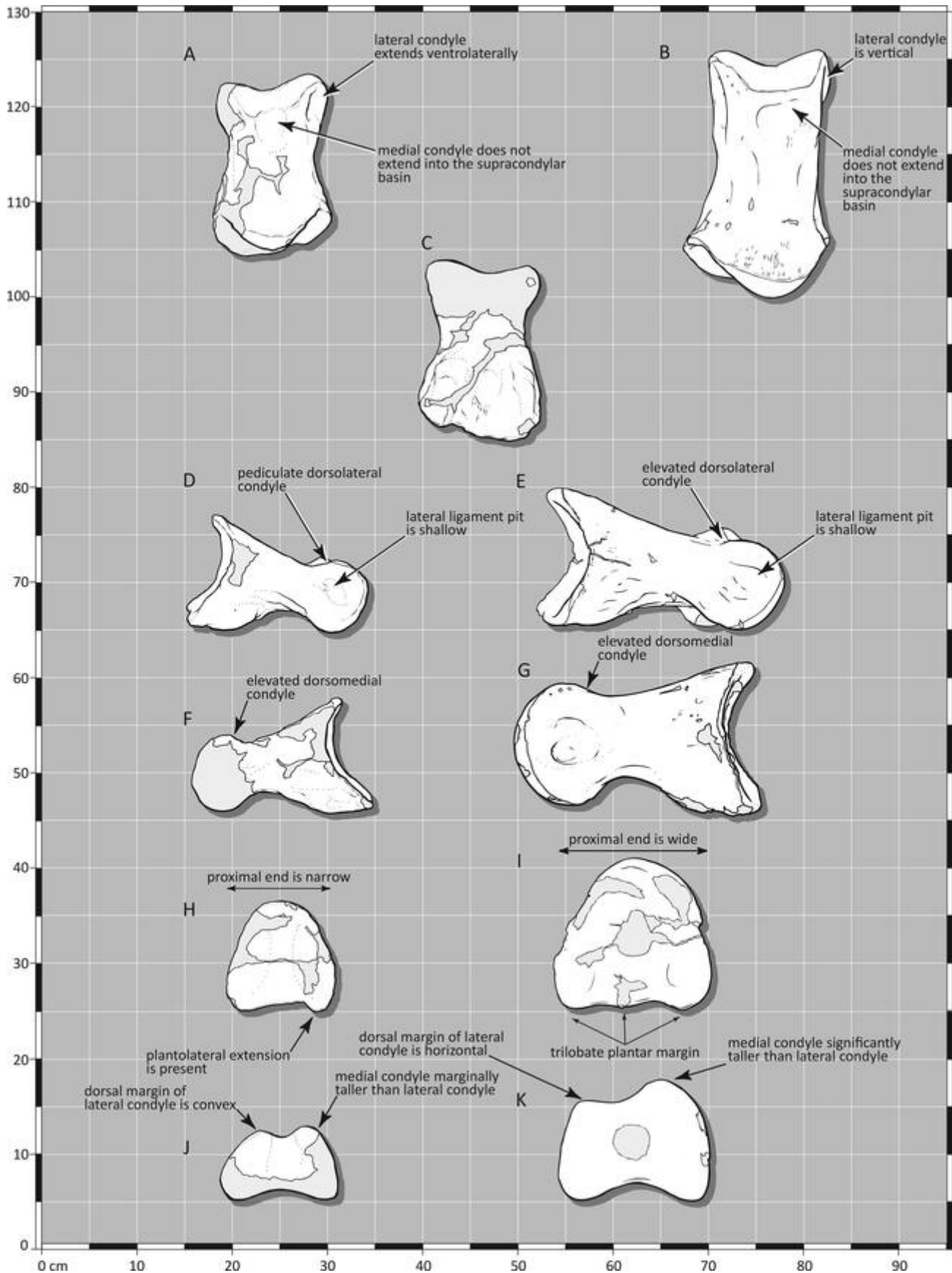
FIGURE 21. The phalanx IV-2 of the lectotype (AMNH FARB 6554) of *Alectrosaurus olseni* in **A**, dorsal; **C**, plantar; **D**, lateral; **F**, medial; **H**, proximal; and **J**, distal views. Comparative illustrations of *Albertosaurus libratus* (ROM 1247) in **B**, dorsal; **E**, lateral; **G**, medial; **I**, proximal; and **K**, distal views. Note the generally dilated distal end of *Alectrosaurus* in contrast to *Albertosaurus*.

The distal margin of the lateral condyle in *Alectrosaurus* is flattened (Figs. 1L, 20E). In contrast, the cranial margin is convex in *Appalachiosaurus* (RMM 6670), *Bistahieversor* (NMMNH P-25049), *Albertosaurus* (AMNH FARB 5218, AMNH FARB 5255, CMN 11593, ROM 1247; Fig. 20F), *D. horneri* (MOR 590), and in *Tyrannosaurus bataar* (PIN 551-2). Variation is seen in *T. rex*, where the margin is convex (BMRP 2002.4.1, LACM 23845) or flattened (FMNH PR2081).

The distal joint surface in *Alectrosaurus* does not lap onto the craniodorsolateral surface of the bone (Figs. 1L, 20E); this condition is also seen in *Appalachiosaurus*, *Albertosaurus libratus* (AMNH FARB 5458, ROM 1247; Fig. 20F), and subadult *T. rex* (BMRP 2002.4.1). In contrast, the joint surface covers the craniodorsolateral surface of the bone in *Bistahieversor* (NMMNH P-25049), *A. sarcophagus* (AMNH FARB 5218, AMNH FARB 5255), and *Tyrannosaurus* (FMNH PR2081, LACM 23845, PIN 551-2).

The scar on the shaft that is cranial to the proximal end of the bone in *Alectrosaurus* is prominent (Figs. 1L, 20E); this condition is also seen in *T. bataar* (PIN 551-2). In contrast, the scar is low in *Appalachiosaurus* (RMM 6670), *Bistahieversor* (NMMNH P-25049), *Albertosaurus libratus* (CMN 2120, CMN 11593), *A. sarcophagus* (AMNH FARB 5218, AMNH FARB 5255), and in *T. rex* (FMNH PR2081). The scar is absent from subadult *A. libratus* (ROM 1247; Fig. 20F), *D. horneri* (MOR 590), and subadult *T. rex* (BMRP 2002.4.1).

In dorsal view, the plantomedial flange of the proximal joint surface in *Alectrosaurus* extends caudally beyond the caudal margin of the proximal end of the bone (Figs. 1L, 20A); this is also seen in *Appalachiosaurus* (RMM 6670), *Bistahieversor* (NMMNH P-25049), *Albertosaurus libratus* (CMN 11593, ROM 1247; Fig. 20B), *T. bataar* (MgD-I/29, PIN 551-2), and subadult *T. rex* (BMRP 2002.4.1). In contrast, the flange extends only marginally such that the caudoplantar margin is transversely oriented in *A. sarcophagus* (AMNH FARB 5218, AMNH FARB 5255) or subtly concave as seen in *D. horneri* (MOR 590). In *T. rex*, the proximal end of the bone is separated from the lateral flange by a concavity, but it does not extend beyond the caudal edge of the bone (FMNH PR2081).

The supracondylar basin in *Alectrosaurus* occupies approximately one third of the shaft length (Fig. 20A); this is also seen in *Appalachiosaurus* (RMM 6670) and in *Albertosaurus libratus* (CMN 11593). In contrast, the basin is restricted to one quarter of shaft length in *Bistahieversor* (NMMNH P-25049), *Albertosaurus* (AMNH FARB 5218, AMNH FARB 5255, ROM 1247; Fig. 20B), *D. horneri* (MOR 590), and in *Tyrannosaurus* (BMRP 2002.4.1, FMNH PR2081, MgD-I/29, MgD-I/36, PIN 551-2).

In plantar view, in *Alectrosaurus* a low tubercle is present between the collateral ridges that approaches the caudal margin of the bone (Fig. 20C); this is also seen in *D. horneri* (MOR 590) and *Tyrannosaurus* (FMNH PR2081, PIN 551-2). In contrast, the tubercle is far cranial to the caudal margin of the bone in *Bistahieversor* (NMMNH P-25049) and *Albertosaurus* (AMNH FARB 5218, AMNH FARB 5255, CMN 2120, CMN 11593, ROM 1247; Fig. 20D). Variation is seen in *T. bataar*, where the tubercle is positioned cranially in some specimens (MgD-I/29).

Digit IV, Phalanx 2

The dorsolateral condyle in *Alectrosaurus* is pediculate (Figs. 1L, 21D). In contrast, the condyle is elevated in *Daspletosaurus* (CMN 350, MOR 590) and *T. rex* (BMRP 2002.4.1, FMNH PR2081, LACM 23845); the condyle is level with the dorsal surface in *Appalachiosaurus* (RMM 6670), *Bistahieversor* (NMMNH P-25049), and in *Albertosaurus sarcophagus* (AMNH FARB 5218, AMNH FARB 5255). Variation is seen in *T. bataar* (PIN 551-2) where the condyle is elevated or pediculate.

Variation is also seen in *A. libratus* where the condyle is elevated (AMNH FARB 5458, CMN 2120, CMN 11593, ROM 1247; Fig. 21E) or level (AMNH FARB 5434).

The dorsomedial condyle in *Alectrosaurus* is elevated (Fig. 21F); this condition is also seen in *Albertosaurus libratus* (CMN 2120, CMN 11593, ROM 1247; Fig. 21G), *Daspletosaurus* (CMN 350, MOR 590), *T. bataar* (PIN 551-2), and *T. rex* (BMRP 2002.4.1, FMNH PR2081). The plantolateral condyle in *Alectrosaurus* is elevated (Figs. 1L, 21D); this is also seen in *Albertosaurus libratus* (AMNH FARB 5458, CMN 2120, CMN 11593, ROM 1247; Fig. 21E) and *Daspletosaurus* (CMN 350, MOR 590). Unfortunately, the plantomedial condyle is missing. See Table S4 for a taxonomic summary. Measurements of digit IV-2 are given in Table 1; polymorphic and ontogenetic characters are listed in Table S2 and Table S3, respectively.

In proximal view the bone in *Alectrosaurus* is narrow (Fig. 21H). In contrast, the proximal surface is wide in *Bistahieversor* (NMMNH P-25049), *Albertosaurus* (AMNH FARB 5218, AMNH FARB 5255, CMN 11593, ROM 1247; Fig. 21I), *D. horneri* (MOR 590), and in *T. rex* (BMRP 2002.4.1, FMNH PR2081; LACM 23845). Both conditions are seen in *T. bataar* (PIN 551-2).

The plantar margin in *Alectrosaurus* is horizontal, with a plantar extension at its lateral edge (Fig. 21H); this condition is also seen in *Bistahieversor* (NMMNH P-25049). A distinct lateral extension and a subtle medial extension is seen in *D. horneri* (MOR 590), In contrast, the margin is concave, but the extension is present in *Appalachiosaurus* (RMM 6670). Also, the plantar margin is trilobate, with plantar extensions at the medial and lateral edges and on the midline in *Albertosaurus* (AMNH FARB 5218, AMNH FARB 5231, CMN 11593, ROM 1247; Fig. 21I) and in subadult *T. rex* (BMRP 2002.4.1). An indistinct trilobate condition is seen in the type specimen of *A. libratus* (CMN 2120).

In distal view, the medial condyle in *Alectrosaurus* is not significantly taller than the lateral condyle (Fig. 21J). In contrast, the medial condyle is significantly taller than the lateral condyle in *Appalachiosaurus* (RMM 6670), *Bistahieversor* (NMMNH P-25049), *Albertosaurus sarcophagus* (AMNH FARB 5218, AMNH FARB 5255), *Daspletosaurus* (CMN 350, MOR 590), and *T. bataar* (PIN 551-2). Variation is seen in *A. libratus*, where the condyle is either not taller than the lateral condyle (AMNH FARB 5434) or it is taller than the lateral condyle (CMN 11593, ROM 1247; Fig. 21K). Variation is seen in *T. rex* where the medial condyle is tall in a subadult (BMRP 2002.4.1, LACM 23845), but it is not taller in an adult (FMNH PR2081).

The dorsal margin of the lateral condyle in *Alectrosaurus* is convex (Fig. 21J); this is also seen in *Albertosaurus sarcophagus* (AMNH FARB 5218, AMNH FARB 5255), *D. horneri* (MOR 590), and *Tyrannosaurus* (BMRP 2002.4.1, FMNH PR2081, LACM 23845, PIN 551-2). In contrast, the dorsal margin of the condyle is horizontal in *Appalachiosaurus* (RMM 6670), *Bistahieversor* (NMMNH P-25049), *Albertosaurus libratus* (AMNH FARB 5434, CMN 11593, ROM 1247; Fig. 21K), and *Daspletosaurus torosus* (CMN 350).

In lateral view, the collateral ligament pit in *Alectrosaurus* is very shallow (Figs. 1L, 21D); this condition is also seen in *D. horneri* (MOR 590) and in subadult *T. rex* (BMRP 2002.4.1). In *Albertosaurus libratus* (AMNH FARB 5434), the pit is flat, almost level with the lateral surface of the bone. The pit is shallow in *Appalachiosaurus* (RMM 6670) and in *Albertosaurus libratus* (AMNH FARB 5458, CMN 11593, ROM 1247; Fig. 21E), whereas it is deep in the type specimen of *A. libratus* (CMN 2120), *Daspletosaurus torosus* (CMN 350), and *Tyrannosaurus* (FMNH PR2081, LACM 23845, MgD-I/29, PIN 551-2). Variation is seen in *A. sarcophagus* where the pit is deep (AMNH FARB 5255) or shallow (AMNH FARB 5218).
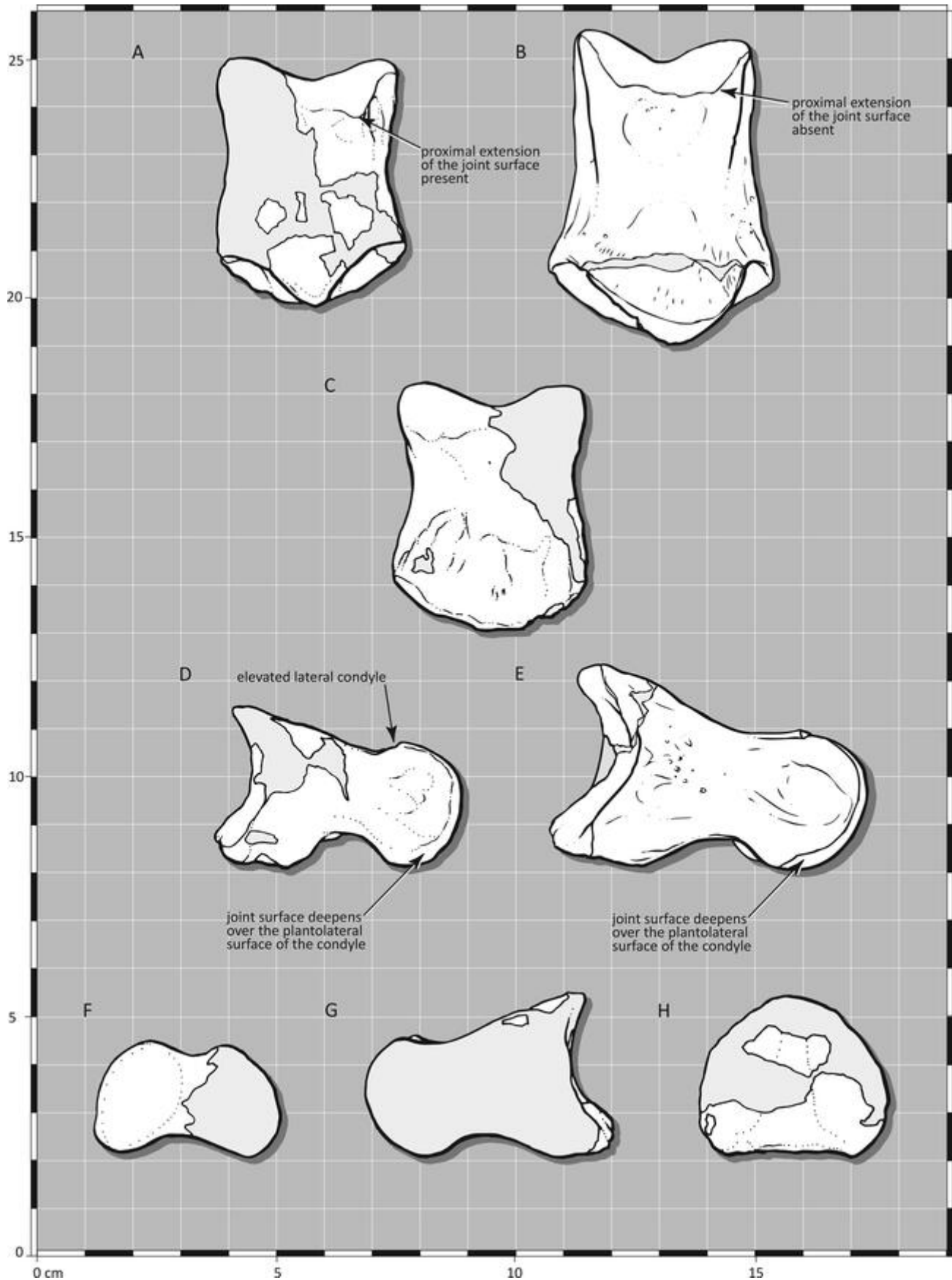
FIGURE 22. The phalanx IV-3 of the lectotype (AMNH FARB 6554) of *Alectrosaurus olseni* in **A**, dorsal; **C**, plantar; **D**, lateral; **F**, distal; **G**, medial; and **H**, proximal views. Comparative illustrations of *Albertosaurus libratus* (ROM 1247) in **B**, dorsal; and **E**, lateral views. Note the generally dilated distal end of *Alectrosaurus* in contrast to *Albertosaurus*.

In dorsal view, the lateral condyle in *Alectrosaurus* extends lateroplantarly such that it is almost entirely visible (Fig. 21A). In contrast, the condyle does not extend into view in *Appalachiosaurus* (RMM 6670), *Bistahieversor* (NMMNH P-25049), *Albertosaurus sarcophagus* (AMNH FARB 5218, AMNH FARB 5255), *D. horneri* (MOR 590), and in *Tyrannosaurus* (BMRP 2002.4.1, FMNH PR2081, LACM 23845, PIN 551-2). Variation is seen in *A. libratus*, where the condyle extends marginally into view (CMN 2120, ROM 1247; Fig. 21B) or it does not extend into view (AMNH FARB 5434).

The distal condylar surface of the medial condyle in *Alectrosaurus* does not intrude onto the supracondylar basin (Fig. 21A); this condition is also seen in *Appalachiosaurus* (RMM 6670), *Bistahieversor* (NMMNH P-25049), *Albertosaurus* (AMNH FARB 5218, AMNH FARB 5255, CMN 11593, ROM 1247; Fig. 21B), *Daspletosaurus* (CMN 350, MOR 590), and in *Tyrannosaurus* (BMRP 2002.4.1, FMNH PR2081, LACM 23845, PIN 551-2). In contrast, the condyle extends into the basin in large specimens of *Albertosaurus* (AMNH FARB 5218, AMNH FARB 5434).

Digit IV, Phalanx 3

The dorsolateral condyle in *Alectrosaurus* is elevated (Figs. 1L, 22D); this condition is also seen in *Bistahieversor* (NMMNH P-25049), *Albertosaurus libratus* (CMN 2120, CMN 11593, ROM 1247; Fig. 22E), *D. horneri* (MOR 590), and in *T. bataar* (PIN 551-2). Variation is seen in *T. rex*, where the condyle is elevated in subadults (BMRP 2002.4.1, LACM 23845) whereas it is pediculate in an adult (FMNH PR2081). Variation is seen in *A. sarcophagus* where the condyle is pediculate (AMNH FARB 5218, AMNH FARB 5397) or level (AMNH FARB 5255). Unfortunately, the dorsomedial condyle in *Alectrosaurus* is missing.

The plantolateral condyle in *Alectrosaurus* is elevated (Figs. 1L, 22D); this condition is also seen in *Albertosaurus libratus* (CMN 2120, CMN 11593, ROM 1247; Fig. 22E), *D. horneri* (MOR 590), *T. bataar* (PIN 551-2), and in subadult *T. rex* (BMRP 2002.4.1). Variation is seen in *A. sarcophagus*, where the condyle is pediculate (AMNH FARB 5218, AMNH FARB 5397) or level (AMNH FARB 5255) with the plantar surface. Unfortunately, the plantomedial condyle in *Alectrosaurus* is missing; see Table S4 for a taxonomic summary. Measurements of IV-3 are in Table 1; polymorphic and ontogenetic characters are listed in Table S2 and Table S3, respectively.

In lateral view, the joint surface in *Alectrosaurus* is deep beneath the collateral ligament pit (Figs. 1L, 22D); this condition is also seen in subadult *Albertosaurus libratus* (ROM 1247; Fig. 22E), *D. horneri* (MOR 590), possibly *T. rex* (FMNH PR2081), and in *T. bataar* (PIN 551-2). In contrast, the joint surface is shallow in *Bistahieversor* (NMMNH P-25049) and in subadult *T. rex* (BMRP 2002.4.1). Variation is seen in *A. sarcophagus*, where the surface is deep (AMNH FARB 5397) or shallow (AMNH FARB 5218, AMNH FARB 5255); and in *A. libratus*, where the surface is shallow (CMN 2120, CMN 11593).

In dorsal view, the caudodorsal corner of the lateral condyle in *Alectrosaurus* extends caudolaterally beyond the caudal margin of the joint surface (Fig. 22A). A similar extension is present on the medial condyle in *Bistahieversor* (NMMNH P-25049) and *Albertosaurus sarcophagus* (AMNH FARB 5218, AMNH FARB 5397). In contrast, an extension is absent from *A. libratus* (ROM 1247; Fig. 22B), *D. horneri* (MOR 590), and *Tyrannosaurus* (BMRP 2002.4.1, LACM 23845, PIN 551-2).

Digit IV, Phalanx 4

The dorsolateral condyle in *Alectrosaurus* is pediculate (Figs. 1L, 23D); this condition is also seen in *Albertosaurus libratus*

(AMNH FARB 5458, CMN 11593, ROM 1247; Fig. 23E) and *D. horneri* (MOR 590). In contrast, the condyle is elevated in the type specimen of *A. libratus* (CMN 2120) and *T. bataar* (PIN 551-2). The lateral dorsal condyle is level dorsally in *Appalachiosaurus* (RMM 6670), *Bistahieversor* (NMMNH P-25049), *Albertosaurus sarcophagus* (AMNH FARB 5218), and *T. rex* (LACM 23845); in two specimens of *A. sarcophagus* (AMNH FARB 5255, AMNH FARB 5397), the condyle is level dorsally. The dorsal margin extends cranioplantarly to the condyle surface in *Appalachiosaurus* (RMM 6670). The dorsomedial condyle in *Alectrosaurus* is elevated (Fig. 23F), as in *T. bataar* (PIN 551-2), whereas the condyle is pediculate in *Albertosaurus libratus* (ROM 1247; Fig. 23G) and *D. horneri* (MOR 590). Variation is seen in one specimen of *A. libratus* (CMN 11593), where it is elevated or on a stout pedicle.

The plantolateral condyle in *Alectrosaurus* is pediculate (Figs. 1L, 23D). Variation is seen in *T. bataar* (PIN 551-2), where the condyle is level or pediculate. This condyle is elevated in *A. libratus* (CMN 11593, ROM 1247; Fig. 23E), *Daspletosaurus* (CMN 350, MOR 590), and subadult *T. rex* (BMRP 2002.4.1). In *A. sarcophagus* (AMNH FARB 5255, AMNH FARB 5397), the condyle is pediculate. The plantomedial condyle in *Alectrosaurus* is elevated (Fig. 23F); this condition is also seen in *Albertosaurus libratus* (CMN 2120, CMN 11593, ROM 1247; Fig. 23G) *D. horneri* (MOR 590), and subadult *T. rex* (BMRP 2002.4.1). In contrast, the condyle is level with the plantar surface in *T. bataar* (PIN 551-2). See Table S4 for a taxonomic summary. Measurements of IV-4 are given in Table 1; polymorphic characters are listed in Table S2.

In proximal view, in *Alectrosaurus* the bone bears deep and wide lateral and medial flanges (Fig. 23H); this condition is also seen in *Appalachiosaurus* (RMM 6670), and *Tyrannosaurus* (LACM 23845, PIN 551-2). In contrast, the flanges are low and narrow in *Bistahieversor* (NMMNH P-25049), *Albertosaurus* (AMNH FARB 5218, AMNH FARB 5255, AMNH FARB 5397, CMN 11593, ROM 1247; Fig. 23I), and in *Daspletosaurus* (CMN 350, MOR 590). The medial flange is narrow in subadult *T. rex* (BMRP 2002.4.1).

In distal view, the lateral condyle in *Alectrosaurus* is significantly deeper than the medial condyle (Fig. 23J); this condition is also seen in *D. horneri* (MOR 590) and *Tyrannosaurus* (LACM 23845, PIN 551-2). In contrast, the lateral condyle is not much taller than the medial condyle in *Bistahieversor* (NMMNH P-25049), *Albertosaurus libratus* (CMN 11593, ROM 1247; Fig. 23K), and in subadult *T. rex* (BMRP 2002.4.1). The lateral condyle is lower than the medial condyle in *Appalachiosaurus* (RMM 6670) and *Albertosaurus sarcophagus* (AMNH FARB 5218, AMNH FARB 5255, AMNH FARB 5397).

In *Alectrosaurus* a narrow cleft separates the distal condyles (Fig. 23A, B). In contrast, a wide gap separates the condyles in *Appalachiosaurus* (RMM 6670), *Bistahieversor* (NMMNH P-25049), *Albertosaurus* (AMNH FARB 5255, AMNH FARB 5397, CMN 2120, CMN 11593), *D. horneri* (MOR 590), and *Tyrannosaurus* (BMRP 2002.4.1, LACM 23845, PIN 551-2).

The plantar surfaces of the condyles in *Alectrosaurus* are bulbous (Fig. 23B); this condition is also seen in *Appalachiosaurus* (RMM 6670), *T. bataar* (PIN 551-2), and in *Bistahieversor* (NMMNH P-25049). In contrast, the condyles are flat or gently convex in *Albertosaurus libratus* (CMN 2120, CMN 11593, ROM 1247; Fig. 23C), *Daspletosaurus* (CMN 350, MOR 590), and subadult *T. rex* (BMRP 2002.4.1, LACM 23845). Variation is seen in *A. sarcophagus*, where the condyles are bulbous (AMNH FARB 5397) or flat (AMNH FARB 5218, AMNH FARB 5255).

In medial view, the axis of the collateral ligament pit in *Alectrosaurus* extends craniodorsally (Fig. 23F); this condition is also seen in *Appalachiosaurus* (RMM 6670), and *T. rex* (LACM 23845). In contrast, the axis extends cranioplantarly in *Bistahieversor* (NMMNH P-25049), *Albertosaurus sarcophagus*
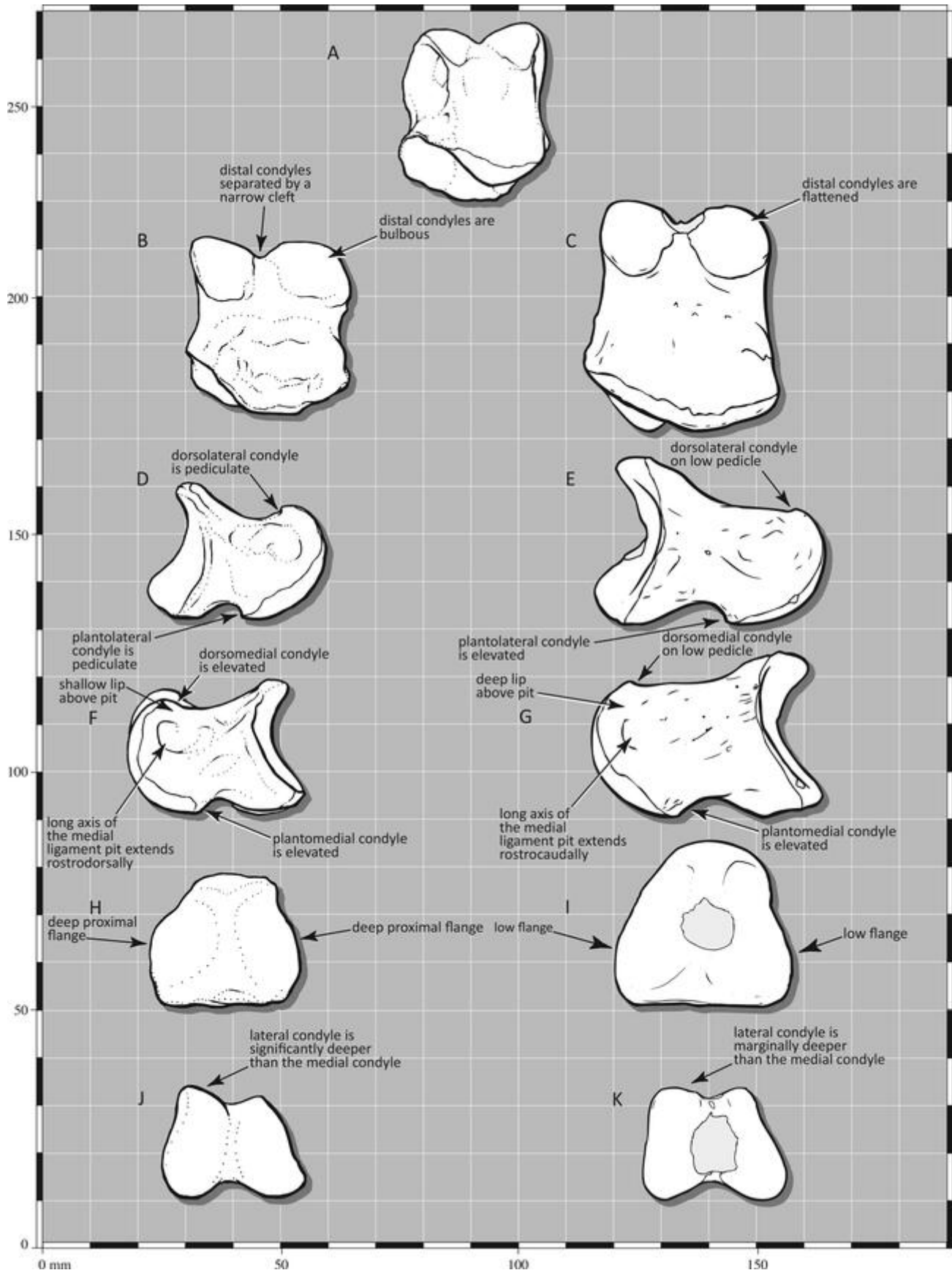
FIGURE 23. The phalanx IV-4 of the lectotype (AMNH FARB 6554) of *Alectrosaurus olseni* in **A**, dorsal; **B**, plantar; **D**, lateral; **F**, medial; **H**, proximal; and **J**, distal views. Comparative illustrations of *Albertosaurus libratus* (ROM 1247) in **C**, plantar; **E**, lateral; **G**, medial; **I**, proximal; and **K**, distal views. Note the greatly dilated distal end of *Alectrosaurus* in contrast to *Albertosaurus*.
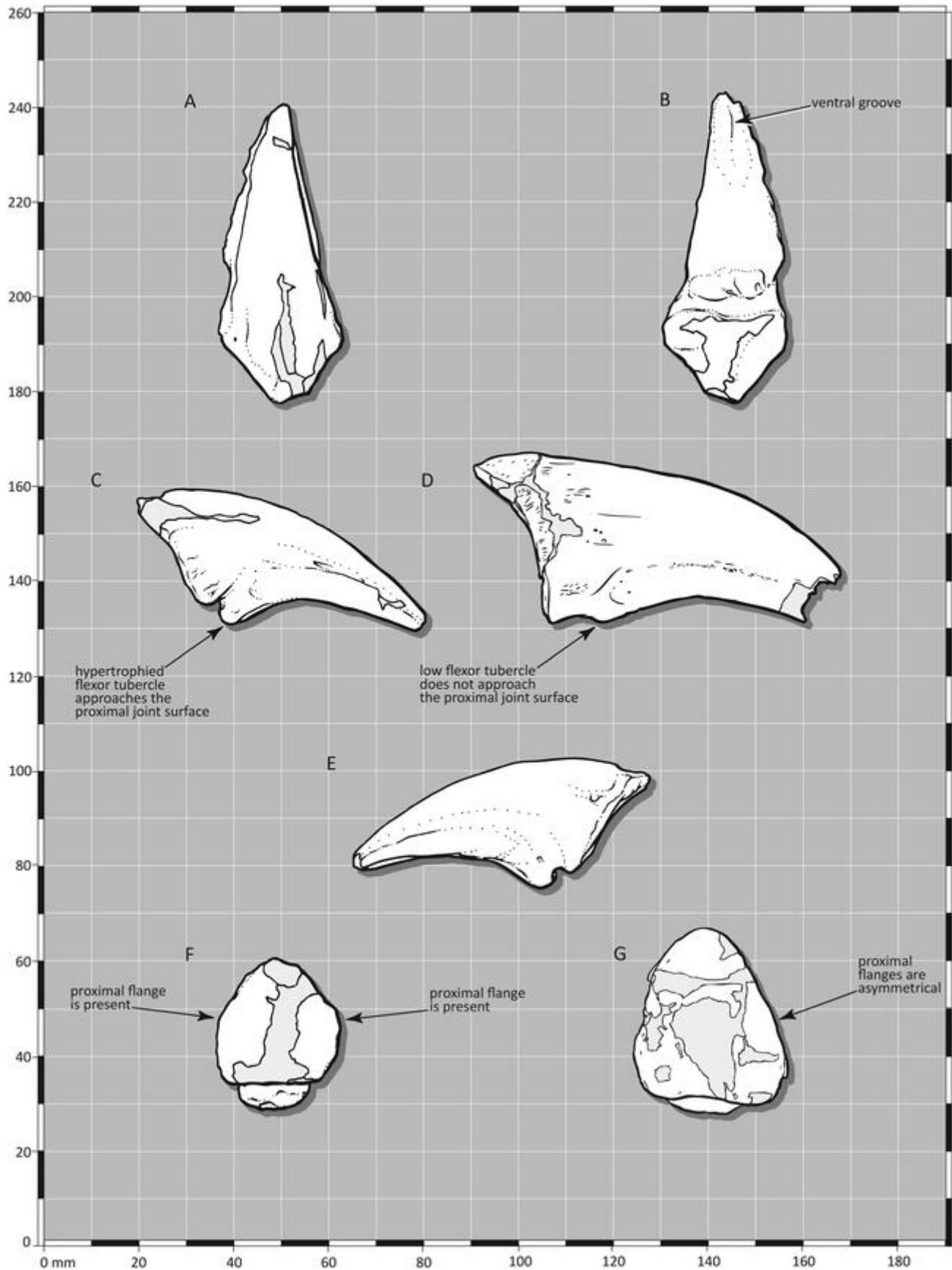
FIGURE 24. The phalanx IV-5 of the lectotype (AMNH FARB 6554) of *Alectrosaurus olseni* in **A**, dorsal; **B**, plantar; **C**, lateral; **E**, medial; and **F**, proximal views. Comparative illustrations of *Albertosaurus libratus* (ROM 1247) in **D**, lateral; and **G**, proximal views.
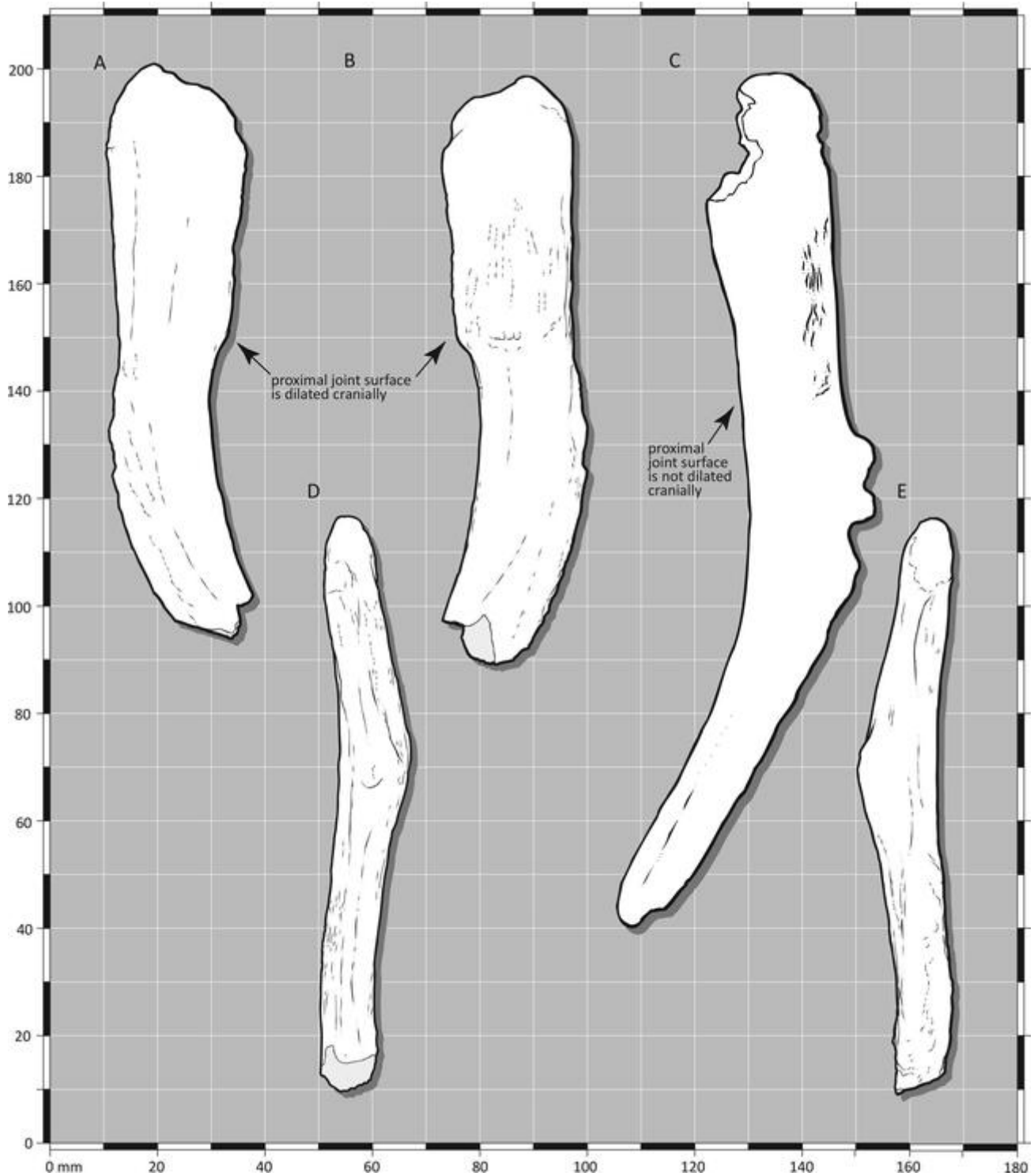
FIGURE 25. Metatarsal V of the lectotype (AMNH FARB 6554) of *Alectrosaurus olseni* in **A**, lateral; **B**, medial; **D**, cranial; and **E**, plantar views. Comparative illustration of *Albertosaurus sarcophagus* (CMN 11315) in **C**, medial view.

(AMNH FARB 5218, AMNH FARB 5255, AMNH FARB 5397), and subadult *T. rex* (BMRP 2002.4.1). The long axis extends craniocaudally in *A. libratus* (CMN 11593, ROM 1247; Fig. 23G) and in *Daspletosaurus* (CMN 350, MOR 590). Individual variation is seen in *T. bataar* (PIN 551-2) where the axis extends cranioplantarly or craniocaudally.

The ridge above the medial collateral pit in *Alectrosaurus* is dorsoplantarly shallow (Fig. 23F); this condition is also seen in *Albertosaurus libratus* (CMN 11593), *Daspletosaurus torosus* (CMN 350). In contrast, the ridge is deep in *Appalachiosaurus* (RMM 6670), *Bistahieversor* (NMMNH P-25049), *Albertosaurus* (AMNH FARB 5218, AMNH FARB 5255, AMNH FARB 5397,

CMN 2120, ROM 1247; Fig. 23G), *D. horneri* (MOR 590), and *T. bataar* (PIN 551-2).

Digit IV, Phalanx 5

In plantar view, a longitudinal groove excavates the distal third of the ungual in *Alectrosaurus* (Fig. 24B); a shallow groove is seen in *D. horneri* (MOR 590). In contrast, a plantar groove is absent from the unguals of *Bistahieversor* (NMMNH P-25049: D II, III), *Albertosaurus libratus* (CMN 11593, ROM 1247: D I, II, III), and *Tyrannosaurus* (BMRP 2002.4.1: D IV; FMNH PR2081: D II; PIN 551-2: D II, D III). Measurements of IV-5 are in Table 1.

In lateral view, the flexor tubercle in *Alectrosaurus* is large and it nearly reaches the level of the proximal joint surface (Figs. 1K, 24C, E, F) (Mader and Bradley, 1989). As noted above, this condition is unique among tyrannosauroids except for *T. bataar*. In *Albertosaurus libratus* (ROM 1247; Fig. 24D, G), the tubercle is large, but it does not extend to the proximal surface; in the type specimen (CMN 2120) the tubercle is low. In one specimen of *A. libratus* (CMN 11593), *D. horneri* (MOR 590), and *T. bataar*, the tubercle is large and approaches, but does not reach, the proximal joint surface (MgD-I/29).

In proximal view, the joint surface in *Alectrosaurus* is symmetrical, owing to the presence of dorsoplantarly deep lateral and medial flanges (Fig. 24F); this condition is also seen in *T. rex* (BMRP 2002.4.1, FMNH PR2081). In contrast, this condition is not seen in *Bistahieversor* (NMMNH P-25049). The flanges are asymmetrically developed in *Albertosaurus libratus* (CMN 11593, ROM 1247; Fig. 24G). Flanges are absent from *D. horneri* (MOR 590), but notches in the lateral and medial margins are present.

Metatarsal V

The joint surface for metatarsal IV in *Alectrosaurus* is dilated (widened) such that it emarginates the cranial margin of the bone in lateral and medial views (Figs. 1H, 25A, B). In contrast, an expansion is not seen in *Bistahieversor* (NMMNH P-25049), *Albertosaurus* (AMNH FARB 5232, AMNH FARB 5423, AMNH FARB 5432, CMN 2120, CMN 11315, CMN 11593, ROM 1247; Fig. 25C), *Alioramus* (IGM 100/1844), *Tyrannosaurus* (BMRP 2002.4.1, FMNH PR2081, MgD-I/76, PIN 551-2; Brochu, 2003). Measurements of metatarsal V are given in Table 1; polymorphic and ontogenetic characters are listed in Table S2 and Table S3, respectively.

TYRANNOSAURIDAE Gen. Indet.

Locality and Horizon—Third Asiatic Expedition, 1922, Iren Dabasu, Mongolia (what is now the Inner Mongolia Autonomous Region, People's Republic of China).

Remarks—Granger and Berkey (1922:6) reported that "portions of a small carnivorous dinosaur skull with two or three teeth" were collected in Iren Dabasu, Mongolia. The AMNH catalog database states that the fossil, AMNH FARB 6266, was collected by Granger and identifies the specimen as *Deinodon* ? sp., a tyrannosaurid. Unfortunately, the fossils reported here were not labeled with specimen numbers. When this author (TDC) studied the fragments, a catalog card associated with the box identified them as AMNH FARB 6556. Regardless, the skull fragments and teeth do match the report of Granger and Berkey (1922) and the information in the AMNH database; therefore, AMNH FARB 6266 is regarded here as the correct number, which was also reported by Brochu (2003).

AMNH FARB 6266 was collected the year before the lectotype of *Alectrosaurus* was discovered, and, in the absence of overlapping bones, AMNH FARB 6266 is cautiously referred here to Tyrannosauridae indeterminate. The future discovery of an associated skull and hind limb will resolve this equivocation in taxonomic identity.

This collection of fossils includes 75 fragments, which include premaxillary and lateral teeth, a fragmentary lacrimal, jugal, pterygoid, and ectopterygoid. The presence of D-shaped premaxillary teeth indicates the specimen is a derived tyrannosauroid, and the presence of a jugal pneumatic recess with a secondary fossa identifies it as a tyrannosaurid. The absence of hindlimb bones prevents comparison with the lectotype of *Alectrosaurus olseni*. The most complete, and identifiable, fragments are described here in the event that associated cranial and hindlimb bones are collected from the Iren Dabasu Formation in the future.

DESCRIPTION

Lacrimal—The left lacrimal is represented by the proximal parts of the rostral ramus, supraorbital process, and ventral ramus (Fig. 26A–C). The fragment is damaged in several places: the caudolateral surface of the bone is sheared off and missing; the base of the supraorbital process is present, and its lateral surface is also sheared off; the rostral ramus is broken off ahead of the cornual process; finally, the rostral margin of the ventral ramus is sheared off below the antorbital fossa of the rostral ramus. In dorsal view, the surface rostral and caudal to the cornual process is missing. In medial view, the rostral portion of the joint surface for the prefrontal is missing. Measurements are in Table 2.

In comparison with other tyrannosauroids, the fragment is most similar to that of *Raptorex kriegsteini* (Sereno et al., 2009) and with a lacrimal of a presumably juvenile *T. rex* (FMNH PR2411). In each specimen, the cornual process is a laterally extending ridge; this condition is unique among tyrannosauroids, where the process is usually oriented dorsolaterally or directly dorsally (Fig. 26A–C). The Iren Dabasu specimen also resembles *Raptorex*, *Albertosaurus sarcophagus*, *Daspletosaurus*, and *Tyrannosaurus*, in having a pneumatic foramen that penetrates the rostromedial surface of the ventral ramus that is termed here the medial pneumatic recess (Fig. 26A). The recess is positioned ventromedial to the lacrimal pneumatic recess and below the rostral ramus, between lateral and medial ridges. The medial ridge is formed by the leading edge of the orbitonasal ridge, whereas the lateral ridge is formed by the rostral edge of the ventral ramus; the medial ridge fades as it extends ventrally, but the lateral ridge is prominent for its entire extent.

The recess and ridges are also seen in *Raptorex* (LH PV18) and in *Alioramus* (IGM 100/1844), whereas this opening is not seen in FMNH PR2411. A medial pneumatic recess is also seen in *Albertosaurus sarcophagus* (CMN 5601) and an enlarged caudally extending variant of this opening is seen in large, presumably, adult tyrannosaurines (CM 9380, CMN 8506). Internally the recess connects to the pneumatic space in the ventral ramus, which opens dorsally into the lacrimal pneumatic recess. Based on these similarities, the Iren Dabasu specimen is a tyrannosaurine and a close relative of *Raptorex*, if *R. kriegsteini* is a member of that clade as indicated by its large maxillary fenestra and low tooth count; these conditions are also seen in juvenile *T. bataar* (MPC-D 107/7).

In addition to its small size, several characters indicate that the Iren Dabasu specimen represents a juvenile animal. In lateral view, the specimen resembles *Raptorex* and small juvenile *T. bataar* (MPC-D 107/7) in having a very narrow ventral ramus, which is narrower than the condition seen in slightly larger juveniles of tyrannosaurids (BMRP 2002.4.1, FMNH PR2411, TMP 1986.144.0001, TMP 1994.143.0001) (Fig. 26A). This similarity indicates that all three specimens are at the
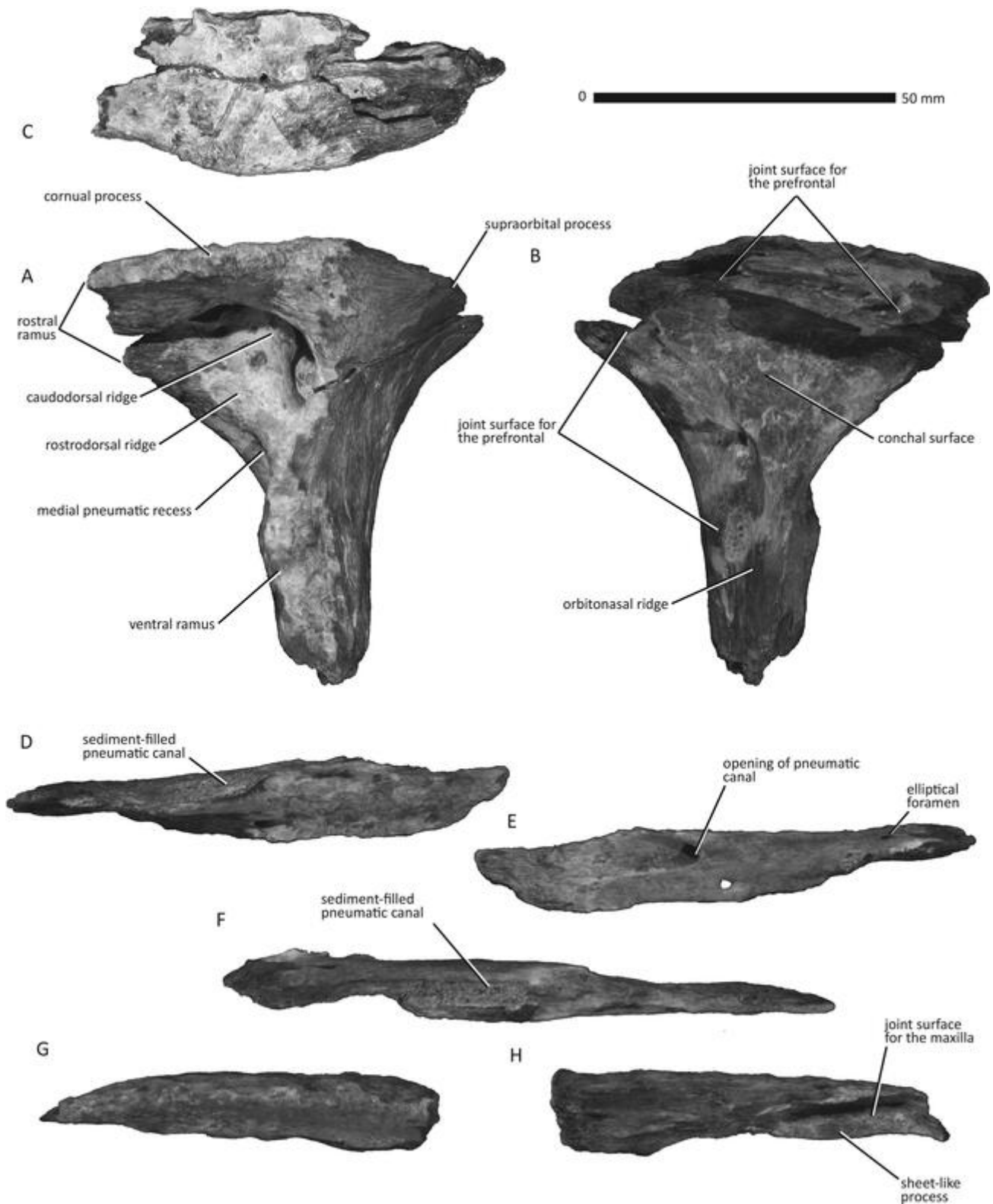
FIGURE 26. Left lacrimal of Tyrannosauridae indeterminate (AMNH FARB 6266) in **A**, lateral; **B**, medial; and **C**, dorsal views; lacrimal fragment A in **D**, lateral; **E**, medial; and **F**, ventral views; lacrimal fragment B in **G**, lateral; and **H**, medial views. **D** and **E** are upside-down.

relatively same early stage of ontogeny. The Iren Dabasu specimen has a large lacrimal pneumatic recess that is deeper than the cornual process, a condition that is seen in *Raptorex* and juveniles and subadults of *A. libratus* (ROM 1247, TMP 1986.144.0001), *Daspletosaurus* (TMP 1994.143.0001), and *Tyrannosaurus rex* (BMRP 2002.4.1).

TABLE 2. Measurements (in millimeters) of the associated tyrannosaurid skull bones and teeth AMNH FARB 6266 from the Iren Dabasu Formation of China. Symbols: ~, approximate measurement at regions of damage; +, underestimate due to missing portions of bone.

Lacrimal	
Total height of fragment	74.4
Total length of fragment	69
Depth of the cornual process above the pneumatic recess	9.1
Width across junction of the rostrodorsal ridge and the lateral surface	13.8
Depth of ventral foramen in the orbitonasal ridge, rostral opening	4.8
Depth of ventral foramen in the orbitonasal ridge, caudal opening	4.4
Jugal	
Total length of fragment	104.5
Total depth of fragment	36.0
Maximum length of pneumatic recess	28
Quadratojugal	
Total height of fragment	95.5
Maximum length of fragment	54.7
Depth of base of the jugal process	22.3+
Ectopterygoid	
Total length of fragment	76.3
Maximum depth of the joint surface for the jugal	17.4
Maximum length of ramus	23.8
Maximum depth of ramus	16.9
Pterygoid	
Total height of fragment	57.4
Total width of fragment	34.6
Length base of basipterygoid process	26.4
Premaxillary tooth A	
Total tooth height	42.0+ (tip of root broken)
Crown height	15.1
Basal width (labial)	5.0
Basal width (lingual)	4.3
Basal length (labiolingual)	8.1
Premaxillary tooth B	
Total tooth height	43.9+ (tip of root broken)
Crown height	16.2+ (tip worn)
Basal width (labial)	5.1
Basal width (lingual)	4.5
Basal length (labiolingual)	8.2
Lateral tooth A	
Total height of fragment	23.1+
Length of fragment	11.9
Width of fragment	7.3
# denticles/5 mm, base of distal carina	15
Lateral tooth B	
Total height of fragment	37.6+
Basal length	14.2+
Basal width	~9.7
Length of crown at midheight	11.6
Width of crown at midheight	7.6
# denticles/5 mm, midheight of mesial carina	20
# denticles/5 mm, basal extent of mesial carina	24
# denticles/5 mm, midheight of distal carina	16
Lateral tooth C	
Total height of fragment	18.8+
Basal length	13.8
Basal width	6.7
Length of crown at midheight	10.6
Width of crown at midheight	5.1
# denticles/5 mm, midheight of mesial carina	21
# denticles/5 mm, basal extent of mesial carina	27
# denticles/5 mm, midheight of distal carina	20
# denticles/5 mm, basal extent of distal carina	27

In lateral view, the caudal margin of the recess curves caudodorsally before extending rostrodorsally, and then rostroventrally. In rostral view, the caudal edge of the external opening of the recess is convex, whereas it is sharp and bladelike dorsally. The preserved portion of the recess indicates that it was low and long; this condition is seen in juvenile *A. libratus* (TMP 1986.144.0001), subadult *A. sarcophagus* (CMN 5601), subadult *Alioramus* (IGM 100/1844), juvenile *Raptorex* (PH LV18), and juvenile and subadult *Tyrannosaurus* (BMRP 2002.4.1, MPC-D 107/7). Finally, the surface of the bone is deeply concave above the lacrimal pneumatic recess (Fig. 26A); this condition is also seen in juvenile and subadult tyrannosaurids (e.g., ROM 1247, TMP 1986.144.0001). Therefore, the Iren Dabasu specimen almost certainly was a juvenile at death. A small foramen pierces the caudodorsal part of the concavity.

In the Iren Dabasu specimen, the cornual process is a low ridge that extends along the dorsolateral edge of the dorsal ramus that barely interrupts the dorsal margin of the bone (Fig. 26A). This condition is seen elsewhere among derived tyrannosauroids only in *Raptorex* (LH PV18) and FMNH PR2411. The process is coarsely textured, especially along its dorsal margin. In dorsal view, the process extends furthest laterally above the rostral fossa within the pneumatic recess before returning rostromedially to the base of the rostral ramus (Fig. 26A, C). In contrast, it is widest at the caudal end of the recess in FMNH PR2411.

In dorsal view, the lateral edge of the cornual process is convex and coarsely textured; it extends rostrolaterally at a low angle before curving rostromedially to the rostral ramus (Fig. 26C). Three ridges coarsen the dorsal and dorsolateral surfaces of the process rostrally, and one ridge coarsens the surface caudally, at the level of the caudal margin of the pneumatic recess. Otherwise, the dorsal surface of this region is irregular in texture and it is pierced by four small foramina. The dorsal surface of the bone is concave next to the cornual process, and it becomes convex along the joint surface for the nasal. In cross section, the dorsum of the bone is convex along the lateral edge of the rostral ramus, it is concave medial to that ridge before becoming convex again along the medial two thirds of the dorsal surface.

In lateral view, a rostrodorsally extending ridge bounds the lacrimal pneumatic recess ventrally, which splits into a wide caudodorsally extending ridge that extends up the medial wall of the recess, and another ridge that extends rostrally along the ventral edge of the antorbital fossa (Fig. 26A). The caudodorsally extending ridge separates two deep fossae; a caudal fossa that extends toward the supraorbital process, and a rostral fossa that is positioned below the cornual process. The fossae extend dorsally to excavate the ceiling of the recess. All of these features are seen in derived tyrannosauroids. In contrast to the Iren Dabasu specimen and other derived tyrannosauroids, the caudodorsal ridge is a narrow and short strut in *Raptorex* (LH PV18), subadult *A. sarcophagus* (TMP 2000.045.0026), and *Alioramus* (IGM 100/1844).

In lateral view, the convex and prominent ridge that bounds the lacrimal pneumatic recess ventrally in the Iren Dabasu specimen is hollowed by a pneumatic space. The fossa above this ridge, and ahead of the caudodorsal ridge, is deeply excavated and it is perforated by a small foramen at its greatest depth (Fig. 26A). The foramen almost certainly exited through the medial surface of the bone. The fossa behind the caudodorsal ridge is only visible marginally in lateral view; it also extends ventrally into the ventral ramus to at least the depth where the antorbital fossa diverges rostrodorsally from the ramus. The fossa is pierced rostrally by a small foramen and two tiny foramina caudally; the small foramina pierce a canal that exits the orbitonasal ridge caudally.

In medial view, the joint surface for the prefrontal is a deep groove that extends rostroventrally along the caudoventral

margin of the bone, from the supraorbital process to the ventral ramus (Fig. 26B). The groove is deepest proximally, and it is shallow distally. Proximally, a flange extends caudally along the rostromedial edge of the contact, which would have overlapped the rostral edge of the prefrontal. The caudal half of the contact extends caudomedially, is coarse, and extends further medially than the rostral half of the contact. The rostral half of the joint surface is inset relative to the flat surface of the conchal region. A large part of the midregion of the joint surface is missing, where a foramen pierces the orbitonasal ridge. The distal end of the joint surface is almost certainly represented by a deep pocket in the caudomedial surface of the ventral ramus that is pierced by two small foramina (Fig. 26B).

The conchal surface is the flat region that is bounded caudoventrally and dorsally by the divergent parts of the joint surface for the prefrontal (Fig. 26B). The conchal surface is not excavated by a deep fossa or foramen as is seen in tyrannosaurines, but two small foramina pierce the surface. The surface is gently convex centrally, which is bounded rostrally by a low, but rostrocaudally wide groove. The rostral margin of the conchal surface extends rostrodorsally along an indistinct curve between the orbitonasal ridge and the proximal region of the rostral ramus. The deep and coarse groove for the dorsal arm of the prefrontal extends above the conchal surface. The joint surface is positioned immediately below the dorsal surface of the bone. The contact is dorsoventrally deep and it appears to bifurcate rostrally, where the dorsal half does not extend as far medially as the ventral shelf (Fig. 26B).

In lateral view, the ventral ramus blends with antorbital fossa of the dorsal ramus (Fig. 26A). This condition is also seen in *Albertosaurus libratus* (AMNH FARB 5664, ROM 1247), *Raptorex* (PH LV18), *Daspletosaurus* (TMP 1994.143.0001), and *T. rex* (AMNH FARB 5027, CM 79057, CM 9380, CMNH 7541, MOR 1125). This wide distribution indicates that this feature is almost certainly not taxonomically informative. Damage prevents description of the contour of the rostral margin of the ramus.

In rostral view, the ridges that bound the medial pneumatic recess form a groove that extends ventrally, where it is pierced by a second large foramen that penetrates the orbitonasal ridge; a shallow fossa separates this opening from the recess. In caudal view, the ventral foramen opens through the orbitonasal ridge above the rostroventral end of the joint surface for the prefrontal. In medial view, the preserved part of the orbitonasal ridge is situated midway between the rostral and caudal margins of the ventral ramus (Fig. 26B). This condition is also seen in *A. libratus* (ROM 1247) and in *A. sarcophagus* (CMN 5601). In contrast, the ridge reaches the caudal margin in *Raptorex* (PH LV18), FMNH PR2411, and tyrannosaurines in general.

Lacrimal? Fragment A—A long (83.6 + mm) and mediolaterally narrow (8.2 mm) splinter might represent a portion of the antorbital fossa of the rostral ramus of the left lacrimal (Fig. 26D, E, F); the fragment has a maximum depth of 14.3 mm. Although there is no fit between this fragment and the rest of the lacrimal, the gray discoloration of the cortical bone and the brown medullary bone matches the two specimens. Also, the lacrimal has a pneumatic canal that extends rostrally deep to the antorbital fossa, a condition that is also seen in the fragment. This canal opens medially as a deep channel that excavates the medial surface of the bone before fading (Fig. 26E). Therefore, the position and orientation of the canal is the point of reference for orienting the fragment, where the canal opens rostromedially, and extends through the ventral half of the fragment. If the orientation is correct, then this fragment is from the left lacrimal.

In 'lateral' view, the internal surface of the bone is revealed by breakage, where the matrix-filled pneumatic canal is exposed along the caudal half of the fragment (Fig. 26D). The intact surface is inflated external to the canal, which flattens rostrally opposite its medial opening. A foramen extends rostrodorsolaterally through the bone and forms a deep sulcus before fading rostrally, above the swelling. In 'ventral' view, a narrow groove extends forward from the pneumatic canal, widening and deepening toward the rostral end of the bone. Above this groove, is the gently convex medial surface (Fig. 26F).

In 'medial' view, the surface of the fragment is tubular caudally and flat rostrally (Fig. 26E). The flat condition of the rostral half extends caudally above the convex tubular region that is inflated, presumably by the internal pneumatic canal. The large pneumatic foramen, positioned ahead of the midlength of the fragment, exits close to the ventral margin of the fragment (Fig. 26E). The surrounding bone is flat, but it is convex caudal to the opening. A foramen pierces the fragment caudodorsal to the large opening. The cortical bone is missing from the rostral end of the fragment, making it impossible to determine if it bore the joint surface for the maxilla. Along the convex caudal half of the fragment, the medial surface extends ventrolaterally, where it is pierced by an elliptical foramen next to the broken end (Fig. 26E). The pneumatic canal, which is filled with matrix, can be seen in ventral view (Fig. 25F).

Lacrimal? Fragment B—A second fragment (length: 66.2 mm, depth: 14.8 mm, width: 11.5 mm) might represent the dorsal part of the rostral ramus (Fig. 26G, H), but a fit cannot be obtained between it and the other portions of lacrimal. The form of the fragment is consistent with the other fragments in several regards: (1) the external surface is coarsely textured, which matches the subcutaneous surface of the most complete fragment; (2) the external gray cortical bone and brown medullary bone match the other fragments; (3) the ventral surface of the fragment is wide and concave, matching the laterally extending cornual process; (4) the lateral edge of the shelf is coarsely textured, as on the cornual process of the lacrimal. If correctly identified, then this fragment is the dorsolateral part of the rostral ramus of the left lacrimal.

In medial view, the ventral surface of the distal end is incised by a short groove, possibly to receive the caudolateral process of the nasal or the dorsal prong of the ascending ramus of the maxilla (Fig. 26H). In ventral view, a chamber hollows the medial surface, medial to a sheet that extends ventromedially from the coarse dorsolateral ridge. Rostrally, the chamber deviates laterally to connect with a groove that is situated opposite the joint surface for the nasal. The medial groove widens ahead of the joint surface for the nasal, toward the lateral edge of the bone.

A second groove is present, which is positioned medial to the lateral groove; a ventrally extending sheet-like process that ends rostrally in a point separates the grooves (Fig. 26H). The medial surface of the sheet was almost certainly covered by the joint surface for the maxilla. The deep, ventromedially opening cleft is preserved on an intact portion of the medial surface; the groove extends rostrodorsally, producing a notch in the rostral tip of the fragment. This groove may have received the lateral edge of the nasal.

Jugal—The maxillary ramus of the left jugal is preserved, which is missing its ventrolateral edge and surface, and most of the dorsal margin (Fig. 27). All of the cortical bone is missing from the medial surface. Measurements are in Table 2. The maxillary ramus is dorsoventrally shallow. The suborbital region is shallower than the ramus; this feature is seen in other derived tyrannosauroids (Fig. 27A, B). In the antorbital fossa, a secondary fossa is present; this condition is also seen in all tyrannosaurids (Fig. 27A). Although a pneumatic recess and a secondary fossa is in the antorbital fossa of the jugal in *Sinraptor dongi* (Currie and Zhao, 1993), the vertical ridge in the secondary fossa in that species is not seen in Tyrannosauridae. These features indicate this fossil represents a taxon that is more
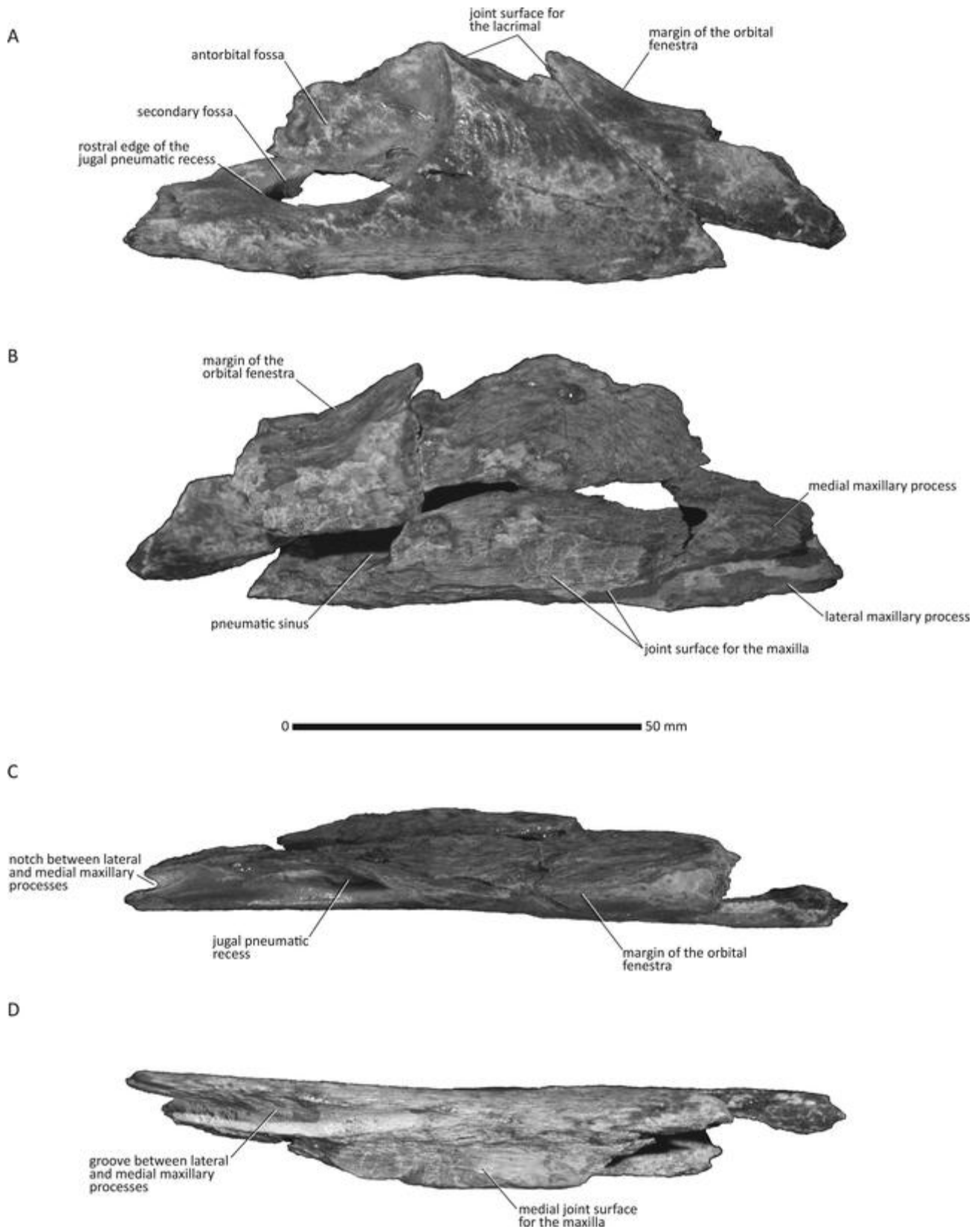
FIGURE 27. Maxillary process of the left jugal of Tyrannosauridae indeterminate (AMNH FARB 6266) in **A**, lateral; **B**, medial; **C**, dorsal; and **D**, ventral views.
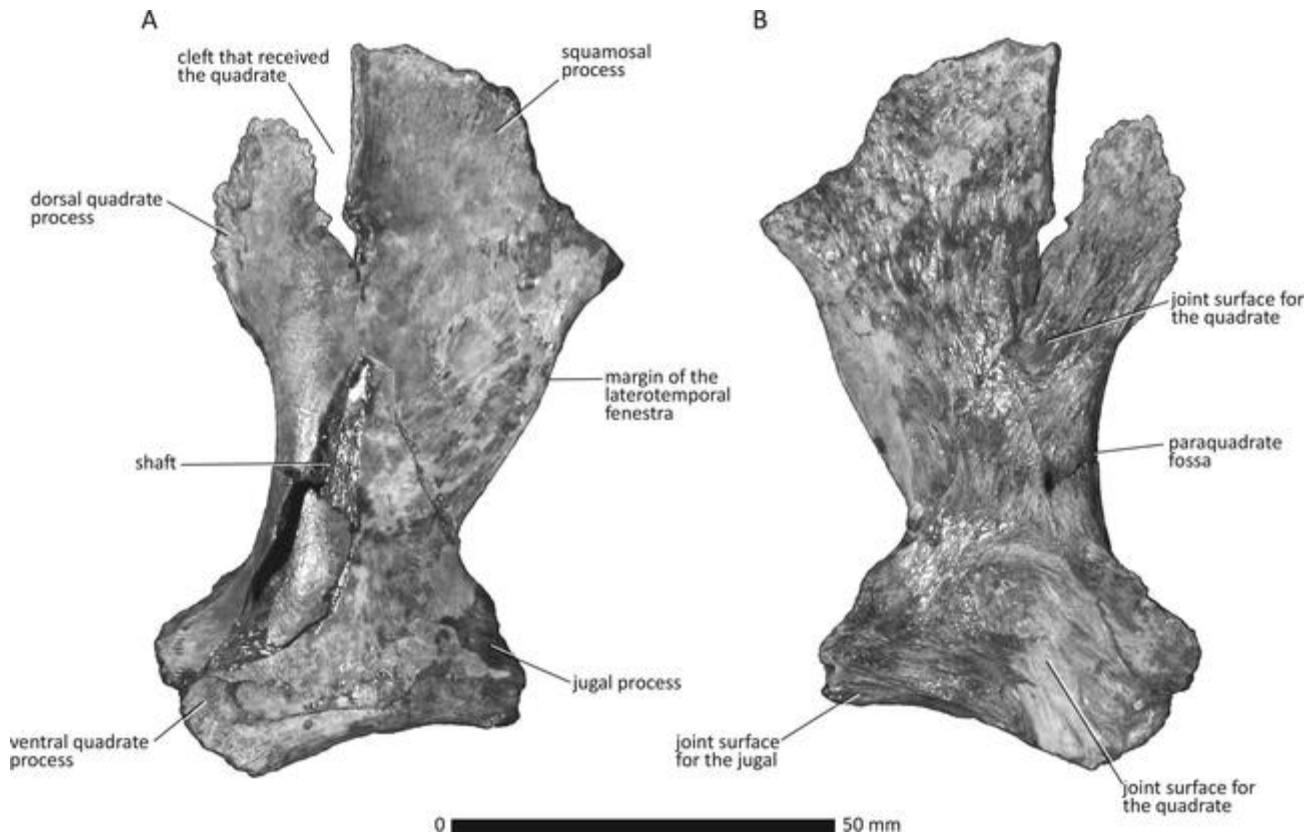
FIGURE 28. Right quadratojugal of Tyrannosauridae indeterminate (AMNH FARB 6266) in **A**, lateral and **B**, medial views.

highly derived than *Bistahieversor*, the sister taxon of Tyrannosauridae that has the recess, but lacks the secondary fossa.

Below the antorbital fossa the subcutaneous surface is dorsoventrally shallow (Fig. 27A); this condition is seen in juveniles of *A. libratus* (TMP 1986.144.0001), *Raptorex* (PH IV18), and subadult *Alioramus* (IGM 100/1844). In lateral view, the dorsal half of the secondary fossa is exposed to view, where it is lens-shaped, not circular (accordingly, in AMNH FARB 6266 the antorbital fossa extends deeply above the secondary fossa). This condition is seen in non tyrannosaurines and in juvenile and subadult tyrannosaurines, whereas the circular condition (i.e., maximally exposed by resorption) is seen in adult tyrannosaurines.

The rostral end of the maxillary ramus is divided into medial and lateral processes that received the dorsal jugal process of the maxilla between them. In dorsal view, a notch separates the lateral and medial processes (Fig. 27C); the maxilla fits into a deep groove between them that extends caudally from the notch. The joint surface for the maxilla is seen in lateral view on the medial process, which extends further dorsally than the lateral process.

In medial view, the medial half of the joint surface for the maxilla is wider than the lateral half (Fig. 27B). The lateral joint surface is subvertically (i.e., it slopes at a steep angle ventrolaterally) oriented, and the preserved portions of the joint surface are smooth. It is separated from the medial joint surface by a deep groove that is approximately 1.9 mm wide. In ventral view, the slot separates the processes at midlength and it extends caudally along the midline before curving caudolaterally to the lateral edge of the bone (Fig. 27D). Thereafter, the bone is missing. The medial joint surface slopes ventrolaterally

at a steep (45°) angle; it is smooth and becomes less steep caudally, becoming nearly horizontal.

In lateral view, the antorbital fossa is deeply inset into the bone, especially rostrally where it is inset from the lateral surface (Fig. 27A). This forms a shelf that extends caudally to the pneumatic recess whereupon the shelf becomes a shallow groove. The groove extends to the caudal edge of the recess and then to the level of the joint surface for the lacrimal. The shelf between the fossa and the subcutaneous surface is narrow ahead of the recess. In dorsal view, the rostral end of the ramus is narrow such that the antorbital fossa extends along a steep convex curve to the subcutaneous surface (Fig. 27C). Rostrally the fossa slopes directly to the subcutaneous surface, but caudally the narrow shelf and groove separates it from the subcutaneous surface lateral to the jugal recess. The preserved portion of the joint surface for the maxilla stops 8.0 mm ahead of the recess.

The pneumatic recess extends rostrally into the bone for a few millimeters ahead of its rostral margin. This condition is also seen in *Albertosaurus libratus* (TMP 1986.144.0001), *A. sarcophagus* (TMP 1981.010.0001), *Raptorex* (PH LV18), *Alioramus* (IGM 100/1844), *Daspletosaurus* (CMN 11594), and in *Tyrannosaurus rex* (FMNH PR2081). The sinus also extends ventrally from the recess into the bone. The caudal edge of the recess merges within the antorbital fossa below the level of the joint surface for the lacrimal; caudal to this a distinct edge between the fossa and subcutaneous surface is produced by the groove that follows the lateral edge of the fossa.

The joint surface for the lacrimal extends caudoventrally and ends in a shallow concavity that does not extend into the bone as a pocket (Fig. 27A). This condition is also seen in *Raptorex* (PH LV18) and *Alioramus* (IGM 100/1844); in other

tyrannosaurids the joint surface is a deep groove or pit, where a ridge overlaps the joint surface laterally. The condition seen in the Iren Dabasu specimen is almost certainly not ontogenetic, because a deep and overlapped joint surface is seen in juvenile *Albertosaurus libratus* (TMP 1986.144.0001). A small foramen penetrates the lateral surface ventral to the joint surface for the lacrimal.

As in other tyrannosauroids the subcutaneous surface of the bone is textured, in this case by low and vertically oriented ridges that curve rostroventrally. The orientation of the lateral surface of the bone changes from rostrally to caudally: it is vertical rostroventral to the recess, where the lateral surface is gently concave below the antorbital fossa (Fig. 27A). The lateral surface then curves ventromedially caudal to the level of the joint surface for the lacrimal, where it is convex caudoventral to the joint surface for the lacrimal. These contours are consistent with what is seen in other derived tyrannosauroids, where the external surface is convex below the orbital fenestra, and flattens ahead of that region.

Quadratojugal—The right quadratojugal is present, but it is missing its caudodorsal region, the rostrodorsal part of the squamosal process, the distal part of the jugal process, the caudal edge of the ventral quadrate process, the surface of the paraquadrate fossa, and most of the medial surface of the bone (Fig. 28). Also, the shaft of the bone is damaged. Measurements are in Table 2.

As in other derived tyrannosauroids, the bone consists of dorsal and ventral rami. The dorsal ramus expands rostrally as the squamosal process, which is separated caudodorsally from the dorsal quadrate process by a cleft. The ventral ramus extends rostrally as the jugal process, and caudally as the short ventral quadrate process. As noted, the dorsal margin is deeply notched to receive a lateral process from the quadrate (Fig. 28). The cleft, although incomplete is rostrocaudally narrow and deep, extending 22.0 mm into the bone. A distinct ridge extends along the rostral margin of the notch, representing the medial surface of the joint surface for the quadrate that has extended laterally (Fig. 28A).

In lateral view, the preserved dorsal margin, ahead of the quadrate notch extends rostroventrally at a very low angle (Fig. 28A). This condition is also seen in subadult *A. libratus* (TMP 1996.036.0001), adult *A. sarcophagus* (TMP 1981.010.0001), subadult *Alioramus* (IGM 100/1844), adult *Daspletosaurus* (CMN 8506), and in adult *T. rex* (FMNH PR2081). In contrast, this margin extends steeply rostroventrally in juveniles of *Daspletosaurus* (TMP 1994.143.0001) and *T. rex* (BMRP 2002.4.1, CMNH 7541), which produces a deep notch in the dorsal margin of the bone.

The lateral surface of the squamosal process is concave, which is deepest toward the rostral margin of the bone, and dorsally ahead of the quadrate cleft; the bone expands laterally along its dorsal margin ahead of the cleft (Fig. 28A). The shaft is convex ventral to the quadrate notch, and this region of the bone is not penetrated by a foramen. The
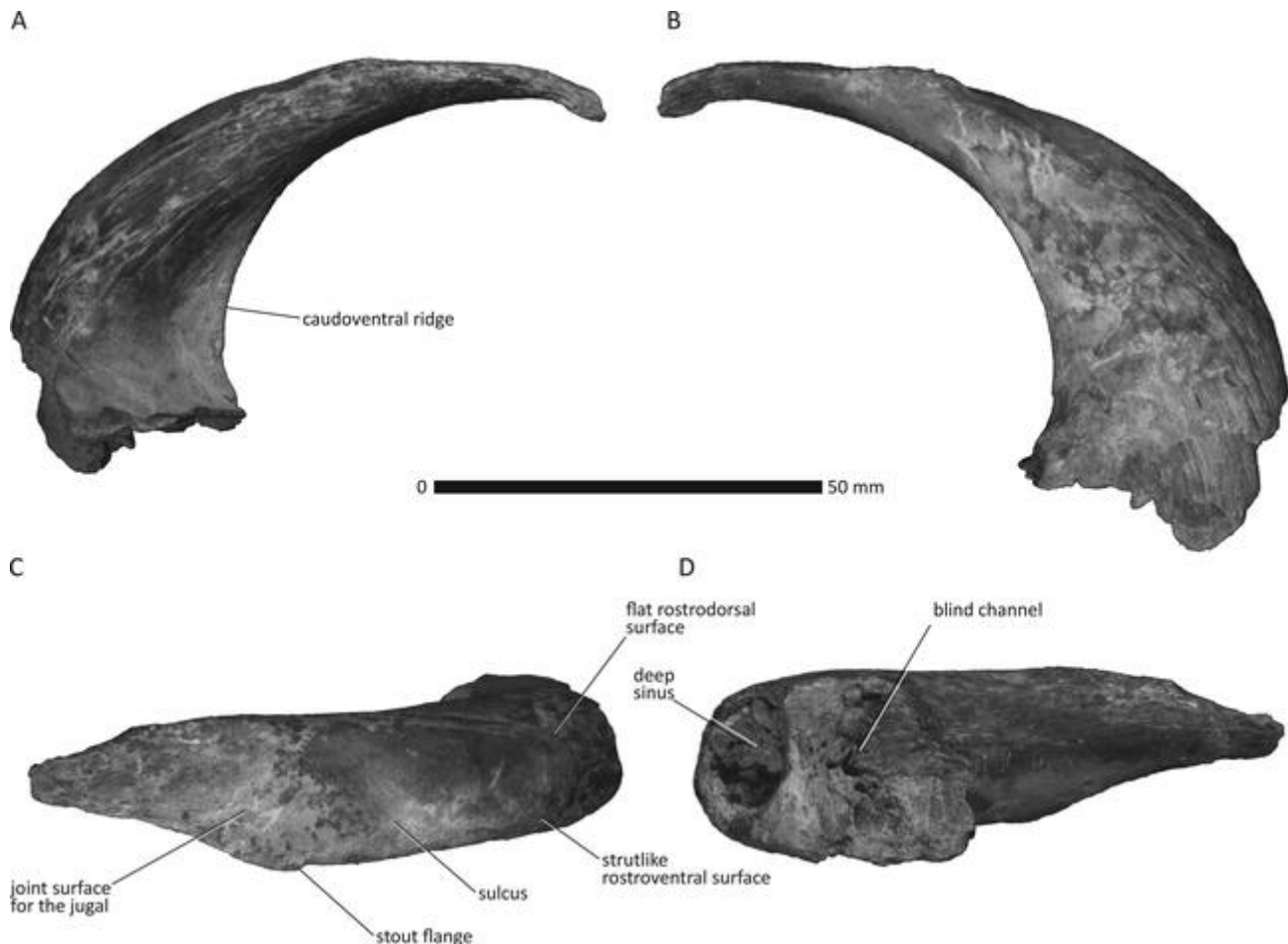

FIGURE 29. Jugal process of the right ectopterygoid of Tyrannosauridae indeterminate (AMNH FARB 6266) in **A**, dorsal; **B**, ventral; **C**, lateral; and **D**, medial views.

dorsal quadrate process is a wide expansion caudal to the quadrate notch; the process is convex with an irregular caudal margin (Fig. 28). This condition is seen in all other derived tyrannosauroids.

In lateral view, the preserved margin of the laterotemporal fenestra is unusual among derived tyrannosauroids. First, it lacks a distinct 'stalk,' a constricted vertical region that separates the ventral ramus from the dorsal ramus (Fig. 28A). This stalk is usually defined by concave rostral and caudal margins. In the Iren Dabasu specimen, only the caudal margin is concave, whereas rostrally there is an abrupt transition between the convex rostral margin of the squamosal process and the jugal process. An abrupt transition is also seen in an isolated (and unnumbered) specimen in the collections of the CMN, almost certainly from the Dinosaur Park Formation of Alberta. Second, the ventral part of the margin is distinctly convex and above the convexity it is concave (Fig. 28). Although an undulating margin is seen in some other derived tyrannosauroids, none match the contours seen in the Iren Dabasu specimen.

The margin of the laterotemporal fenestra extends steeply rostrodorsally in the Iren Dabasu specimen (Fig. 28). Variation in the orientation of the margin, either extending steeply rostrodorsally or at a lower angle, is seen in several species, including *Albertosaurus sarcophagus* (CMN 11315: steep, TMP 1981.010.0001: not steep), *A. libratus* (TMP 1991.036.500: steep, TMP 2000.012.0011: not steep), *T. rex* (BMRP 2002.4.1: steep, MOR 555: not steep). Therefore, this feature may not be taxonomically informative. In medial view, the medial surface of the squamosal process extends rostrolaterally to its leading edge; muscle scars lightly coarsen that inclined surface (Fig. 28B).

In medial view, it appears that the dorsal joint surface for the quadrate extends below the level of the slot that received the quadrate. The paraquadrate fossa is shallowly incised into the bone, represented by a narrow groove along the caudomedial margin of the shaft (Fig. 28B). A similar condition is seen in adult *T. rex* (MOR 555, MOR 980, MOR 1125, RSM 2523.8), where the fossa is not seen in medial view. However, it is possible that the condition in the Iren Dabasu specimen is an artifact of damage; in contrast, the fossa is deep and widely visible in medial view in other tyrannosaurids, including subadult *T. rex* (BMRP 2002.4.1).

The ventral joint surface for the quadrate is a deep pocket below the shaft, and low ridges that extend caudoventrally coarsen it centrally (Fig. 28B). The caudoventral part of the joint surface is coarsely textured by deep grooves separated by five irregular ridges. The joint surface generally faces ventromedially; it is almost horizontal dorsally and becomes almost vertical ventrally. Ahead of the joint surface, that for the jugal faces ventrolaterally, becoming progressively steep (vertical) rostrally; caudally it thins into a shallow groove along the ventral margin to receive the tip of the ventral quadratojugal process of the jugal. The joint surface is somewhat deeply incised into the bone, such that a ridge bounds it dorsally. The ventral margin of the bone is concave below the shaft.

Ectopterygoid—The jugal ramus of the right ectopterygoid is preserved (Fig. 29). In dorsal view, the base of the process widens and curves caudally very close to the joint surface for the jugal, indicating that the jugal process was very short when the bone was complete (Fig. 29A). Measurements are in Table 2.

A dorsoventrally thin ridge extended from the body of the bone to the jugal process along the caudoventral edge of the process, which fades distally opposite to the joint surface for the jugal (Fig. 29A). The ventral position of this ridge is also seen in *A. libratus* (ROM 1247), *Alioramus* (IGM 100/1844), *Daspletosaurus* (CMN 8506, CMN 11594), and adult *T. rex* (CM 9380, CM 79057). In contrast, it is positioned toward the dorsal edge of the process in subadult *T. rex* (BMRP 2002.4.1).

In medial view, the broken surface reveals that the pneumatic sinus extended deeply laterally into the rostral portion of the jugal ramus, whereas caudally the sinus ends as a blind channel in the base of the process (Fig. 29D). The jugal process is not inflated, as indicated by the narrow condition of the process, the small sinus that extends into it, and by the prominent web-like ridge that extends along its caudoventral surface. In contrast, the process is inflated in relatively small, presumably immature, tyrannosaurid specimens, including the holotype of *Alioramus altai* (IGM 100/1844) and in subadult *Tyrannosaurus* (BMRP 2002.4.1, MgD-I/24).

In the Iren Dabasu specimen the dorsal surface of the jugal process is strongly convex, whereas the ventral surface is flat (Fig. 29B). The dorsum is convex along the midlength of the ramus, whereas it is convex at the rostral edge of the ramus in *Albertosaurus sarcophagus* (AMNH FARB 5218). In the Iren Dabasu specimen, the ridge along the caudoventral edge of the process is thin and bladelike proximally. In contrast, the inflated condition seen in other derived tyrannosauroids obscures this feature in dorsal view. In the Iren Dabasu specimen, the rostroventral surface of the process is strutlike, whereas in *A. sarcophagus* (AMNH FARB 5218) the strut is rostrodorsal in position. Also in AMNH FARB 6266, the rostral surface is flattened to produce a rostrodorsally facing flat surface, whereas the surface is uniformly convex in *A. sarcophagus* (AMNH FARB 5218).

In lateral view, the jugal process expands at the base of the joint surface for the jugal; the rostroventral edge of the joint surface is separated from the ramus by a shallow notch, producing a stout ventrally oriented flange (Fig. 29C). This condition is also seen in *Alioramus* (IGM 100/1844). In contrast, a large triangular flange is seen caudoventral to the notch (if it is not broken and missing) in large specimens of *T. rex* (MOR 1125). In the Iren Dabasu specimen, the joint surface is concave basally and it is convex dorsally, a condition that extends distally. The ventral margin of the process below the joint surface is concave and generally extends caudodorsally; this condition is seen in other tyrannosaurids (IGM 100/1844, MOR 1125). A shallow sulcus extends rostroventrally ahead of the joint surface that fades as it reaches the ventral surface of the bone. A much shallower version of this groove is seen in *Albertosaurus sarcophagus* (AMNH FARB 5218).

Pterygoid—A portion of the quadrate ramus of the right bone preserves the junction between the quadrate process, basipterygoid process, and the palatine ramus (Fig. 30). Measurements are in Table 2. This fragment conforms to the morphology of *T. rex* (AMNH FARB 5117), except the palatine ramus is narrower, and so the basipterygoid process extends further rostrally than in *T. rex*, where the ramus is as wide as the base of the process. The basipterygoid process extends almost to the caudal edge of the quadrate process, whereas in *T. rex* it stops short of the caudal edge of the process.

Dentition, Premaxillary Crown A—This tooth is nearly complete, which includes the crown and root; there is minor damage to the tip of the root (Fig. 31A–D). In labial view, the enamel is missing from the basal half of the crown (Fig. 31A). With the crown held facing downward and the lingual surface facing the viewer, the crown curves to the right, indicating that the tooth is from the right premaxilla. This crown has the typical morphology seen in the premaxillary teeth of other derived tyrannosauroids, including a D-shaped cross section, where the crown is linguolabially long, but mesiodistally narrow, and the carinae face lingually on either side of a prominent lingual ridge (Fig. 31B). Measurements and denticle counts are in Table 2.

In lingual view, the bases of six denticles are present on the mesial surface of the mesial carina; all other trace of them is worn away from the enamel. The carinae converge basally and
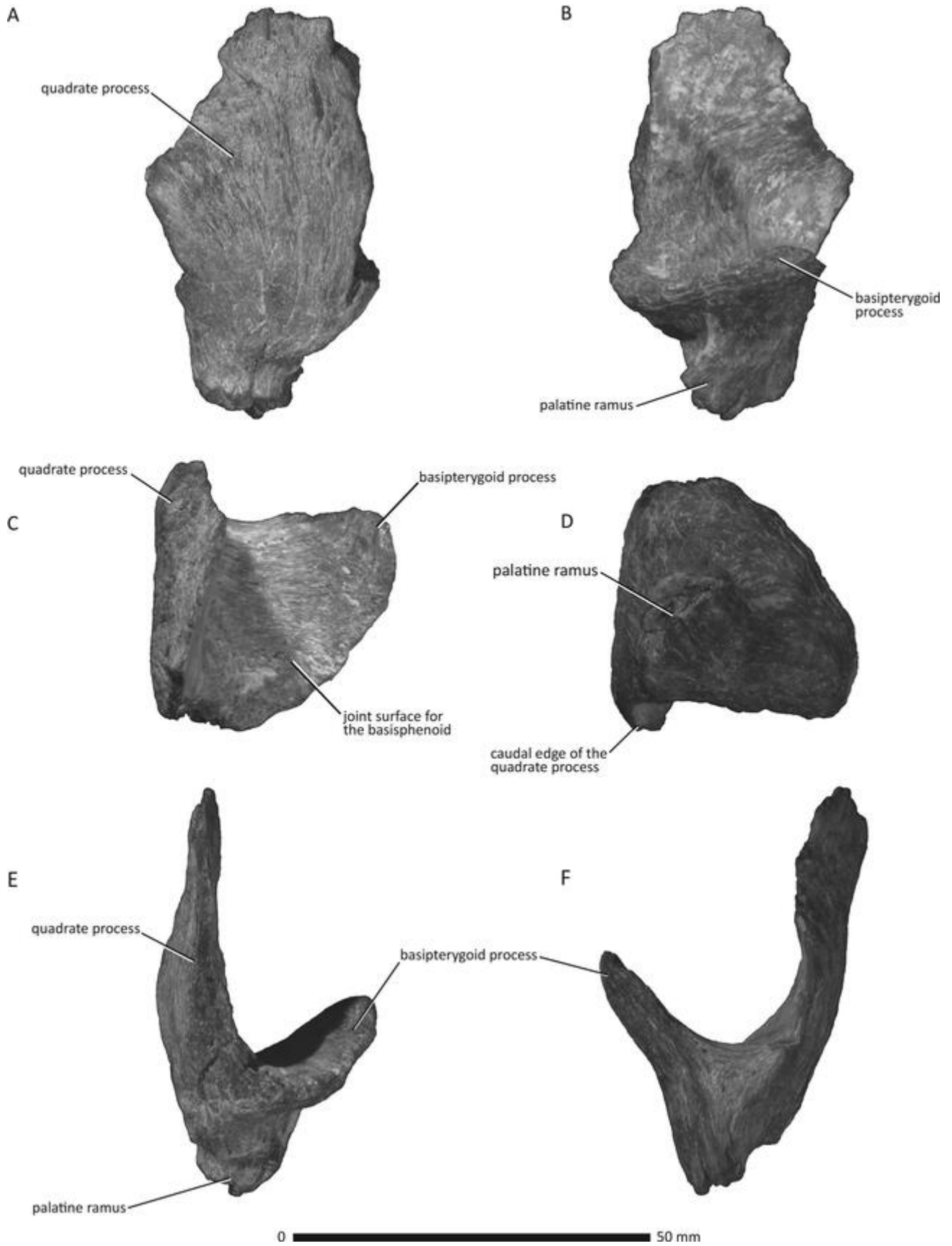
FIGURE 30. Partial right pterygoid of Tyrannosauridae indeterminate (AMNH FARB 6266) in **A**, lateral; **B**, medial; **C**, dorsal; **D**, ventral; **E**, rostral; and **F**, caudal views.
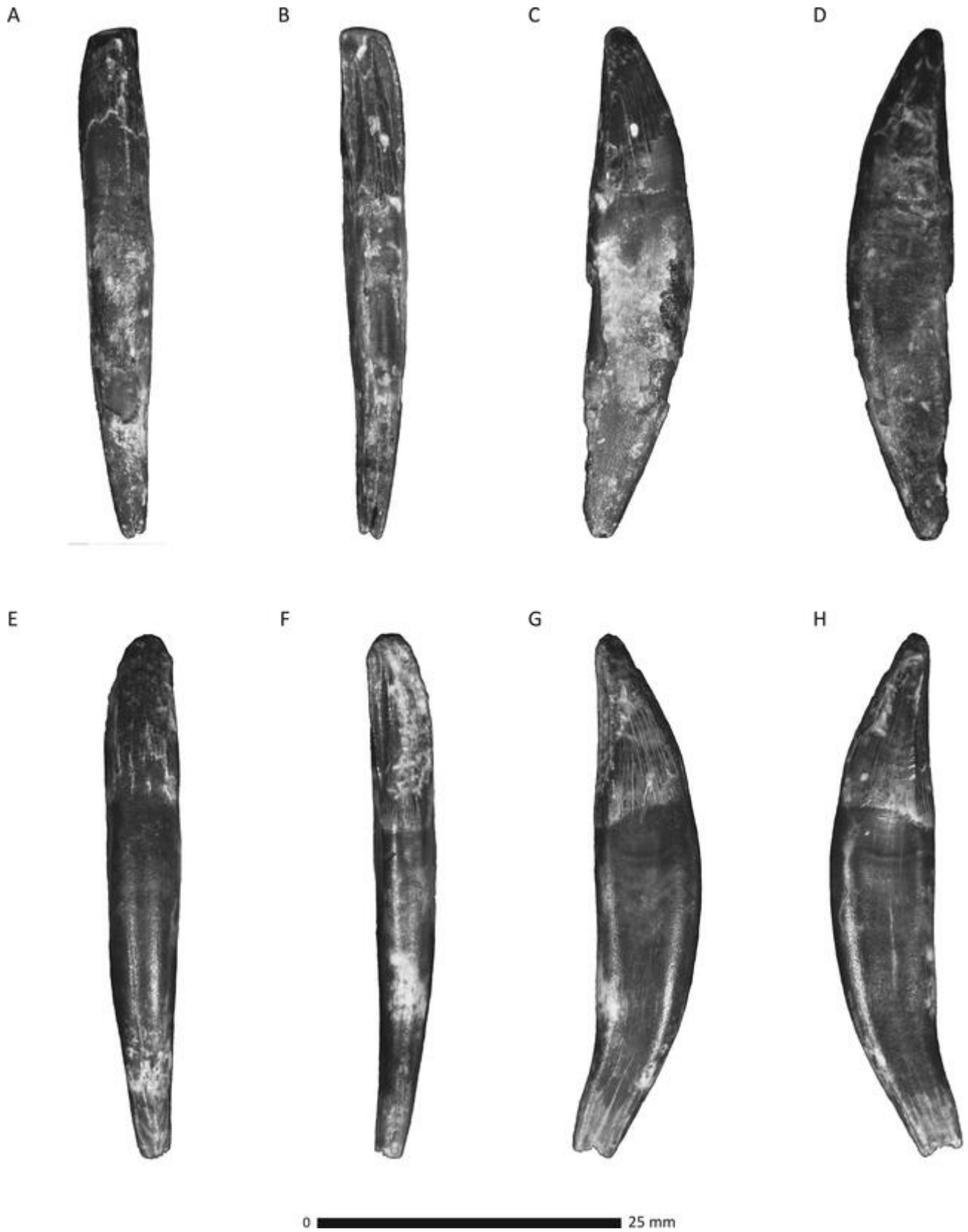
FIGURE 31. AMNH FARB 6266. Premaxillary tooth A in **A**, labial; **B**, lingual; **C**, mesial; and **D**, distal views. Premaxillary tooth B in **E**, labial; **F**, lingual; **G**, mesial; and **H**, distal views.

the lingual surface is narrower than the labial surface of the crown (Fig. 31A, B). Despite damage, the mesial carina appears to fade before it reaches the lingual ridge. The distal carina may have reached the lingual ridge, but this region is unclear. The distal carina is positioned labially relative to the mesial carina.

A groove separates each carina from the lingual ridge; the mesial groove widens and flattens (i.e., faces fully lingually) apically, whereas the distal groove only widens slightly (Fig. 31B). This difference in width reflects the apicodistal orientation of the ridge; i.e., the lingual ridge is positioned closer to the distal carina than the mesial carina toward the apex of the crown. Fine ridges texture the grooves between the lingual ridge and carinae; the ridges extend apically toward the carinae at a relatively steep angle.

The lingual ridge is approximately half the crown width apically, and it widens until it spans the width of the crown basal to the carinae. The ridge is bilobate, where a groove separates the ridge into mesial and distal halves. The groove is mesial in position (i.e., it is not exactly at the midwidth of the ridge) and the mesial part of the ridge does not extend as far lingually as the distal part; i.e., the distal half is more prominent than the mesial half (Fig. 31B). The groove shallows apically, where the two parts of the ridge merge together. The ridge follows the curve of the crown, which extends distally at its apex. Low irregular ridges that trend apicobasally texture the lingual ridge.

In lingual view, the apex of the crown is worn, and the wear facet extends further basally along the mesial carina than the distal carina (Fig. 31B). On the lingual ridge, the apical wear facet extends further basally on the distal half of the ridge, but it does not reach the groove that separates it into mesial and distal halves. The wear is more extensive on the distal half of the lingual ridge than the mesial half, where the carinae, apex of the crown, and lingual ridge are most heavily worn. In contrast, the grooves between the lingual ridge and carinae are only worn apically, and the distal groove is more extensively worn than the mesial groove.

In mesial view, the tip of the crown and the preserved part of the carina are worn from use (Fig. 31C). Enamel on the mesiolabial surface is exfoliated away. The surface of the enamel is textured by low irregular and intersecting ridges that trend from mesiolabially to mesiolingually at a steep angle, presumably at the same angle as the grooves between the bases of the denticles. The texture is most heavily worn down apically. Although worn and incomplete, the mesial carina is concave at the midheight of the crown. Also in mesial view, the lingual ridge is visible from the base to the apex. The mesial surface of the crown is concave next to the basal third of the carina.

In labial view, the enamel of the basal half of the crown is worn away and missing; above this, the enamel texture is worn smooth from use in life (Fig. 31A). Two deep wear facets have worn the apex down to the dentine, which is deeply grooved by use. One wear facet is large and excavates the apicomesial surface and the other is a third of its size and is connected to it, which is located on the apicolabial surface on the midline. The worn tip slopes mesiobasally along a convex arc. As in other tyrannosaurids, the apical half to third of the crown curves distally, where the mesial edge of the crown is a uniform convex arc, whereas the distal edge is concave, and its apical extent is convex.

In distal view, the surface of the crown is concave next to the basal half of the carina (Fig. 31D). The texture of the enamel is the same as on the mesial surface, and it is worn smooth apically. The lingual ridge is prominent and it is visible from the base to the apex, where it is worn down (Fig. 31D). Although worn and damaged, the carina follows a concave curve throughout its length. The apical portion of the distal carina is worn down to the dentine.

Dentition, Premaxillary Crown B—As with the preceding tooth, the tooth is incisiform and it is labiolingually longer than mesiodistally wide, with a prominent lingual ridge (Fig. 31E–H). The tooth is virtually complete, but most of the enamel is missing from the labial surface and mesial surface, and from the mesial half of the lingual surface. Measurements and denticle counts are in Table 2. The curvature of the crown indicates it is from the right side.

In lingual view, the crown curves distally from its midheight and the carinae converge basally (Fig. 31F). In distal and mesial views, the sides of the crown are concave between the carinae and the labial surface of the crown; each concavity extends basally, where they widen and deepen along the root. The enamel of the lingual surface extends further basally than that of the labial surface. An apical wear facet is present.

In mesial view, enamel bands are present on the crown, which are convex-down and extend from the carina toward the labial surface; they are heavily worn down. The mesial carina fades before reaching the crown base; the margin of the heavily worn carina is concave throughout its length (Fig. 31G). The basal margin of the enamel is level until it deviates basally below the carina and extends across the lingual ridge. The lingual ridge is visible from the base to the apex The enamel texture is the same as in the preceding tooth and it is generally worn, especially closest to the apex.

In distal view, as on the mesial surface, enamel bands are present on the basal half of the tooth (Fig. 31H). The carina is smooth and appears to be worn down, and there are no traces of denticles. The carina fades toward the base of the crown. The surface texture is smoothest at the basal part of the crown, which extends onto the base of the labial surface.

In lingual view, although damaged, the lingual ridge is bilobate as in the preceding crown, where the distal part is twice as wide as the mesial part. The distal half of the ridge is scoured by a long vertical groove that is one sixth the crown height (Fig. 31F). The grooves that separate the carinae from the lingual ridge appear to be the same width, but the mesial edge is damaged, so the mesial groove may have been wider as is seen in the other tooth. Both grooves are textured as in the preceding tooth. The apical worn surface is convex and curves apicolabially over the crown tip.

Dentition, Lateral Tooth A—This lateral tooth is represented by the apical part of a crown, where the basal part is missing and all of the enamel is missing from its apical half (Fig. 32A–D). In labial view, enamel is only present on the distal half of the crown (Fig. 32A). All of the denticles are chipped and missing their apices. The surface between the denticles and the crown surface is gently concave. Measurements and denticles counts are in Table 2. Interdenticle grooves, where present, are short and trend mesiobasally; the notches between the denticle are ampulla-shaped.

In distal view, the carina curves labially (Fig. 32D). Although the enamel is missing, the apex curves apicolabially, where the lingual edge extends toward the apex short of the crown tip, whereas the labial surface extends to the apex along a uniform low angle. In apical view, the external surface of the crown is strongly convex in frontal section between the carinae and it extends to both at the same angle. The labial surface is flatter than the lingual surface; the labial surface along its course has a more strongly convex mesial half than distal half.

In labial view, convex-down enamel bands are present in the basal region of the fragment. The enamel surface is textured by broken and irregular ridges that trend apicobasally. On the lingual surface almost all of the surface texture is worn off (Fig. 32B).

Dentition, Lateral Tooth B—This incomplete crown has a heavily eroded surface, where almost all of the enamel is

FIGURE 32. AMNH FARB 6266. Lateral tooth A in **A**, labial; **B**, lingual; **C**, mesial; and **D**, distal views. Lateral tooth B in **E**, labial; **F**, lingual; **G**, mesial; and **H**, distal views. Lateral tooth C in **I**, labial; **J**, lingual; **K**, mesial; and **L**, distal views.

missing lingually (Fig. 32E–H). The root is completely missing. In side view, the crown is pointed and curved, as is typically seen in theropod lateral teeth (Fig. 32E, F). Measurements and denticle counts are in Table 2.

In mesial view, the carina descends from the apex on the midline and almost immediately deviates onto the mesiolingual surface, after which it is vertically oriented and fades between the midheight and the base (Fig. 32G). In cross section, a mesiolabial heel (a distinct corner formed between the side and front of the crown) is not pronounced because the labial surface does not abruptly curve toward the carina, although the curve is more distinct than the gentle curve it follows to the distal carina.

In mesial and distal views the apex is directed labially, owing to the strong curvature along the lingual edge of the crown to the apex (Fig. 32G, H). In cross section, the lingual surface of the crown is convex, but turns abruptly distolabially to join the distal carina. Therefore, the distal carina is closest to the labial edge of the tooth, a feature that is useful for identifying the lingual and labial sides of isolated crowns (Fig. 32H). The distal carina descends vertically from the apex along the apical third of the crown, and thereafter it curves labially; the basalmost extent of the carina is missing.

Lateral Tooth C—This crown is exceedingly apicobasally short and labiolingually narrow, indicating that it may be from the distal region of the tooth row of the dentary. The root is missing and the apex is absent, possibly due to wear sustained during life (Fig. 32I–L). Distinct enamel bands are present on both surfaces of the tooth (Fig. 32I, J). In basal view, the root in cross section is indented at midlength on both sides, but this concavity does not extend onto the crown for more than 0.5 millimeters. Measurements and denticles counts are in Table 2.

In mesial view, the mesial carina extends to the base of the crown; it is vertical before curving labially below the midheight to reach the crown base (Fig. 32K). The adjacent crown surface is missing enamel next to the basal quarter of the carina. The distal carina extends from apicolingually to basolabially and it appears to be vertical above the crown base (Fig. 32L).

In apical view, the lingual surface is convex and curves abruptly to the distal carina at the distal quarter of the crown. The mesial three-quarters of the lingual surface is strongly convex. The labial surface is convex, and extends from the distal carina at a low angle before curving more abruptly to the mesial carina, producing a low mesiolabial heel basally that diminishes apically. The mesiolabial heel corresponds to the wide base of the crown, which becomes progressively lenticular in cross section toward the apex.

The mesial denticles are hatchet shaped and their long axes trend apically. On both sides, the interdenticle grooves extend for a short distance onto the crown for a few millimeters and they are oriented basally more steeply than the denticles. In mesial view, the denticles are wider than deep, but they are deeper than wide basally (Fig. 32K). In labial view, the distal grooves are short and shallow, and extend basally at only a slight angle relative to the denticles (Fig. 32I). The denticles extend apically and are longer than those of the mesial carina. The distal denticles are much longer than deep, at least 2.0–2.5 longer than deep whereas the mesial denticles are as deep as they are long. The lingual grooves are deeper, larger, and extend at a steeper angle basally than those on the labial side; basally the grooves are shallow and short.

DISCUSSION

Autapomorphies of *Alectrosaurus olseni* (This Study)—Mader and Bradley's (1989) restudy of *Alectrosaurus* identified three autapomorphies of the taxon; to those I add 30 characters. This list is intended to aid workers in identifying tyrannosauroid

hind limb fossils from the Iren Dabasu Formation, and its lateral equivalents, on a bone-by-bone basis. The expanded and pediculate condition seen in the metatarsals and phalanges are almost certainly a part of a single functional complex, but they are listed here separately as an aid to identification.

1. A spike-like process extends from the caudodorsal surface of the medial condyle of the femur;
2. the oval scar on the caudal surface of the femur is lateral to the midline;
3. an abrupt expansion in length of the cranial margin of the fibula at the distal joint surface for the tibia;
4. the tendon pit adjacent to the ventrolateral buttress of the astragalus undercuts the medial surface of the buttress;
5. the medial ligament pit of MTT I lies in a deep groove;
6. the lateral flange of MTT I is triangular and culminates in a point;
7. the apex of the distal joint surface of MTT I is situated medial to the midline of the bone;
8. the lateral plantar condyle of I-1 extends plantolaterally;
9. the dorsolateral condyle of MTT II is pediculate and the joint surface extends beyond the pedicle as a crest;
10. the dorsal margin of the proximal surface of II-2 is pointed;
11. the lateral dorsal condyle of II-2 in dorsal view reaches the midlength of the collateral ligament pit;
12. a deep and narrow cleft separates the distal condyles of II-2;
13. the medial condyle of II-2 projects below the plantar margin of the bone;
14. the center of the flexor groove of II-2 is convex;
15. the flexor tubercle of the unguals of digits II–IV is hypertrophied and reaches the level of the proximal joint surface (Mader and Bradley, 1989);
16. the proximal joint surface of the unguals of digits II–IV bears a low vertical ridge on the midline;
17. the dorsolateral and plantolateral condyles of MTT III are pediculate;
18. in cranial view, the dorsal margin of the distal condyle of MTT III is horizontally oriented;
19. the medial edge of the distal joint surface of MTT III extends beyond the shaft margin;
20. in plantar view, the distal joint surface of MTT III is hyperextended onto the shaft (Mader and Bradley, 1989);
21. D III is short (ratio of D III:mtt III = 0.63, in contrast to the range (0.71–0.80) seen in other tyrannosaurids; Mader and Bradley, 1989:49);
22. in distal view, the lateral condyle of III-1 is significantly deeper than the medial condyle;
23. in plantar view, the caudal margin of the distal condyle of III-1 is convex;
24. in plantar view, the lateral ridge that bounds the flexor groove of III-2 is a prominent keel;
25. rugosities are absent above the collateral ligament pits of III-3;
26. in dorsal view, the wide caudal region of the shaft of III-3 is limited to the caudal third of the shaft;
27. the cranioplantar surfaces of the distal condyles of III-3 are strongly convex;
28. in medial view, the scar caudodorsal to the collateral ligament pit is low in III-3;
29. in dorsal view, the dorsal craniocaudally extending ridge of the ungual of D III is situated medial the midline of the bone;
30. the cleft that separates the condyles of MTT IV extends onto the distal end of the joint surface;
31. the medial condyle of IV-1 is subtly deeper than the lateral condyle;
32. a narrow cleft separates the distal condyles in IV-4;
33. the dorsal half of the joint surface for MTT IV of MTT V is dilated cranially.

Autapomorphies of Other Tyrannosauroids—The postcranial skeleton of tyrannosauroids has generally been neglected in the search for phylogenetically informative variation. For instance, the hind limb has not been treated at the level of comparative detail seen here and in recent phylogenetic studies of Tyrannosauroidea, the hind limb is represented by only 8% of the data set (e.g., Brusatte et al., 2010). Exceptions to this are few in number (e.g., Osborn, 1906; Lambe, 1917; Parks, 1928; Brochu, 2003; Brusatte et al., 2012). In general, emphasis is given to the skull in descriptions (Osborn, 1912; Russell, 1970, Carr, 1999; Hurum and Sabath, 2003; Carr and Williamson, 2004, 2010; Carr et al., 2011) and in cladistic analyses (e.g., Holtz, 2001; Currie et al. 2003; Brusatte et al., 2010; Carr and Williamson, 2010; Carr et al., 2011). Given the variation that is seen in the hind limb, as shown here, it has potential as a source of phylogenetically informative data. During the course of this study diagnostic characters for several taxa were identified. Although the characters listed here appear to be unique to each taxon, some specimens may possess variants that are seen in other taxa because of the high amount of variation that is seen in the clade. Therefore, diagnostic nature of these characters requires testing in a cladistic analysis.

Dryptosaurus aquilunguis—The ventromedial heel of MTT IV is absent.

Appalachiosaurus montgomeriensis—The distal margin of III-1 is convex.

Bistahieversor sealeyi—A concavity is present at the base of the proximal joint surface of I-1.

Albertosaurus

1. The dorsal margin of the lateral cnemial process of the tibia extends cranioventrally at a steep angle;
2. plantarly, the joint surface of the lateral condyle of I-1 reaches or extends past the caudal margin of the collateral ligament pit;
3. in dorsal view, the distal condyle of IV-2 extends into the supracondylar pit.

A. libratus—In medial view, the proximal joint surface of II-3 does not extend onto the dorsal surface of the bone.

A. sarcophagus—The joint surface for the fibula is on the ventrolateral surface of the lateral cnemial process of the tibia.

Daspletosaurus—The plantomedial condyle is level with the diaphysis in mtt III.

D. torosus—The joint surface for the fibula on the ascending process of the astragalus is deeply excavated and a prominent ridge extends along the medial edge of the joint surface.

D. horneri

1. Lateral processs of mtt II that abuts mtt IV is as wide as it is long;
2. plantolateral condyle of II-2 is subtly pediculate;
3. plantomedial condyle of II-2 extends at a low angle;
4. flexor groove of II-2 is concavoconvex;
5. plantar condyles of mtt IV are subtly pediculate;
6. distal condylar region of IV-1 is pediculate across midline on extensor surface;
7. flanges are absent from the proximal surface of IV-5.

Tyrannosaurus—The oval scar of the femur is on the caudomedial edge of the bone.

T. bataar—The medial margin of the proximal surface of IV-1 is concave.

"*Alectrosaurus*" Fossils from Mongolia and Uzbekistan—This study permits an evaluation of the referral of the fossils to *Alectrosaurus* that have been figured in the literature. Tyrannosaurid specimens collected from Turonian deposits in Uzbekistan were referred to *Alectrosaurus* (Nessov, 1995). Nessov figured several bones that he referred to "*Alectrosaurus* sp.," which include the ungual of pedal D I (1995:fig. 1.1) and a phalanx (1995:fig. 1.16). The ungual is not referable to *Alectrosaurus* because the dorsal part of the proximal joint surface is short and the flexor tubercle is massively developed; otherwise, the ungual resembles that of a tyrannosaurid manual ungual given its curvature and the large size and distal position (relative to the proximal joint surface) of the flexor tubercle. The proximal phalanx appears to be from D IV, but the image lacks sufficient detail to make comparisons with the lectotype of *Alectrosaurus*. Nessov also figured two pedal unguals in dorsal view (1995:fig. 2.13, 14), which is insufficient for comparison with those of the lectotype. Finally, he figured a pedal ungual in side views (1995: fig. 10.9, 10) that entirely lacks a flexor tubercle and so resembles the condition seen in ornithomimid pedal unguals in that regard; therefore, it is not referable to *Alectrosaurus* either.

Nessov included photographs of a tyrannosaurid femur in cranial and caudal views (1995:fig. 10.1). The oval scar is situated medial to the caudal midline of the bone and is not situated on the caudomedial edge of the bone, indicating that it is not referable to either *Alectrosaurus* or *Tyrannosaurus*. On the basis of these fossils, there is presently no evidence to support the hypothesis of the presence of *Alectrosaurus* in the Turonian of Uzbekistan, which is consistent with the later (Campanian) occurrence of the lectotype. In fact, these fossils are probably referable to *Timurlengia* (Brusatte et al., 2016).

Perle (1977) referred two specimens (GIN 100/50, GIN 100/51) from Outer Mongolia to *Alectrosaurus* on the basis of hind limb proportions. These fossils include hind limb material, including a complete metatarsus associated with (deduced from the same specimen number, IGM 100/51) a partial ilium and incomplete skull. However, there are some differences. Unlike the lectotype of *Alectrosaurus*, the flexor tubercle of the manual ungual of GIN 100/50 is hypertrophied (Perle, 1977:fig. 3), a condition that is present in other tyrannosaurid specimens (AMNH FARB 5397, AMNH FARB 5937, AMNH FARB 29067); in dorsal view, the entire distal end of MTT III (GIN 100/51; Perle, 1977:fig. 5) is widened relative to the shaft of the bone; and MTT III is pinched out (concealed) for half of its length behind the adjacent metatarsals—this state is unique among tyrannosaurids because the middle bone is only concealed proximally in articulated metatarsi (AMNH FARB 5423, CMN 2120, FMNH PR2081, NMMNH P-25049, PIN 551-2, PIN 552-1, PIN 552-2, ROM 1247; Lambe, 1917; Maleev, 1974; Brochu, 2003). Although incomplete, the proximal-most portion of the right MTT III of the lectotype of *Alectrosaurus* is relatively wide and it is not covered by joint surfaces for the adjacent metatarsals, indicating that the bone was not concealed at midheight as in the referred fossil. Thus, there is reason to be skeptical of the referral of the Mongolian fossils to *Alectrosaurus*.

The Mongolian fossils were collected at Baishin Tsav in the East Gobi, from the upper part of the Bain Shire Formation, the fauna of which is most similar to that of the Iren Dabasu Formation and may be its lateral equivalent (Currie and Eberth, 1993). First-hand study of GIN 100/50, GIN 100/51, and additional "*Alectrosaurus*" fossils from southeastern Mongolia and northern China collected since the lectotype (Currie, 2000a), are required to resolve their identity.

CONCLUSIONS

(1) The hind limb of the lectotype of *Alectrosaurus olseni* is specialized relative to that of other tyrannosauroids, and the taxon can be characterized on the basis of 33 diagnostic characters, indicating that even isolated hind limb bones of this species can be identified with confidence. Tyrannosauroid fossils collected from the Turonian of Uzbekistan are

not convincingly referred to *Alectrosaurus*, probably represent *Timurlengia*, but those from the Campanian of Mongolia require restudy.

(2) The associated partial skull and dentition from the Iren Dabasu Formation cannot be referred to *A. olseni* because it does not share diagnostic bones with the lectotype. The narrow condition of the lateral teeth, the relative development of the skull bones, and the small size of the specimen indicate that it represents a juvenile. The lacrimal bone is most similar to that of *Raptorex kriegsteini* and to juvenile *T. rex*; however, the laterally extending cornual process is smooth in *Raptorex*, whereas it is rugose in the Iren Dabasu specimen and in juvenile *T. rex*. The large maxillary fenestra in the holotype of *Raptorex*, a juvenile, is also seen in *T. bataar* (Tsuihiji et al., 2011). It is therefore possible that *Raptorex* and the taxon represented by the Iren Dabasu skull are most closely allied with derived tyrannosaurines. Three characters are unique to the specimen: (1) the strongly undulating margin of the laterotemporal fenestra, (2) the narrow paraquadrate fossa of the quadratojugal as seen in medial view, and (3) the narrow and sharp ridge along the caudoventral edge of the jugal process of the ectopterygoid. Future discoveries of associated skulls and hind limbs will settle its identity.

LIST OF SUPPLEMENTARY FILES

Supplementary File 1: Tables S1–S4, Carr.Supplementary.R2_-_LL.docx

LITERATURE CITED

Baumel, J. J., & Witmer, L. M. (1993). Osteologica. In J. J. Baumel, A. S. King, J. E. Breazile, H. E. Evans, & J. C. Vanden Berge (Eds.), *Handbook of Avian Anatomy: Nomina Anatomic Avium* (pp. 45–132). Cambridge: Publications of the Nuttall Ornithological Club, No. 23.

Brochu, C. A. (2003). Osteology of *Tyrannosaurus rex*: insights from a nearly complete skeleton and high-resolution computed tomographic analysis of the skull. *Journal of Vertebrate Paleontology*, 22(Suppl. 4), 1–138.

Brownstein, C. D. (2021). Dinosaurs from the Santonian-Campanian Atlantic coastline substantiate phylogenetic signature of vicariance in Cretaceous North America. *Royal Society Open Science*, 8. https://doi.org/10.1098/rsos.210127

Brusatte, S. L., Norell, M. A., Carr, T. D., Erickson, G. M., Hutchinson, J. R., Balanoff, A. M., Bever, G. S., Choiniere, J. N., Makovicky, P. J., & Xu, X. (2010). Tyrannosaur paleobiology: new research on ancient exemplar organisms. *Science*, 329, 1481–1485.

Brusatte, S. L., Carr, T. D., & Norell, M. A. (2012). The osteology of *Alioramus*, a gracile and long-snouted tyrannosaurid (Dinosauria: Theropoda) from the Late Cretaceous of Mongolia. *Bulletin of the American Museum of Natural History*, 336, 1–197.

Brusatte, S. L., Averianov, A., Sues, H.-D., & Butler, I. B. (2016). New tyrannosaur from the mid-Cretaceous of Uzbekistan clarifies the evolution of giant body sizes and advanced senses in tyrant dinosaurs. *Proceedings of the National Academy of Sciences USA*, 113(13), 3447. https://doi.org/10.1073/pnas.1600140113

Brusatte, S. L. & Carr, T. D. (2016), The phylogeny and evolutionary history of tyrannosauroid dinosaurs. *Scientific Reports 6*, 20252. https://doi.org/10.1038/srep20252

Carr, T. D. (1999). Craniofacial ontogeny in Tyrannosauridae (Dinosauria, Theropoda). *Journal of Vertebrate Paleontology*, 19 (3), 497–520.

Carr, T. D., & Williamson, T. E. (2004). Diversity of late Maastrichtian Tyrannosauridae (Dinosauria, Coelurosauria) from western North America. *Zoological Journal of the Linnean Society*, 142, 479–523.

Carr, T. D. (2020). A high-resolution growth series of *Tyrannosaurus rex* obtained from multiple lines of evidence. *PeerJ 8*: e9192. https://doi.org/10.7717/peerj.9192

Carr, T. D., & Williamson, T. E. (2010). *Bistahieversor sealeyi*, gen. et sp. nov., a new tyrannosauroid from New Mexico and the origin of deep snouts in Tyrannosauroidea. *Journal of Vertebrate Paleontology 30* (1), 1–10. http://doi.org/10.1080/02724630903413032

Carr, T. D., T. E. Williamson, & D. R. Schwimmer. (2005). A new genus and species of tyrannosauroid from the Late Cretaceous (Middle Campanian) Demopolis Formation of Alabama. *Journal of Vertebrate Paleontology* 25: 119–143.

Carr, T. D., Williamson, T. E., Britt, B. B., & Stadtman, K. (2011). Evidence for high taxonomic and morphologic tyrannosaurid diversity in the Late Cretaceous (Late Campanian) of the American Southwest and a new short-skulled tyrannosaurid from the Kaiparowits Formation of Utah. *Naturwissenschaften*, 98(3), 241–246.

Carr, T. D., Varricchio, D. J., Sedlmayr, J. C., Roberts, E. M., & Moore, J. R. (2017). A new tyrannosaur with evidence for anagenesis and crocodile-like facial sensory system. *Scientific Reports*, 7, 44942. https://doi.org/10.1038/srep44942

Carr, T. D., Napoli, J.G., Brusatte, S. L., Holtz, T. R. Jr., Hone, D. W. E., Williamson, T. E., & Zanno, L.E. (2022). Insufficient evidence for multiple species of *Tyrannosaurus* in the Latest Cretaceous of North America: A comment on "The tyrant lizard king, queen and emperor: multiple lines of morphological and stratigraphic evidence support subtle evolution and probable speciation within the North American genus *Tyrannosaurus*." *Evolutionary Biology*, 49: 327–341. https://doi.org/10.1007/s11692-002-09573-1

Carrano, M. T., & Hutchinson, J. R. (2002). Pelvic and hindlimb musculature of *Tyrannosaurus rex* (Dinosauria: Theropoda). *Journal of Morphology*, 253, 207–228. https://doi.org/10.1002/jmpr.10018

Currie, P. J. (2000a). Theropods from the Cretaceous of Mongolia. In M. Benton, E. Kurochkin, M. Shishkin, & D. Unwin (Eds.), *The Age of Dinosaurs in Russia and Mongolia* (pp. 434–455). Cambridge University Press.

Currie, P. J. (2000b). Possible evidence of gregarious behavior in tyrannosaurids. *Gaia*, 15, 271–277.

Currie, P. J., Rigby, J. K., & Sloan, R. E. (1990). Theropod teeth from the Judith River Formation of southern Alberta, Canada. In K. Carpenter & P. J. Currie (Eds.), *Dinosaur Systematics: Perspectives and Approaches* (pp. 107–125). Cambridge University Press.

Currie, P. J., & Eberth, D. A. (1993). Palaeontology, sedimentology and palaeoecology of the Iren Dabasu Formation (Upper Cretaceous), Inner Mongolia, People's Republic of China. *Cretaceous Research*, 14(2), 127–144. https://doi.org/10.1006/cres.1993.1011

Currie, P. J. & Zhao, X. J. (1993). A new carnosaur (Dinosauria, Theropoda) from the Jurassic of Xinjiang, People's Republic of

China. *Canadian Journal of Earth Sciences*, *30*(10), 2037–2081. https://doi.org/10.1139/e93-179

Currie, P. J., & Dong, Z. (2001). New information on *Shanshanosaurus huoyanshanensis*, a juvenile tyrannosaurid (Theropoda, Dinosauria) from the Late Cretaceous of China. *Canadian Journal of Earth Sciences*, *38*(12), 1729–1737. https://doi.org/10.1139/e01-042

Currie, P. J., Hurum, J., & Sabath, K. (2003). Skull structure and evolution in tyrannosaurid dinosaurs. *Acta Palaeontologica Polonica*, *48*(2), 227–234.

Fowler, D. W., Woodward, H. N., Freedman, E. A., Larson, P. L., & Horner, J. R. (2011). Reanalysis of "*Raptorex kriegsteini*": a juvenile tyrannosaurid dinosaur from Mongolia. *PLoS ONE*, *6*(6), 1–7. https://doi.org/10.1371/journal.pone.0021376

Gilmore, C. W. (1933). On the dinosaurian fauna of the Iren Dabasu Formation. *Bulletin of the American Museum of Natural History*, *67*, 23–78.

Granger, W. & Berkey, C. P. (1922). Discovery of Cretaceous and older Tertiary strata in Mongolia. *American Museum Novitates 42*:1–7.

Holtz, T. R., Jr. (2001). The phylogeny and taxonomy of the Tyrannosauridae. In D. H. Tanke & K. Carpenter (Eds.), *Mesozoic Vertebrate Life* (pp. 64–83). Indiana University Press.

Hurum, J. H., & Sabath, K. (2003). Giant theropod dinosaurs from Asia and North America: skulls of *Tarbosaurus bataar* and *Tyrannosaurus rex* compared. *Acta Palaeontologica Polonica*, *48*(2),161–190.

Kurzanov, S. M. (1976). A new Late Cretaceous carnosaur from Nogon-Tsav, Mongolia. *Joint Soviet-Mongolian Paleontological Expedition Transactions*, *3*, 93–104. [In Russian with English summary]

Lambe, L. M. (1917). The Cretaceous theropodous dinosaur *Gorgosaurus*. *Memoirs of the Geological Survey of Canada*, *100*(83), 1–84.

Li, D., Norell, M. A., Gao, K., Smith, N. D., & Makovicky, P.J. (2009). A longirostrine tyrannosauroid from the Early Cretaceous of China. *Proceedings of the Royal Society Series B*, *277*(1679): 183–190. https://doi.org/10.1098/rsbp.2009.0249

Loewen, M. A., Irmis, R. B., Sertich, J. J. W., Currie, P. J., Sampson, S. D. (2013). Tyrant dinosaur evolution tracks the rise and fall of Late Cretaceous oceans. *PLoS ONE 8*(11), Article e79420. https://doi.org/10.1371/journal.pone.0079420

Mader, B. J., & Bradley, R. L. (1989). A redescription and revised diagnosis of the syntypes of the Mongolian tyrannosaur *Alectrosaurus olseni*. *Journal of Vertebrate Paleontology*, *9*(1), 41–55.

Maleev, E. A. (1974). [Gigantic carnosaurs of the family Tyrannosauridae.] *Joint Soviet-Mongolian Palaeontological Expedition, Transactions 1*, 132–191. [In Russian with English summary]

Marsh, O. C. (1881). Classification of the Dinosauria. *American Journal of Science 3*(23), 81–86.

Matthew, W. D., & Brown, B. (1923). Preliminary notices of skeletons and skulls of Deinodontidae from the Cretaceous of Alberta. *American Museum Novitates*, *89*, 1–9.

Molnar, R. E., Kurzanov, S. M., & Dong, Z. (1990). Carnosauria. In D. B. Weishampel, P. Dodson, and H. Osmólska (Eds.), *The Dinosauria* (pp. 169–209). University of California Press.

Nesbitt, S. J., Denton Jr, R. K., Loewen, M. A., Brusatte, S. L., Smith, N. D., Turner, A. H., Kirkland, J. I., McDonald, A. T., Wolfe, D. G. (2019). A mid-Cretaceous tyrannosauroid and the origin of North American end-Cretaceous dinosaur assemblage. *Nature Ecology and Evolution*, *3*, 892–899. https://doi.org/10.1038/s41559-019-0888-0

Nessov, L. A. (1995). Dinosaurs of the Northern Eurasia: new data about assemblages, ecology and paleobiogeography, St. Petersburg State University, *Institute of the Earth Crust, St. Petersburg*, 1-156 [In Russian] https://doi.org/10.30906/1026-2296-1996-3-2-206-208

Newbrey, M. G., Brinkman, D. B., Winkler, D. A., Freedman, E. A., Neuman, A. G., Fowler, D. W., & Woodward, H. N. (2013). Teleost centrum and jaw elements from the Upper Cretaceous Nemegt Formation (Campanian-Maastrichtian) of Mongolia and a re-identification of the fish centrum found with the theropod *Raptorex kriegsteini*. In G. Arratia, H.-P. Schultze, & M. V. H. Wilson (eds.), *Mesozoic Fishes 5 – Global Diversity and Evolution* (pp. 291–304). Verlag Dr. Friedrich Pfeil.

Osborn, H. F. (1905). *Tyrannosaurus* and other Cretaceous carnivorous dinosaurs. *Bulletin of the American Museum of Natural History 21*, 259–265.

Osborn, H. F. (1906) *Tyrannosaurus*, Upper Cretaceous carnivorous dinosaur. (Second Communication). *Bulletin of the American Museum of Natural History*, *22*(16), 281–296.

Osborn, H. F. (1912) Crania of *Tyrannosaurus* and *Allosaurus*. *Memoirs of the American Museum of Natural History*, *1*(1), 1–30.

Parks, W. A. (1928). *Albertosaurus arctunguis*, a new species of theropodous dinosaur from the Edmonton Formation of Alberta. *University of Toronto Studies (Geological Series)*, *25*, 3–42.

Perle, A. (1977). [On the first discovery of *Alectrosaurus* (Tyrannosauridae, Theropoda) in the Late Cretaceous of Mongolia. *Problems of Mongolian Geology*, 3, 104–113.] [In Russian]

Russell, D. A. (1970). Tyrannosaurs from the Late Cretaceous of western Canada. *National Museum of Natural Science Publications in Palaeontology 1*, 1–34.

Seeley, H. G. (1888). On the classification of the fossil animals commonly named Dinosauria. *Proceedings of the Royal Society of London 43*(258-265), 165–171. https://doi.org/10.1098/rspl.1887.0117

Sereno, P.C., Tan, L., Brusatte, S.L., Kriegstein, J., Zhao, X., & Cloward, K. (2009). Tyrannosaurid skeletal design first evolved at small body size. *Science*, *326*(5951), 418–422. https://doi.org/10.1126/science.1177428

Tsuihiji, T., Watabe, M., Tsogtbaatar, K., Tsubamoto, T., Barsbold, R., Suzuki, S., Lee, A. H., Ridgely, R. C., Kawahara, Y., & Witmer, L. M. (2011). Cranial osteology of a juvenile specimen of *Tarbosaurus bataar* (Theropoda, Tyrannosauridae) from the Nemegt Formation (Upper Cretaceous) of Bugin Tsav, Mongolia. *Journal of Vertebrate Paleontology*, *31*(3), 497–517. https://doi.org/10.1080/02724634.2011.557116

Turner, A. H., Makovicky, P. J., & Norell, M. A. (2012). A review of dromaeosaurid systematics and paravian phylogeny. *Bulletin of the American Museum of Natural History*, *2012*(371):1–206. https://doi.org/10.11206/748.1

Wu, X.-C., Shi, J-R, Dong, L.-Y., Carr, T. D., Yi, J., & Xu, S-C. (2020). A new tyrannosauroid from the Upper Cretaceous of Shanxi, China. *Cretaceous Research*, *108*, 1–13. https://doi.org/10.1016/j.creres.2019.104357

Zanno, L. E., Tucker, R. T., Canoville, A., Avrahami, H. M., Gates, T. A., & Makovicky, P. J. (2019). Diminutive fleet-footed tyrannosauroid narrows the 70-million-year gap in the North American fossil record. *Communications Biology*, *2*(64), 1–12. https://doi.org/10.1038/s42003-019-0308-7